# DYNAMIC MODELLING OF CATALYTIC SO2 CONVERTER IN A SULFURIC ACID PLANT OF AN INDUSTRIAL SMELTER

by

Jianjun He

Thesis submitted in partial fulfillment
of the requirements for the degree of
Doctor of Philosophy (PhD) in Natural Resources Engineering

Faculty of Graduate Studies
Laurentian University
Sudbury, Ontario, Canada

## THESIS DEFENCE COMMITTEE/COMITÉ DE SOUTENANCE DE THÈSE
**Laurentian Université/Université Laurentienne**
Faculty of Graduate Studies/Faculté des études supérieures

Title of Thesis
Titre de la thèse: DYNAMIC MODELLING OF CATALYTIC $SO_2$ CONVERTER IN A SULFURIC ACID PLANT OF AN INDUSTRIAL SMELTER

Name of Candidate
Nom du candidat: He, Jianjun

Degree
Diplôme: Doctor of Philosophy

Department/Program
Département/Programme: Natural Resoureces Engineering

Date of Defence
Date de la soutenance: April 16, 2018

**APPROVED/APPROUVÉ**

Thesis Examiners/Examinateurs de thèse:

Dr. Helen Shang
(Co-Supervisor/Co-directrice de thèse)

Dr. Junfeng Zhang
(Co-Supervisor/Co-directeur de thèse)

Dr. Ramesh Subramanian
(Committee member/Membre du comité)

Dr. JA Scott
(Committee member/Membre du comité)

Dr. Ali Elkamel
(External Examiner/Examinateur externe)

Dr. Guangdong Yang
(Internal Examiner/Examinateur interne)

Approved for the Faculty of Graduate Studies
Approuvé pour la Faculté des études supérieures
Dr. David Lesbarrères
Monsieur David Lesbarrères
Dean, Faculty of Graduate Studies
Doyen, Faculté des études supérieures

**ACCESSIBILITY CLAUSE AND PERMISSION TO USE**

# Abstract

In industrial nickel and copper production, sulfur dioxide ($SO_2$) is generated from the combustion of sulfide ores. With increasingly tightened regulations on $SO_2$ emissions, a sulfuric acid plant has become a crucial part of industrial smelters. It converts environmentally harmful $SO_2$, which is generated in smelter furnaces, roasters, and Cu-reactors, into commercially beneficial sulfuric acid. This method is recognized as one of the most effective ways to ensure that smelters are able to satisfy the $SO_2$ emission regulations.

A sulfuric acid plant is primarily comprised of a central catalytic $SO_2$ converter, $SO_3$ (sulfur trioxide) absorption towers and a series of interconnected heat exchangers. The catalytic $SO_2$ converter is the key component and the focus of this research. Both steady-state and dynamic models of the converter are developed in this thesis.

A steady-state model of the converter is established in accordance with steady-state mass and energy balances. The developed model provides an explicit relation between $SO_2$ conversion ratio and gas temperature, which is denoted as the heat-up path of the converter. By combining the heat-up path with the equilibrium curve of the $SO_2$ oxidation reaction, an equilibrium state for every converter stage can be obtained. Using the developed steady-state model, simulations are performed to investigate the effect of inlet $SO_2$ molar fraction and gas temperature on the equilibrium conversion ratio.

In an industrial $SO_2$ converter, the $SO_2$ concentration and conversion ratio out of each bed are important variables but are not measured in real time. To monitor these unmeasured variables in industrial operations, a soft sensor is proposed by combining the derived steady-state model with dynamic data analysis. The obtained soft sensor provides a real-time estimation of outlet $SO_2$ concentration and the conversion ratio from measured temperatures. For synchronization between the inlet $SO_2$ concentration and outlet temperature, a first-order exponential data filter is applied to the feed $SO_2$ data. With the filtered signal being used,

the proposed soft sensors give a satisfactory estimation of both outlet $SO_2$ concentration and conversion ratio in the converter stages.

Dynamic modelling is carried out using two different model forms: ordinary differential equation (ODE) and partial differential equation (PDE) models. The ODE model is obtained by applying dynamic mass and energy conservation to the $SO_2$ converter. The resulting model can be used in industrial applications and describes the converter performance even if information of reaction kinetics is not available. A good fit with collected industrial data verifies the validity of the developed ODE model. The effect of process input variables is studied using simulations with the ODE model.

Dynamic modelling is performed by implementing mass and energy balances on both fluid and solid-phase gas flows. The proposed two-phase dynamic model, which takes the PDE form, is able to generate detailed profiles of the $SO_2$ converter within time and space. With the estimated parameters, this two-phase dynamic model generates a good fit between the simulated and measured outlet temperatures. Based on the PDE model, simulations are run to investigate the detailed mechanistic performance of the converter. The detailed PDE model provides useful explanation of, and prediction for the converter behaviour.

## Keywords:

dynamic modelling, catalytic $SO_2$ converter, sulfuric acid plant, industrial smelter

# Acknowledgments

I would like to express my sincere gratitude to my supervisor Dr. Helen Shang, who provided me with the opportunity to start my Ph.D researching, guided me patiently throughout my graduate studies, inspired me with her wisdom and professional expertise, and supported me psychologically and financially. It was a pleasure for me to work and study under her supervision.

I would like to acknowledge the patient guidance of Dr. Junfeng Zhang, who provided me with professional suggestions and helped me solve various problems in the Ph.D research.

Also, I would like to thank my advisory committee: Dr. John A. Scott, Dr. Ramesh Subramanian, Dr. Guangdong Yang and Dr. Ali Elkamel for their valuable time in helping me with my Ph.D work and giving me insightful opinions to improve my thesis.

The financial support from Natural Sciences and Engineering Research Council of Canada (NSERC), Vale Canada Inc. and Laurentian University is gratefully acknowledged. The industrial data and process information from Vales Copper Cliff Smelter are especially appreciated. The support and guidance by Chris Doyle, Dan Legrand and Paul Kenny from Vale is particularly appreciated.

# Contents

# Nomenclature

| | |
|---|---|
| $a_p$ | specific area, 1/m |
| $b_p$ | standard enthalpy, J/mol |
| $A_\mu$, $B_\mu$, $C_\mu$ | empirical coefficients regarding viscosity calculation |
| $A_k$, $B_k$, $C_k$ | empirical coefficients regarding thermal conductivity coefficient calculation |
| $A_p$, $B_p$, $C_p$ | empirical coefficients regarding molar heat capacity calculation |
| $D_p$, $E_p$ | empirical coefficients regarding molar heat capacity calculation |
| $A_E$ | empirical constant in Equation (2.24), 0.09357 MJ/(kmol·K) (Davenport and King, 2006) |
| $B_E$ | empirical constant in Equation (2.24), -98.41 MJ/(kmol·K) (Davenport and King, 2006) |
| $c_p$ | heat capacity, J/(kg·K) |
| $C$ | concentration, mol/m$^3$ |
| $d_p$ | catalyst particle diameter, m |
| $D$ | mass diffusion coefficient, m$^2$/sec |
| $D_C$ | catalytic converter diameter, m |
| $h$ | heat transfer coefficient, J/(m$^2$·K·sec) |
| $H$ | enthalpy of gas components, J/mol |
| $\Delta H$ | reaction heat, -98 kJ/mol |
| $j$ | mass diffusion, kg/(m$^2$·sec) |
| $j^*$ | mass transfer between fluid and solid phases, kg/(m$^2$·sec) |
| $k$ | thermal conductivity, J/(m·K·sec) |
| $k_p$ | heat capacity, J/(mol·K) |
| $K_1$, $K_2$, $K_3$, $K_E$ | empirical parameters in reaction rate expression (5.85) |

| | |
|---|---|
| $n_t$ | total molar quantity of gas in the converter stage, mol |
| $M$ | molecular weight, g/mol |
| $N$ | molar flowrate, mol/sec |
| $P$ | pressure, Pa |
| $Pr$ | Prandtl number |
| $\dot{q}$ | heat flux, J/(m$^2$·sec) |
| $Q$ | volume flowrate, m$^3$/sec |
| $\dot{Q}$ | heat flux rate, J/sec |
| $r$ | consumption rate of $SO_2$, mol/min |
| $r_{SO_2}$ | production rate of $SO_2$, mol/(kg-cat·sec) |
| $r_h$ | energy release rate of chemical reation, J/(kg-cat·sec) |
| $r_s$ | chemical production rate, mol/(kg-cat·sec) |
| $R$ | ideal gas constant, 0.008314 kJ/(mol·K) |
| $R_s$ | chemical production rate, kg/(kg-cat·sec) |
| $Re$ | Reynolds number |
| $S$ | area, m$^2$ |
| $Sc$ | Schmidt number |
| $t$ | time, sec |
| $T$ | temperature, K |
| $T_{cp}$ | specific temperature defined as $T$/1000, $10^{-3}$K |
| $u$ | Darcy velocity, m/sec |
| $v$ | average velocity, m/sec |
| $V$ | volume, m$^3$ |
| $V_{sp}$ | specific volume, m$^3$ |
| $V_m$ | molar volume at normal boiling point, cm$^3$/mol |
| $x$ | gas flow direction |

| | |
|---|---|
| $X$ | molar fraction of gas compoenents |
| $y$, $z$ | radial directions of the catalyst bed |

***Greek symbols***

| | |
|---|---|
| $\alpha$ | first-order exponential filter parameter |
| $\beta$ | mass transfer coefficient, m/sec |
| $\varepsilon$ | porosity |
| $\kappa$ | Darcy permeability, $m^2$ |
| $\lambda$ | parameter related with actural and equilibrium $SO_2$ conversion ratios |
| $\mu$ | viscosity, Pa·sec |
| $\Phi$ | $SO_2$ conversion ratio |
| $\pi$ | ratio of a circle's circumference to its diameter, 3.1416 |
| $\rho$ | density, $kg/m^3$ |

***Superscript***

| | |
|---|---|
| $E$ | equilibrium |
| $in$ | inlet |

***Subscript***

| | |
|---|---|
| $cat$ | catalyst |
| $cs$ | cross-section |
| $cv$ | control volume |
| $f$ | fluid phase |
| $g$ | gas |
| $i$ | represents gas components, $SO_2$, $O_2$, $SO_3$ or nonreactive remainders |
| $k$ | stages of the converter |

| | |
|---|---|
| $min$ | minimum |
| $max$ | maximum |
| $p$ | catalyst particle |
| $re$ | nonreactive remainders in the gas mixture |
| $s$ | solid phase |
| $t$ | total |

# List of Figures

# List of Tables

# Chapter 1

# Introduction

Apart from the sulfur-laden fossil fuel combustion, smelting of sulfide ores to extract the designated metal has become a major source of sulfur dioxide ($SO_2$) emission into the atmosphere (Ciccone and Storbeck, 1997). $SO_2$ is recognized worldwide as a significant air pollutant and the major cause of acid rain, resulting in harmful impacts on human respiratory systems and the environment (Kampa and Castanas, 2008). $SO_2$ generated from industrial smelters was historically directly discharged into the atmosphere without proper treatments, and led to a wide range of severe environmental issues (Chan et al., 1984a,b). In order to reduce $SO_2$ emissions, significant efforts were subsequently made through different abatement programs at many smelters (Hunter Jr. et al., 1975; Donovan et al., 1978; Sudbury and Crawford, 1989; Gunn et al., 1995; Byrdziak et al., 1996; Lobanov et al., 2008; Ma et al., 2012).

Sulfuric acid plants are markedly important in the modern process industry due to wide applications of sulfuric acid products (e.g., fertilizers, metallic ore leaching and petroleum (Kiss et al., 2010)). As they are capable of capturing sulfur dioxide in off-gas, sulfuric acid plants have also become an essential part of many smelters. A typical sulfuric acid plant is primarily composed of a central catalytic $SO_2$ converter, $SO_3$ (sulfur trioxide) absorption towers, and a series of interconnected heat exchangers. The central catalytic converter, where $SO_2$ is oxidized by oxygen ($O_2$) to $SO_3$, is usually built with multistage catalyst beds. It determines the amount

of $SO_2$ captured from the off-gas and is the key unit in a sulfuric acid plant.

## 1.1 Process Description

### 1.1.1 Sulfuric Acid Plant in an Industrial Smelter

Sulfuric acid is a bedrock of the modern chemical industry and is widely used in many industrial sectors. The raw material of sulfuric acid is sulfur dioxide ($SO_2$) gas, which mostly originates from elemental sulfur burning, metal sulfide ore smelting, and/or spent acid (Davenport and King, 2006; Ashar and Golwalkar, 2013). Unlike $SO_2$ gas from sulfur burners, where $SO_2$ concentration is controllable and easily maintained, $SO_2$ in metallurgical off-gas is often dusty and can vary in concentration. This makes the $SO_2$ conversion and acid production more challenging. According to an air pollutant emission report from Environment and Climate Change Canada, 46% of Canada's sulfur oxide ($SO_x$) pollutant in 2015 came from the oil and mineral industries (ECCC, 2017). In Ontario Canada, smelters resulted in over 60% of sulfur dioxide emissions in 2012 (MECC-$SO_2$). In order to control and reduce the $SO_2$ emission, increasingly stringent environmental regulations on discharge levels have been issued in many districts or countries.

Table 1.1: Sulfur dioxide emission allowances, facility budgets on base metal smelting sectors in Ontario Canada (O. Reg. 194/05)

| Facility | Amount (tonnes) | | | |
|---|---|---|---|---|
| | 2006 | 2007-2009 | 2010-2014 | 2015 and after |
| Inco, Sudbury | 265,000 | 175,000 | 175,000 | 66,000 |
| Falconbridge, Sudbury | 66,000 | 66,000 | 66,000 | 25,000 |

Tables 1.1 and 1.2 provide the regulations on sulfur dioxide emission (Ontario Regulation 194/05). It can be seen that the two smelters located in Sudbury, Ontario were required to significantly reduce their $SO_2$ emission allowance and emission density after 2015. According to the regulations, $SO_2$ emissions of these smelters has to be reduced to almost one third of the

Table 1.2: Sulfur dioxide emission intensity rates on base metal smelting sectors in Ontario Canada (O. Reg. 194/05)

| Facility | Intensity Rates* | | |
|---|---|---|---|
| | 2006 | 2007-2014 | 2015 and after |
| Inco, Sudbury | 1.12 | 0.81 | 0.30 |
| Falconbridge, Sudbury | 0.60 | 0.51 | 0.30 |

* [amount of emissions reported]/[the estimated average annual production]

2006 levels. Measures were, therefore, needed for further $SO_2$ emission abatement.

Sulfuric acid plants, where environmentally harmful $SO_2$ is converted into commercially valuable sulfuric acid products, play a critical role in smelter operations and have become an integral component of many industrial smelters. To ensure sound smelter operation in accordance with strict environmental standards, it is important and necessary to perform active research on these sulfuric acid plants. In contrast to those in many other industrial applications, acid plants in smelters have the challenge of dealing with highly varying feed conditions resulting from upstream metallurgical processes.

Methods of manufacturing sulfuric acid may vary at different smelters, but the traditional and most common one is the contact type, which involves the four steps listed below (Schlesinger et al., 2011):

(1) cooling and cleaning the gas;

(2) drying the gas with 93% sulfuric acid;

(3) catalytically oxidizing $SO_2$ to $SO_3$;

(4) absorbing this $SO_3$ into 98.5% $H_2SO_4$ sulfuric acid.

A sulfuric acid plant in an industrial smelter is comprised of a series of unit operations. A model of the plant can be developed by separately modelling individual unit operations and then integrating them to describe the overall plant. In Figure 1.1, a general flowsheet for producing sulfuric acid from smelting and converting off-gas is provided. These processes may vary at different acid plants, but they all follow the basic steps listed above.

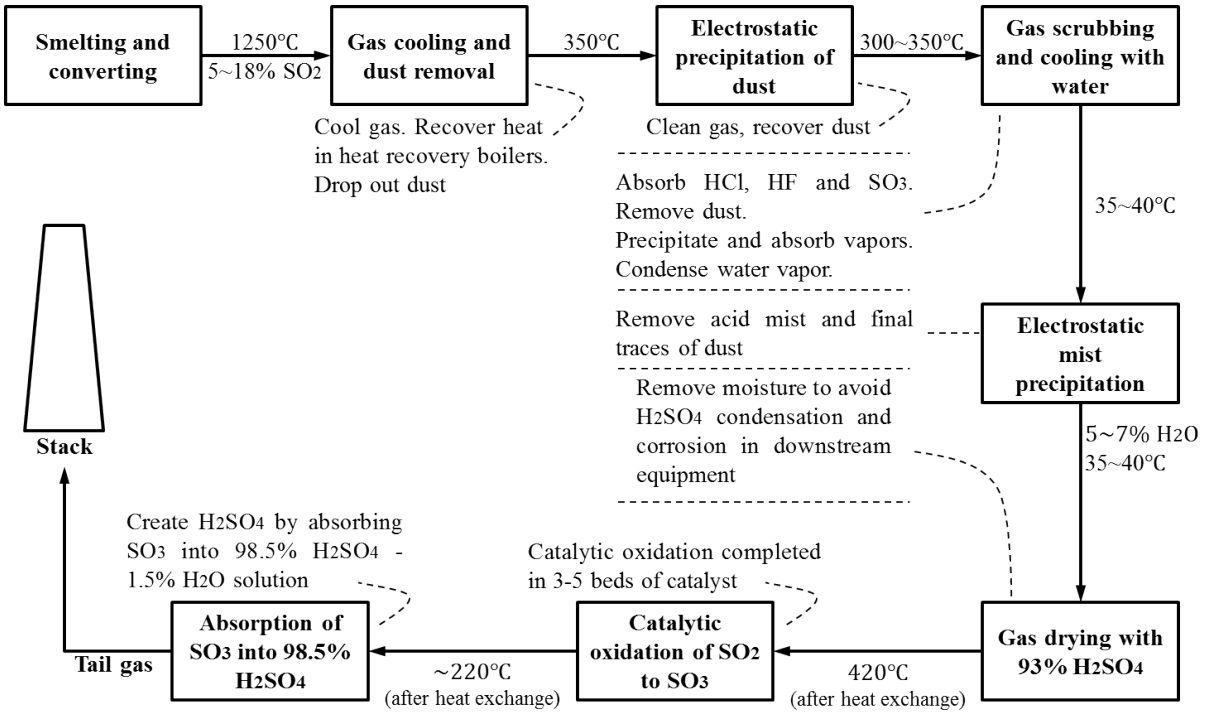


Figure 1.1: Flowsheet of sulfuric acid making from smelting and converting off-gas (Schlesinger et al., 2011)

The first five blocks are off-gas generation and pretreatment in Figure 1.1, which include smelting and converting the raw minerals, gas cooling and dust removal, electrostatic precipitation of dust, and gas scrubbing and cooling with water. They ensure that before catalytic oxidation happens, unwanted or harmful components, such as dust and water, are removed. After pretreatment, the gas blown out of the drying tower, the sixth block in Figure 1.1, contains only $SO_2$, $O_2$ and nonreactive gases, and is ready for $SO_2$ conversion operations.

Figure 1.2 shows the major operating units of a sulfuric acid plant in detail. It involves six heat exchangers, one four-bed catalytic $SO_2$ converter and two absorption towers, which are indicated as blocks 7-8 in Figure 1.1. These are the units that have major impact on capture and fixation of sulfur from the off-gas running through the acid plant.

The catalytic $SO_2$ converter is the central facility in the sulfuric acid plant, which is shown in Figure 1.2 and will be described in detail in Section 1.1.2. The heat exchangers that interconnect the catalytic converter stages, are used to transfer heat between the gas entering and exiting the

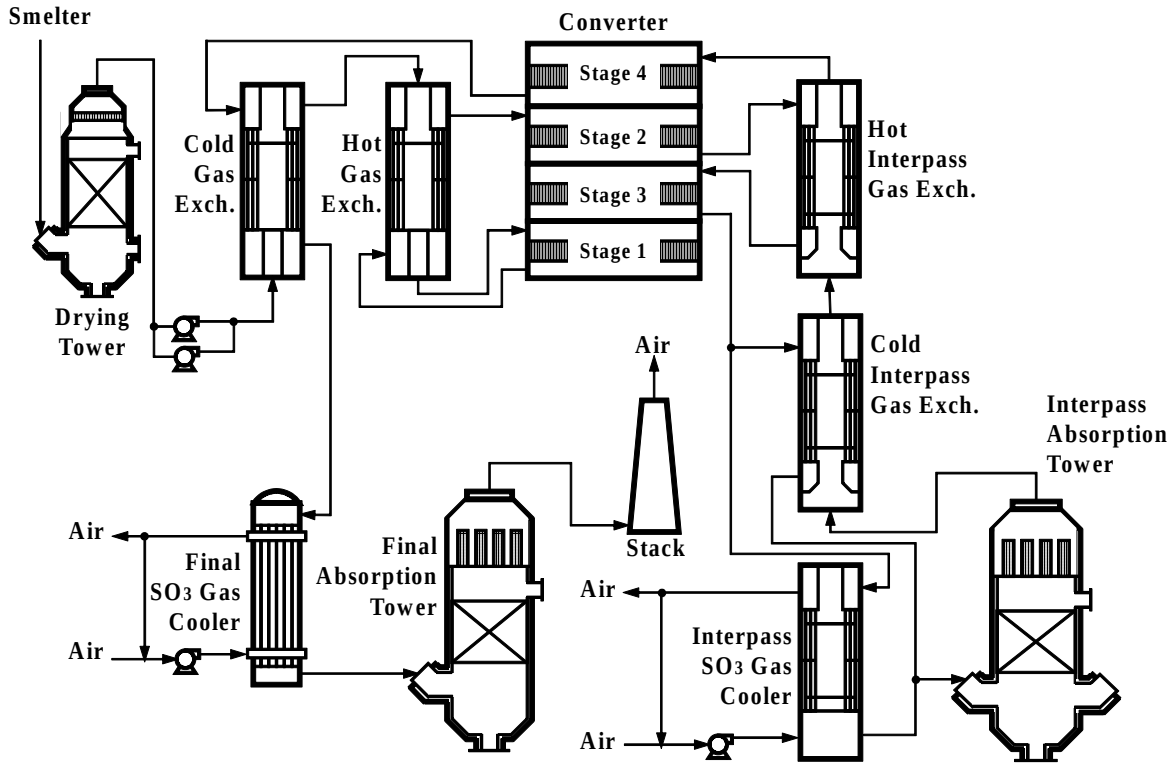


Figure 1.2: Schematic diagram of major operating units in a sulfuric acid plant

converter. They are crucial for a sulfuric acid plant due to the importance of gas temperature manipulation. Temperature is one of the most important and easily measured variables in the plant and good control can ensure more efficient $SO_2$ catalytic oxidation. The heat exchangers are usually chosen based on the design and needs of the smelter and /or sulfuric acid plants. Shell-and-tube types of heat exchangers have been commonly used and by-pass valve control applied for temperature regulation.

Absorption towers installed inside a sulfuric acid plant are where the generated sulfur trioxide ($SO_3$) in the gas stream is absorbed into a 98.5% $H_2SO_4$-1.5% $H_2O$ (sulfuric acid $H_2SO_4$, water $H_2O$) solution and a strengthened acid produced. Figure 1.3 shows a schematic diagram of a $SO_3$ absorption tower. The $SO_3$-laden gas flows in the tower from the bottom and the 98.5% $H_2SO_4$ acid solution enters from the top. They encounter in the packed bed and an

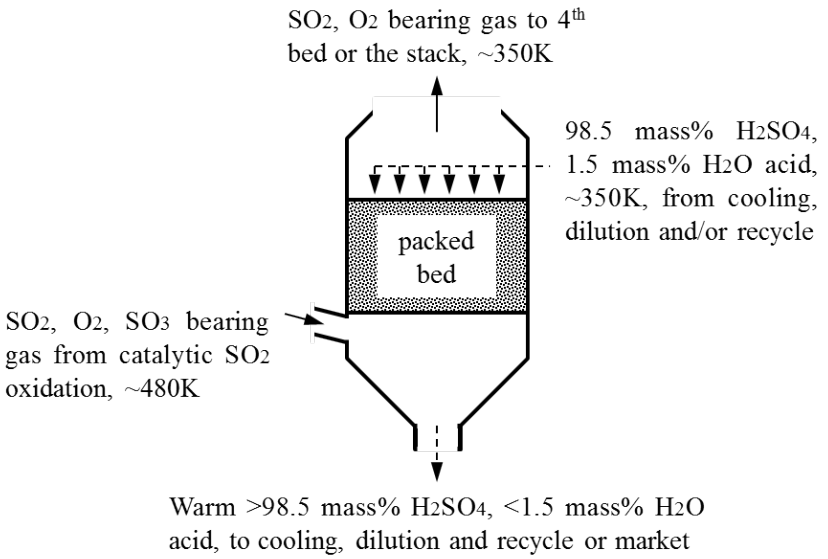


Figure 1.3: Schematic diagram of a $SO_3$ absorption tower (Davenport and King, 2006)

absorption reaction occurs as follows:

$$SO_3(g) + H_2O(l) \rightarrow H_2SO_4(l) \tag{1.1}$$

The reaction (1.1) releases heat and consequently warms up the acid solution. The acid that is warmed up and strengthened comes out from the bottom of the tower and is cooled down, diluted, recycled or marketed after proper treatment.

As shown in Figure 1.2, a double-contact sulfuric acid plant is used with two absorption towers, an intermediate one and a final one. This strategy of double absorption promotes the conversion and capture of $SO_2$ in the converter. After catalytic oxidation through three catalyst beds, the concentration of $SO_3$ increases in the gas flow and slows down the $SO_2$ oxidation reaction. The intermediate absorption tower is designed to absorb $SO_3$ after the first three beds and to decrease the $SO_3$ concentration before the gas enters the fourth bed for the final oxidation. The final absorption tower is used to absorb the $SO_3$ generated in the fourth bed before the off-gas is emitted into atmosphere.

Table 1.3 describes the typical physical features of the intermediate and final absorption

towers. It is noticed that all three physical features of the intermediate tower is higher than those of the final one. This is because most $SO_2$ is oxidized in the first three catalyst beds and more heat and $H_2SO_4$ are generated when a larger amount of $SO_3$ is absorbed in the intermediate absorption tower.

Table 1.3: Typical sulfuric acid design irrigation rates, irrigation densities, inlet/outlet temperature for absorption towers (Guenkel and Cameron, 2000)

| Tower | Sulfuric acid irrigation rate [$m^3$/tonne of 100% $H_2SO_4$ produced] | Sulfuric acid irrigation density [$m^3$/min per $m^2$ of tower cross-section] | Sulfuric acid inlet/outlet temperature [°C] |
|---|---|---|---|
| Intermediate absorption tower | 0.01 | 0.6-0.8 | 80 / 110 |
| Final absorption tower | 0.005 | 0.4 | 80 / 95 |

### 1.1.2 $SO_2$ Converter in a Sulfuric Acid Plant

The catalytic $SO_2$ converter is the key operation in a sulfuric acid plant. $SO_2$ is oxidized in the converter and this determines the final $SO_2$ discharge level to the environment. As the gas stream passes through the catalyst beds installed in the converter, the following catalytic reaction occurs:

$$SO_2 + \frac{1}{2}O_2 \overset{\text{Catalyst}}{\rightleftharpoons} SO_3, \quad \Delta H = -98 \text{ [kJ/mol]}. \tag{1.2}$$

As the forward reaction is exothermic, heat is released and gas temperature increases when this reaction dominates in the converter. Heat exchangers are located between converter stages and designed to regulate the gas temperature in order that $SO_2$ conversion can continue under the desired conditions. In the catalyst bed, as the $SO_2$-laden gas is oxidized to $SO_3$ and the following physical and chemical phenomena occur (Davenport and King, 2006):

(1) consumption of $SO_2$ and $O_2$;

(2) production of $SO_3$;

(3) heating the descending gas;

(4) heat exchange between gas and catalyst bed.

Reaction (1.2) occurring in the converter requires a suitable catalyst. Without this catalyst, the exothermic reaction barely occurs. The typical catalyst used in (1.2) is $V_2O_5$-$K_2SO_4$ based, and contains 5-10% $V_2O_5$, 10-20% $K_2SO_4$, 1-5% $Na_2SO_4$, and 55-70% $SiO_2$ (Schlesinger et al., 2011). $SiO_2$ is an inactive material, but serves as a support for the other components. However, the catalyst is not always active and effective at all ranges of temperature. When the temperature of the catalyst drops below its ignition temperature, which is around 360°C for the $V_2O_5$-$K_2SO_4$ based catalyst, the reaction proceeds very slowly or even stops. Whereas an overly heated catalyst bed, typically over 650°C, could lead to deactivation of catalyst or even unrecoverable damage. The temperature in the converter must, therefore, be maintained between ignition and degradation temperatures, in order to achieve effective $SO_2$ conversion.

Sometimes, the catalyst component $K_2SO_4$ is replaced by cesium sulfate, $Cs_2SO_4$, because a $Cs_2SO_4$-based catalyst can lower the activation temperature as well as provide a higher reaction rate. However, the cesium-based catalyst costs more than the $K_2SO_4$-based one. Some plants, therefore, only apply a Cs-based catalyst to the first catalyst bed where the majority of conversion happens (Schlesinger et al., 2011) or mix with $K_2SO_4$.

Table 1.4: Typical gas temperature and $SO_2$ conversion ratio in each converter stage (Humphris and Javor, 1997)

| | Inlet temperature [°C] | Outlet temperature [°C] | Overall $SO_2$ conversion ratio to the feed [%] |
|---|---|---|---|
| 1st bed | 422 | 624 | 67 |
| 2nd bed | 445 | 511 | 90 |
| 3rd bed | 420 | 438 | 95.7 |
| 4th bed | 413 | 426 | >99 |

Typical gas temperatures and $SO_2$ conversion ratios are tabulated in Table 1.4 for every converter bed. It is noted that over half of the $SO_2$ is converted in the first bed and it is

thus crucial to maintain an optimal operation in this bed to achieve the best overall $SO_2$ conversion. As shown in Table 1.4, conversion efficiency decreases in the subsequent stages due to continuous consumption of $SO_2$. After the off-gas stream passes through all the catalyst beds, over 99% of $SO_2$ will be captured by the acid plant.

## 1.2 Existing Research on Sulfuric Acid Plant

Sulfuric acid plants are essential for the modern process industry due to sulfuric acid's wide range of industrial applications, which include fertilizers, metallic ore leaching, and petroleum (Kiss et al., 2010; Schlesinger et al., 2011). Following the development of vanadium catalysts, the contact process started taking over the traditional chamber process in sulfuric acid plants in the early 1900's. Not only did it sharply increase productivity, it also encouraged improvement of equipment and materials in each area of the process (Friedman, 1999). With awareness of the environmental impacts of sulfur dioxide on our communities, as one of the most effective ways to capture and fix sulfur dioxide from ore processing off-gases (Friedman and Friedman, 2006), sulfuric acid plants have also established a vital environmental protection role.

Among research on sulfuric acid plants, the start-up of the plants gets a lot of attention. Start-up study is important because due to a low temperature of the gas and the catalyst, little or no $SO_2$ will be converted into sulfuric acid before the desired temperature is achieved. As a consequence, unconverted $SO_2$ could be discharged into the atmosphere. Furthermore, a large amount of heat is needed to heat up the plant during the start-up process.

Mann et al. investigated the start-up of a sulfuric acid plant and found that with a proper manipulation of sulfur burning-rate, the problem of over-emitted $SO_2$ could be solved with a fast start-up (Mann et al., 1980). Afterwards, they came up with a new idea to obtain fast and clean start-up, which required suitable flowrate programming in accordance with initial bed temperatures (Mann, 1986). In addition, software system was developed to address start-up problems, with the advantage of applying to all kinds of plant flowsheets (Gosiewski and

Klaudel, 1985).

Along with improvements in sulfuric acid plant technologies, research on the design, modification, optimization and operational problems have been carried out. Based on calculating the conversion and pressure drop, a $SO_2$ optimization program was developed by Donovan et al. that the operators could use of for better plant design and operation (Donovan et al., 1978). The frequent fluctuation of $SO_2$ concentration in the feed gas, as a consequence of multiple feed sources to acid plants, is a challenging problem. An analysis of the dynamic resistance of the concentration drop in the plant was conducted with two selected characteristic flowsheets of metallurgical $SO_2$ oxidation plants, and helped provide an insight into the influence of concentration changes (Gosiewski, 1996).

Dynamic models were provided by Shang et al. for an industrial smelter off-gas system based on mass, momentum, and energy conservation laws (Shang et al., 2008). These served as an alternative method to solve feed gas problem of a sulfuric acid plant by dealing with the source concentration of $SO_2$. Raw material selection and/or upstream technology were mentioned in (Liang and Liang, 2013) and an acid plant studied in terms of equipment, integrity of instrumentation control and the proficiency of personnel operation. Model-based optimization of sulfur recovery with a network design connecting the reactor, furnace and waste heat boiler of the sulfur recovery units together was found useful for integrated process-energy optimization (Manenti et al., 2014).

A good review of unit operations in the plant, including gas cleaning and the contact sections, equipment design, materials and handling stream variables and impurities, can be found in (Friedman and Friedman, 2006).

## 1.3 Existing Research on $SO_2$ Converter

$SO_2$ converters are the central unit operation in a sulfuric acid plant on account of their $SO_2$ capture and conversion function. Due to their importance, research on this facility is crucial

and much of it has been focussed on modelling the $SO_2$ reactors. Mann and his colleagues proposed a dynamic simulation model using ordinary differential equations to describe the unsteady behaviour of the fixed-bed reactors, and it was used as a base to set up fast start-up (Mann et al., 1980). Mann also mentioned that the advantage of using ordinary differential equations over partial differential ones lied in the fact that each bed of the reactor comprised of catalyst pellets and could be easily represented by a set of back mixed stages (Mann, 1986). Using a spreadsheet, Davenport and King presented an introduction to sulfuric acid manufacture with the calculation of steady-state operations (Davenport and King, 2006).

Modelling of the reactors has been beneficial to the operation, optimization, and control of sulfuric acid plants. A one-dimensional heterogeneous model was employed to simulate an adiabatic periodic flow reversal reactor (Snyder and Subramaniam, 1993). It was focussed on simulating the effect of operating conditions and feed gas temperature variations, and found that reaction extinction can be presented by changes in operating conditions. Another one-dimensional two-phase unsteady-state model studied mass conservation of $SO_2$ and the heat for each phase (Hong et al., 1997). To solve this model, which was built with partial differential equations, Hong et al. applied the Crank-Nicolson predictor-corrector method and the numerical results indicated that oxidation of low concentration sulfur dioxide is possible. To handle a low concentration of sulfur dioxide for oxidation, Xiao et al. suggested a converter configuration and a dual position control strategy from modelling, a laboratory reactor and a pilot scale converter (Xiao et al., 1999). The adiabatic assumption is usually made in modelling, even though the adiabatic requirement of the reactors is hard to achieve. Modelling of the reactors and simulation could be used for compensation of the adiabatic requirement and to obtain better model-based performance (Xiao and Yuan, 1996).

By introducing a correction factor into a global rate equation, Wu and his colleagues came up with a heterogeneous transient model to study catalytic oxidation of sulfur dioxide and successfully predicted transient concentration and temperature profiles (Wu et al., 1996).

Through considering the dynamic properties of the vanadium catalyst, mathematical modelling of sulfur dioxide oxidation was carried out using the nonstationary state of the catalyst surface (Vernikovskaya et al., 1999). It was concluded that it can be applied to a conventional double contact/double absorption sulfuric acid plant.

For good temperature control, an experimental and modelling study was made of a packed-bed reactor with the assumption of pseudo-homogeneous perfect plug flow (Nouri and Ouederni, 2013). It was found that conversion decreases with the amount of $SO_2$ and increases with temperature before an optimum is reached. A good reaction rate model can help improve the accuracy and performance of reactor models. Ravindra et al. presented a reaction rate model based on complete wetting of the catalyst particles in a trickle-bed reactor (Ravindra et al., 1997), and this model could predict reaction rate trends during sulfur dioxide oxidation.

An important breakthrough was made with a more detailed dynamic model developed for an acid plant using partial differential equations, and the model was simulated using the software gPROM (Kiss et al., 2010). The model used partial differential equations and developed dynamic models for three-phase slurry and trickle-bed reactors. A method using finite difference approximation for the spatial derivatives was investigated, and the simulations showed that the dynamic approach generates important information on reaction dynamics (Warna and Salmi, 1996).

Even though extensive researches have been done on $SO_2$ converter, some problems still require further investigation. Some important variables, for example, $SO_2$ conversion ratio, are important for $SO_2$ converter modelling, but are rarely measured in the plant. Research on the soft sensor developments for these unmeasured variables are necessary. In addition, the available dynamic models of $SO_2$ converter are complicated and inconvenient for industrial applications, or have mismatch problems with the industrial system. Furthermore, mechanism study inside the $SO_2$ converter is still limited. These problems will all be covered and investigated in my PhD research.

## 1.4 Thesis Organization and Contributions

This dissertation contains six chapters. Chapter 1 presents the process description and literature review over sulfuric acid plants and $SO_2$ converters. The contributions of the research are provided in Chapter 2 to Chapter 5, followed by the conclusions and suggested future work in Chapter 6.

Chapter 2 establishes the steady-state model of catalytic $SO_2$ converter based on steady-state mass and energy balances. The obtained model describes the relation between gas temperature and $SO_2$ conversion ratio under given feed conditions, and provides the base for the dynamic modelling, simplification, and optimization found in the following chapters. Incorporated with the equilibrium curve of reaction (1.2), the potential maximum conversion of the converter can be calculated by using the proposed steady-state relation, which is also called as the heat-up path.

In the derivation of the steady-state model in Chapter 2, expressions of steady-state outlet $SO_2$ concentration and $SO_2$ conversion ratio are obtained. Chapter 3 incorporates the industrial dynamic data analysis with these expressions to derive mathematical soft sensors for outlet $SO_2$ concentration and the $SO_2$ conversion ratio. A first-order exponential filter is applied to the $SO_2$ feed concentration so that synchronization between the filtered concentration and outlet temperature is achieved. The proposed soft sensors are able to estimate the unmeasured variables for the catalytic $SO_2$ converter using available industrial measurements.

In Chapter 4, by applying mass and energy conservation, dynamic modelling of the $SO_2$ converter is carried out in the form of ordinary differential equations (ODE). This dynamic modelling uses the $SO_2$ conversion ratio as the key variable, and gives an acceptable prediction of converter output responses. A good match is achieved between model predicted values and industrial measurements. Based on this ODE model, the effect of input variables on the performance of the converter is investigated.

In Chapter 5, mechanistic modelling for the $SO_2$ converter is studied by considering the gas in both fluid and solid phases. Detailed two-phase dynamic modelling in the form of partial differential equations (PDE) is performed based on mass and energy balances of both the fluid and solid phases. Using the developed dynamic model, spatial profiles of the temperature and concentration are given by simulations, and the effects of the process variables investigated. By analyzing the dynamics of two phases through detailed simulations, the different dynamics of outlet temperature in response to feed $SO_2$ cut-off and restoration can be effectively explained. As the outlet temperature prediction from the two-phase model has a satisfactory fit with industrial data, the model provides, therefore, a useful tool in studying the mechanisms of an industrial $SO_2$ converter and in predicting process performance under different operating conditions.

# Chapter 2

# Steady-State Modelling of the Sulfur Dioxide Converter

Catalytic $SO_2$ converters used in a sulfuric acid plant usually consist of multiple stages (four stages in this thesis), but the operating principle is the same in different stages. Therefore, modelling can be carried out on the first stage and the models for the other stages can be obtained in a similar way.

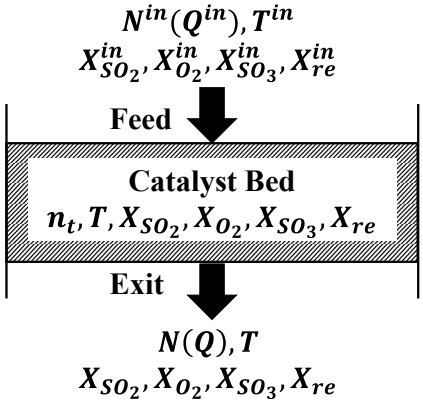


Figure 2.1: Schematic diagram of a catalytic $SO_2$ converter stage

Figure 2.1 describes a catalyst bed with a schematic diagram, including the important variables, where $N$ denotes the molar flow rate, $Q$ represents volume flow rate, $X$ is the mole

fraction (concentration) with subscripts indicating individual components in the gas and the superscript "$in$" standing for the feed condition, $T$ represents the temperature, and $n_t$ is the molar quantity of the gas in the converter stage.

Steady-state model is built based on the steady-state mass and energy balances of the off-gas within the converter stage. It is formulated to explore the relationship among the key variables and to provide a foundation for dynamic modelling and soft sensors. For steady-state modelling, the following assumptions are made:

(1) the converter is assumed to be adiabatic;

(2) temperature difference between gas and catalyst bed is negligible.

## 2.1 Heat-up Path

### 2.1.1 Mass Conservation

Considering a catalyst stage illustrated in Figure 2.1, the offgas contains both reactive components ($SO_2$, $O_2$ and $SO_3$) and nonreactive components (expressed by subscript "$re$" for remainders). According to the reaction (1.2), the conversion involves sulfur (S) and oxygen (O) elements. Applying the mole balances to these two elements during the reaction, yields:

$$X^{in}_{SO_2} N^{in} + X^{in}_{SO_3} N^{in} = X_{SO_2} N + X_{SO_3} N \tag{2.1}$$

$$2X^{in}_{SO_2} N^{in} + 2X^{in}_{O_2} N^{in} + 3X^{in}_{SO_3} N^{in} = 2X_{SO_2} N + 2X_{O_2} N + 3X_{SO_3} N \tag{2.2}$$

As the nonreactive components are not involved in the reaction, the mole balance on these components can simply be written as:

$$X^{in}_{re} N^{in} = X_{re} N \tag{2.3}$$

The molar fraction of the remainder gas in the offgas can be expressed as:

$$X_{re}^{in} = 1 - X_{SO_2}^{in} - X_{O_2}^{in} - X_{SO_3}^{in} \tag{2.4}$$

$$X_{re} = 1 - X_{SO_2} - X_{O_2} - X_{SO_3} \tag{2.5}$$

In a $SO_2$ converter, it is important to examine the ratio of oxidized $SO_2$ at each stage under different conditions. This conversion ratio $\Phi$ reflects the performance of the converter and can be defined as the ratio of $SO_2$ that is oxidized to $SO_3$:

$$\Phi = \frac{X_{SO_2}^{in} N^{in} - X_{SO_2} N}{X_{SO_2}^{in} N^{in}}. \tag{2.6}$$

Based on (2.6), $X_{SO_2}$ can be written as a function of the conversion ratio and feed conditions:

$$X_{SO_2} = (1 - \Phi) X_{SO_2}^{in} \frac{N^{in}}{N}. \tag{2.7}$$

The expressions for $X_{O_2}$, $X_{SO_3}$ and $X_{re}$ are obtained by substituting (2.7) to Equations (2.1 - 2.3):

$$X_{O_2} = \left( X_{O_2}^{in} - \frac{1}{2} \Phi X_{SO_2}^{in} \right) \frac{N^{in}}{N}, \tag{2.8}$$

$$X_{SO_3} = \left( X_{SO_3}^{in} + \Phi X_{SO_2}^{in} \right) \frac{N^{in}}{N}, \tag{2.9}$$

$$X_{re} = \left( 1 - X_{SO_2}^{in} - X_{O_2}^{in} - X_{SO_3}^{in} \right) \frac{N^{in}}{N}, \tag{2.10}$$

For the reaction (1.2), for each mole of $SO_2$ being converted, there is one half mole reduction in the total mole amount. The outlet mole flow rate $N$ can therefore be written as:

$$N = \left( 1 - \frac{1}{2} \Phi X_{SO_2}^{in} \right) N^{in}, \tag{2.11}$$

and the ratio of $N^{in}$ to $N$ is:

$$\frac{N^{in}}{N} = \frac{1}{1 - \frac{1}{2}\Phi X^{in}_{SO_2}}. \tag{2.12}$$

Substituting Equation (2.12) into Equations (2.7 - 2.10), the mole fractions of different components are then derived:

$$X_{SO_2} = \frac{(1-\Phi)X^{in}_{SO_2}}{1 - \frac{1}{2}\Phi X^{in}_{SO_2}}, \tag{2.13}$$

$$X_{O_2} = \frac{X^{in}_{O_2} - \frac{1}{2}\Phi X^{in}_{SO_2}}{1 - \frac{1}{2}\Phi X^{in}_{SO_2}}, \tag{2.14}$$

$$X_{SO_3} = \frac{X^{in}_{SO_3} + \Phi X^{in}_{SO_2}}{1 - \frac{1}{2}\Phi X^{in}_{SO_2}}, \tag{2.15}$$

$$X_{re} = \frac{1 - X^{in}_{SO_2} - X^{in}_{O_2} - X^{in}_{SO_3}}{1 - \frac{1}{2}\Phi X^{in}_{SO_2}}. \tag{2.16}$$

It is noted that under a specified feed condition, the mole fractions of all components vary with the conversion ratio. Substituting (2.11) into (2.6), the conversion ratio $\Phi$ also takes the form as a function of $X_{SO_2}$:

$$\Phi = \frac{X^{in}_{SO_2} - X_{SO_2}}{X^{in}_{SO_2} - \frac{1}{2}X_{SO_2}X^{in}_{SO_2}}. \tag{2.17}$$

The equation above can be used to exactly calculate the conversion ratio when $SO_2$ concentration is measured.

### 2.1.2 Energy Conservation

If the converter is assumed to be adiabatic, the steady-state energy balance in the catalyst bed illustrated in Figure 2.1 can thus be written as:

$$\begin{aligned} &X^{in}_{SO_2}N^{in}H^{in}_{SO_2} + X^{in}_{O_2}N^{in}H^{in}_{O_2} + X^{in}_{SO_3}N^{in}H^{in}_{SO_3} + X^{in}_{re}N^{in}H^{in}_{re} \\ &= X_{SO_2}NH_{SO_2} + X_{O_2}NH_{O_2} + X_{SO_3}NH_{SO_3} + X_{re}NH_{re}, \end{aligned} \tag{2.18}$$

where $H$ [J/mol] denotes the enthalpy of every mole gas component. Substituting Equations (2.7 - 2.10) to (2.18), the energy equation becomes:

$$\begin{aligned} &X^{in}_{SO_2}(H^{in}_{SO_2} - H_{SO_2}) + X^{in}_{O_2}(H^{in}_{O_2} - H_{O_2}) + X^{in}_{SO_3}(H^{in}_{SO_3} - H_{SO_3}) + X^{in}_{re}(H^{in}_{re} - H_{re}) \\ &= -\left(H_{SO_2} + \frac{1}{2}H_{O_2} - H_{SO_3}\right)\Phi X^{in}_{SO_2}. \end{aligned} \tag{2.19}$$

The enthalpies in the above equation are functions of temperature. While temperature changes within a given range, the relation between enthalpy and temperature can be approximated to be linear (Davenport and King, 2006),

$$H = k_p T + b_p, \tag{2.20}$$

where $k_p$ is the heat capacity of the gas and $b_p$ is the standard enthalpy. The values of $k_p$ and $b_p$ for the offgas components are given as (Davenport and King, 2006):

$$\begin{aligned} k_{p,SO_2} &= 0.05161 \quad \text{[kJ/(mol·K)]}, \quad b_{p,SO_2} = -314.3 \quad \text{[kJ/mol]} \\ k_{p,O_2} &= 0.03333 \quad \text{[kJ/(mol·K)]}, \quad b_{p,O_2} = -10.79 \quad \text{[kJ/mol]} \\ k_{p,SO_3} &= 0.07144 \quad \text{[kJ/(mol·K)]}, \quad b_{p,SO_3} = -420.6 \quad \text{[kJ/mol]} \\ k_{p,N_2} &= 0.03110 \quad \text{[kJ/(mol·K)]}, \quad b_{p,N_2} = -9.797 \quad \text{[kJ/mol]} \end{aligned}$$

As the majority of nonreactive components is nitrogen gas, the heat capacity and the standard enthalpy of the remainders are assumed to be equal to the ones of nitrogen gas. Substituting Equation (2.20) to (2.19), the conversion ratio $\Phi$ is found related with the gas temperature in the following expression:

$$\Phi = \frac{(X^{in}_{SO_2} k_{p,SO_2} + X^{in}_{O_2} k_{p,O_2} + X^{in}_{SO_3} k_{p,SO_3} + X^{in}_{re} k_{p,N_2})(T - T^{in})}{\left[\left(k_{p,SO_2} + \frac{1}{2} k_{p,O_2} - k_{p,SO_3}\right) T + \left(b_{p,SO_2} + \frac{1}{2} b_{p,O_2} - b_{p,SO_3}\right)\right] X^{in}_{SO_2}} \tag{2.21}$$

From Equation (2.21), the conversion ratio is a nonlinear function of temperature. Evolvement of conversion ratio with temperature is termed as heat-up path. Simulating Equation (2.21) leads to a heat-up path as in Figure 2.2. It displays how the $SO_2$ conversion ratio $\Phi$ varies with temperature under a given feed condition. It is observed that the relation between the conversion ratio $\Phi$ and temperature $T$ appears to be a straight line although they are related in a nonlinear form according to Equation (2.21).

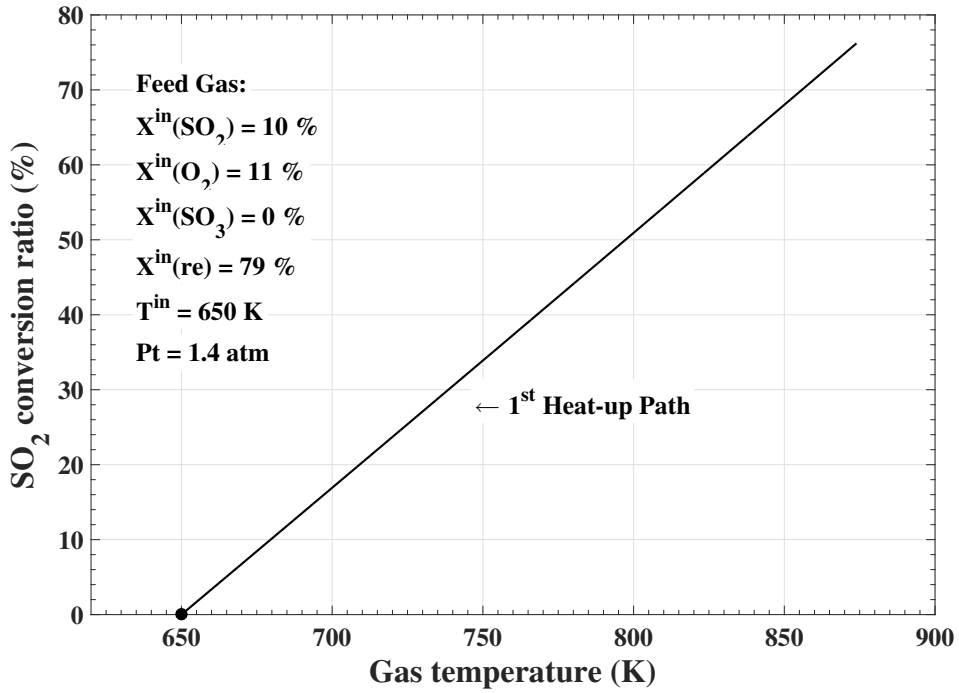


Figure 2.2: First-bed heat-up path under a given feed condition

The approximate linearity can be obtained by approximating (2.21). Defining two molar specific heat coefficients as:

$$k_p^{in} = X_{SO_2}^{in} k_{SO_2} + X_{O_2}^{in} k_{O_2} + X_{SO_3}^{in} k_{SO_3} + X_{re}^{in} k_{N_2},$$
$$k_p = X_{SO_2} k_{SO_2} + X_{O_2} k_{O_2} + X_{SO_3} k_{SO_3} + X_{re} k_{N_2},$$

under the normal operating condition, it holds that:

$$\left| \left( k_{p,SO_2} + \frac{1}{2} k_{p,O_2} - k_{p,SO_3} \right) T \right| << \left| b_{p,SO_2} + \frac{1}{2} b_{p,O_2} - b_{p,SO_3} \right|$$

and

$$b_{p,SO_2} + \frac{1}{2} b_{p,O_2} - b_{p,SO_3} \approx -\Delta H \tag{2.22}$$

where $-\Delta H$ indicates the standard reaction enthalpy in reaction (1.2). Equation (2.21) can then be approximated as:

$$\Phi \approx \frac{k_p^{in}}{(-\Delta H) X_{SO_2}^{in}} (T - T^{in}) \tag{2.23}$$

Relation between the conversion ratio and temperature is, therefore, approximately linear. A similar linear expression to Equation (2.23) is mentioned in (Mann, 1986). Equation (2.23) indicates that the slope of the heat-up path in Figure 2.2 changes with different feed composition while the feed temperature determines the beginning intercept of the heat-up path. $k_p^{in}$ represents the molar heat capacity of the inlet feed gas. For the offgas generated under regular operations, the value of $k_p$ barely varies. Therefore, the slope of heat-up path is mainly controlled by the inlet $SO_2$ concentration. Under the assumptions that $X_{O2}^{in}/X_{SO_2}^{in} = 1.1$ and $X_{SO_3}^{in} = 0$, Figure 2.3 simulates the heat-up path under two different inlet $SO_2$ concentrations. The path with a 10% inlet $SO_2$ has a steeper increase than the one with 11%. Under the same feed gas temperature, the simulation results in Figure 2.3 suggest that at a certain steady-state gas temperature, e.g. 800K, a higher steady-state conversion ratio can be achieved with a lower inlet $SO_2$ concentration. However, more temperature increment is observed for strong $SO_2$ inlet

as per percentage conversion occurs due to more amount of $SO_2$ is converted.

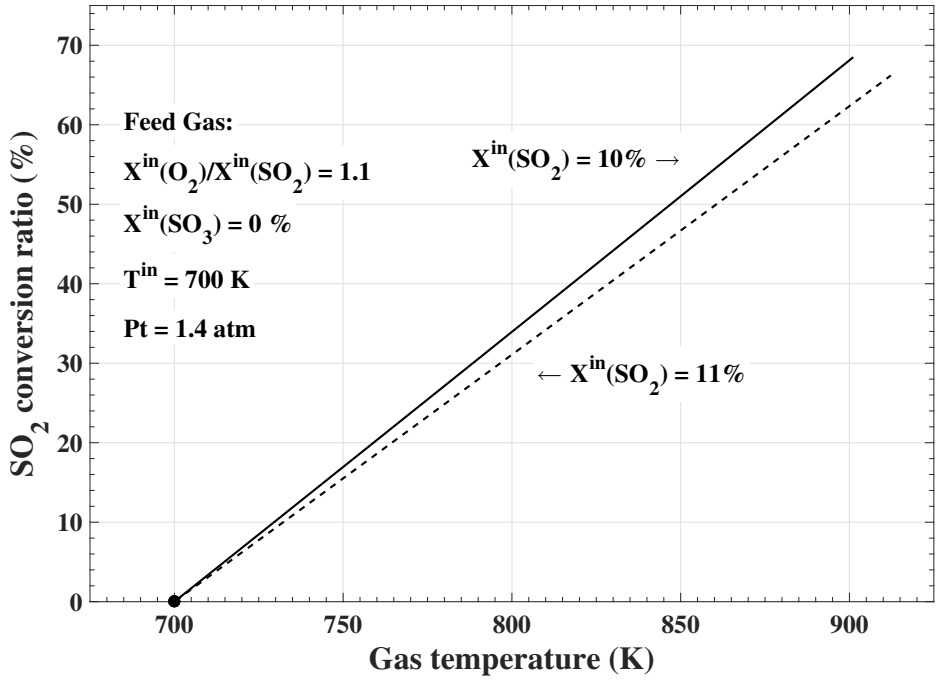


Figure 2.3: First-bed heat-up path under different inlet $SO_2$ concentrations

## 2.2 Equilibrium State

As the reaction (1.2) proceeds, the conversion ratio and temperature increase along the heat-up path in Figure 2.2. With more $SO_2$ is converted to $SO_3$, the forward reaction rate decreases and the reverse reaction rate increases. When the net reaction rate becomes zero, the reaction reaches equilibrium. At equilibrium, the conversion ratio is related to temperature by the following form (Davenport and King, 2006):

$$T^E = \frac{-B_E}{A_E + R \cdot \ln\left[\dfrac{X^{in}_{SO_3} + X^{in}_{SO_2}\Phi^E}{(1-\Phi^E)\,X^{in}_{SO_2}} \cdot \left(\dfrac{1 - 0.5X^{in}_{SO_2}\Phi^E}{X^{in}_{O_2} - 0.5X^{in}_{SO_2}\Phi^E}\right)^{\frac{1}{2}} \cdot P_t^{-\frac{1}{2}}\right]}. \tag{2.24}$$

where $P_t$ indicates the total pressure and $R$ is the gas constant. $A_E$ and $B_E$ are empirical constants and their values are given:

$$A_E = 0.09357 \qquad \text{[MJ/(kmol} \cdot \text{K)]},$$

$$B_E = -98.41 \qquad \text{[MJ/kmol]},$$

$$R = 0.008314 \qquad \text{[kJ/(mol} \cdot \text{K)]}.$$

From (2.24), the equilibrium conversion ratio is a function of equilibrium temperature, feed concentrations and the total pressure. With a given feed concentration and total pressure, conversion of $SO_2$ increases along the heat-up path and converges to the equilibrium curve with time but can never go beyond the equilibrium point, as in Figure 2.4. This equilibrium state at the interception point indicates the theoretical maximum conversion of $SO_2$ under the given conditions.

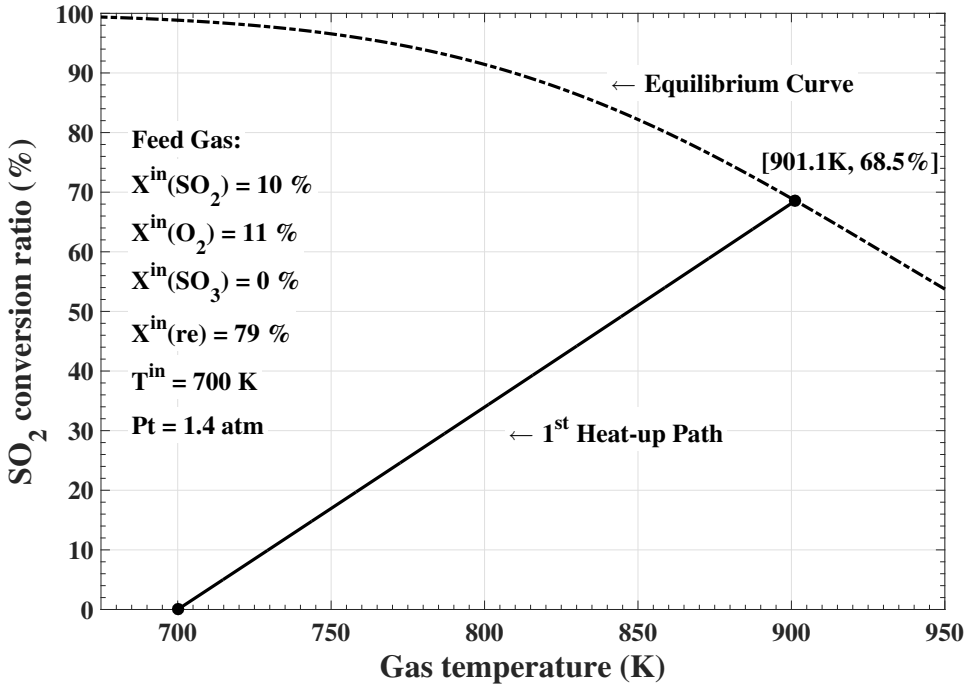


Figure 2.4: Equilibrium curve combining the first-bed heat-up path

## 2.3 Simulation

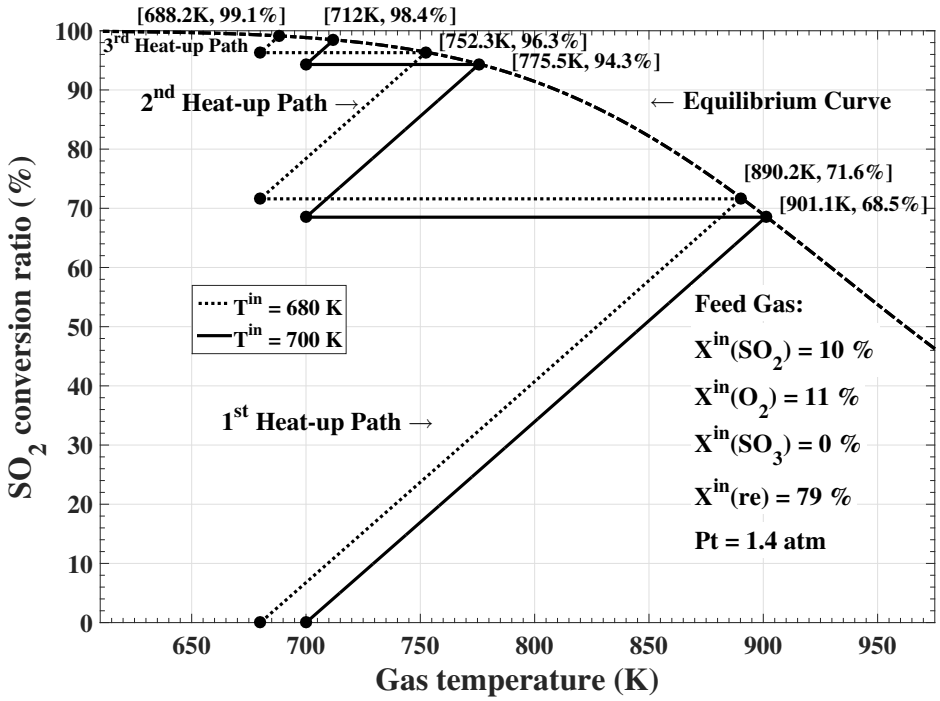


Figure 2.5: Conversion-temperature diagram for three catalyst beds under different inlet temperatures

The heat-up paths with two different inlet temperature is simulated, as shown in Figure 2.5. For simplicity, inlet temperature of all converter stages is set to be equal. Simulation results verify that the majority of conversion (over 50%) occurs in the first bed. $SO_2$ conversion ratio is becoming less when the off-gas passes more stages as a results of the reducing amount of $SO_2$ in the gas. Under the given operating conditions displayed in the figure, the total equilibrium conversion of $SO_2$ could be above 98% after the gas has been oxidized in three beds. However, it is impossible to reach the equilibrium point in real acid plant operations, because the equilibrium of each bed is difficult to obtain. As the process proceeds along the heat-up paths, $SO_3$ is generated and impedes the oxidation of $SO_2$ by the reverse reaction in (1.2). The effect of $SO_3$ becomes more and more significant when the process gets close to the equilibrium, which makes it impossible to reach the equilibrium in reality. The theoretical conversion in Figure

2.5 provides the theoretical maximum conversion of the converter but cannot be obtained in industrial operations. From Figure 2.5, it is noticed that a lower initial temperature is in favor of a higher equilibrium conversion ratio and a lower equilibrium temperature. This equilibrium conversion advantage gets less apparent after the gas passes more beds. Lower inlet temperature is preferred for $SO_2$ conversion, but the lower limit of the inlet gas temperature is always determined by the catalyst ignition temperature, for example, $\sim$635K for the typical $V_2O_5$-$K_2SO_4$ type of catalyst. In order to decrease the lower limit of inlet temperature, a new Cs-promoted type of catalyst is found helpful by replacing the catalyst component $K_2SO_4$ with cesium sulfate ($Cs_2SO_4$) (Schlesinger et al., 2011).

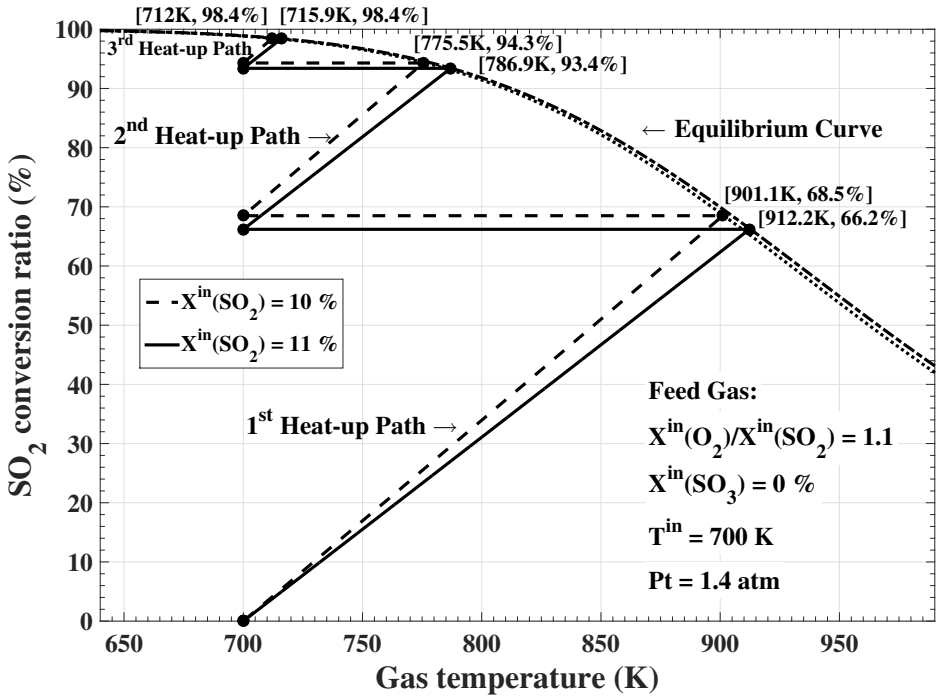


Figure 2.6: Conversion-temperature diagram for three catalyst beds under different inlet $SO_2$ concentrations

The effect of inlet $SO_2$ concentration is investigated in Figure 2.6 for the three-bed heat-up path. It is noticed that the inlet concentration affects the slope of the heat-up path. Higher inlet concentration leads to smaller slope in the heat-up path. The effect of inlet concentration is more noticeable for the first two beds. From Figure 2.6, for the first two beds, a lower initial inlet $SO_2$

concentration results in a higher equilibrium conversion but a lower equilibrium temperature. For the third bed, the effect of inlet concentration on $SO_2$ conversion becomes negligible. Even though lower inlet $SO_2$ concentration has a larger equilibrium conversion, an adequate $SO_2$ concentration is required in the industrial operation in order to maintain an initial high reaction rate.

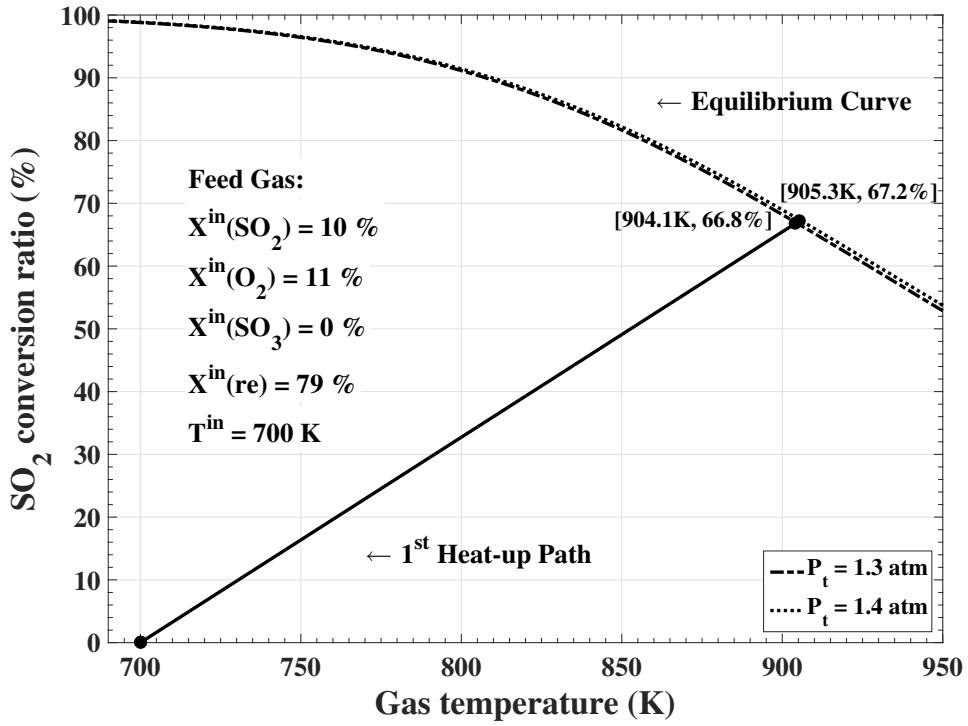


Figure 2.7: Conversion-temperature diagram for the first bed under different gas pressures

Pressure could have important effect on gas-phase reaction (1.2). Under different gas pressures, conversion-temperature diagrams for the first bed are shown in Figure 2.7. According to heat-up path expression (2.21), pressure doesn't affect the steady-state heat-up path. As shown in Figure 2.7, theoretical maximum equilibrium conversion ratio increases with gas pressure. However, for a 0.1 atm increment in pressure, only 0.4% maximum equilibrium conversion changes is observed. Comparing to the effects of inlet temperature and $SO_2$ concentration, effect of gas pressure under normal operations is negligible.

## 2.4 Summary

In this chapter, a steady-state model of the catalytic $SO_2$ converter is derived by applying steady-state mass and energy balances. $SO_2$ conversion ratio is defined and introduced. $SO_2$ conversion ratio defines the percentage of oxidized $SO_2$ over the feed $SO_2$, and can serve as a key performance indicator for the given converter. Based on steady-state model, the relation between conversion ratio and gas temperature is obtained. The graphic representation of the steady-state relation, termed as heat-up path, describes how gas temperature affects the $SO_2$ conversion and provides an important base for dynamic modelling in the following chapters.

The heat-up path indicates that the conversion ratio increases with gas temperature along the approximately linear path. With $SO_2$ conversion ratio building up, more $SO_2$ is converted to $SO_3$. Once the net reaction rate of reaction (1.2) gets zero, equilibrium of the reaction is obtained and $SO_2$ conversion stops. Interception of heat-up path and the equilibrium curve shows the equilibrium state under given feed conditions. This equilibrium state indicates the potential maximum $SO_2$ conversion that a converter can achieve. As the growing production of $SO_3$ impedes the consumption $SO_2$, conversion slows down when the reaction approaches equilibrium.

Simulations are performed to investigate the effect of inlet $SO_2$ concentration and gas temperature on the multi-stage heat-up path and equilibrium $SO_2$ conversion. It shows that the inlet temperature affects the intercept of the heat-up path and the feed $SO_2$ concentration affects the slope of the path. From the simulation results, a lower inlet temperature and $SO_2$ concentration are in favour to achieve a higher equilibrium conversion. However, the inlet gas temperature is always limited by the catalyst activation temperature. To allow reaction (1.2) to start, the inlet gas temperature has to be over the catalyst activation temperature. As for inlet $SO_2$, a low $SO_2$ concentration leads to slow reaction and is not desirable for efficient $SO_2$ conversion in the acid plant.

# Chapter 3

# Mathematical Soft Sensors

Soft sensors are developed to provide real-time estimates of quality variables or key performance indicators based on easily measured information using proper models. These techniques have been widely studied and implemented in process industries (Fortuna et al., 2007), as alternatives to expensive monitoring instruments (Dong et al., 1995) or solutions to obtaining unmeasured critical variables (Wu and Luo, 2009). Various soft sensors have been developed based on specific needs of different industrial processes, as for example, gas emission monitor for an industrial heater (Dong et al., 1995), hydrogen sulfide concentration estimate for a sulfur recovery unit (Di Bella et al., 2007), coal and gas outburst prediction (Yan et al., 2009), black liquor concentration monitor and control in a paper and pulp industry (Amazouz and Platon, 2011). In a $SO_2$ converter, important variables include temperature and $SO_2$ concentration. In industrial operations, temperature of a converter is extensively measured at various locations of all converter stages, but concentration of $SO_2$ is barely measured, or sometimes only at the feed point. Conversion ratio of $SO_2$, as a key performance indicator, can be conveniently calculated if concentration of $SO_2$ is known. Development of a soft sensor for conversion ratio and/or concentration of $SO_2$ is therefore of great interest in monitoring the acid plants in smelters.

Development of a soft sensor for converters requires a proper model that can be used to

estimate the conversion ratio and concentration of $SO_2$. Although modelling of the converters have been investigated by many researchers (Snyder and Subramaniam, 1993; Hong et al., 1997; Xiao and Yuan, 1996; Wu et al., 1996), most of these models were not developed for the converters in industrial smelters. Even for dynamic models developed for the converters in industrial smelters, they may not be able to serve as soft sensors due to model-plant mismatch, a large number of unknown parameters as well as difficulty in parameter estimations fit with the industrial operations. A steady-state model can be reliably built with known parameters but it cannot be used as real-time soft sensor due to dynamic characteristics of the industrial process. In this chapter, mathematical soft sensors are developed based on modification of the steady-state models derived in Chapter 2 and real-time industrial data analysis. The obtained soft sensors are simple to implement and can provide real-time estimates for the conversion ratio and concentration of $SO_2$ in a $SO_2$ converter.

## 3.1 Soft Sensors Development and Application

### 3.1.1 Steady-State Relations

In Chapter 2, based on the steady-state mass and energy balances, heat-up path of a catalytic $SO_2$ converter is proposed and the $SO_2$ conversion ratio is obtained as:

$$\Phi = \frac{(X^{in}_{SO_2}k_{p,SO_2} + X^{in}_{O_2}k_{p,O_2} + X^{in}_{SO_3}k_{p,SO_3} + X^{in}_{re}k_{p,N_2})(T - T^{in})}{\left[\left(k_{p,SO_2} + \frac{1}{2}k_{p,O_2} - k_{p,SO_3}\right)T + \left(b_{SO_2} + \frac{1}{2}b_{O_2} - b_{SO_3}\right)\right]X^{in}_{SO_2}} \tag{3.1}$$

From Equation (3.1), it is noticed that $SO_2$ conversion $\Phi$ can be calculated and obtained when feed gas concentrations, inlet and outlet temperatures are available. Besides, as described in Equation (2.13), that is,

$$X_{SO_2} = \frac{(1-\Phi)X^{in}_{SO_2}}{1 - \frac{1}{2}\Phi X^{in}_{SO_2}}, \tag{3.2}$$

the outlet $SO_2$ concentration is derived when $\Phi$ is achieved from Equation (3.1) and collected measurements.

### 3.1.2 Dynamic Data Analysis

In obtaining a real-time estimate of $SO_2$ conversion ratio, it is necessary to explore the variable dynamics. One-month industrial operating data with sampling time of 1 min were collected and examined for variable dynamics. For a multi-stage converter, most conversion occurs in the first stage and it is more important to closely monitor the performance of the first stage than that of other stages. The analysis in this section is thus focused on the first stage, although it can be extended to other stages. There are four main variables involved in the system, as in Equation (3.1), with $X_{SO_2}^{in}$ and $T^{in}$ being input variables, and $T$ and $\Phi$ being output variables. Measured variables include $X_{SO_2}^{in}$, $T^{in}$ and $T$. A soft sensor is to estimate $\Phi$ based on measurement of $X_{SO_2}^{in}$, $T^{in}$ and $T$, as illustrated in Figure 3.1.

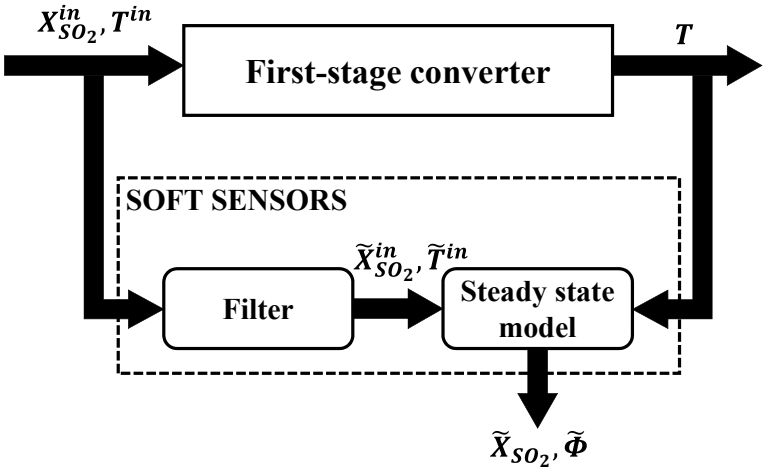


Figure 3.1: Structure of the $X_{SO_2}$ and $\Phi$ soft sensors for a $SO_2$ converter stage.

As inlet temperature $T^{in}$ is controlled using heat exchangers to ensure a desired value,

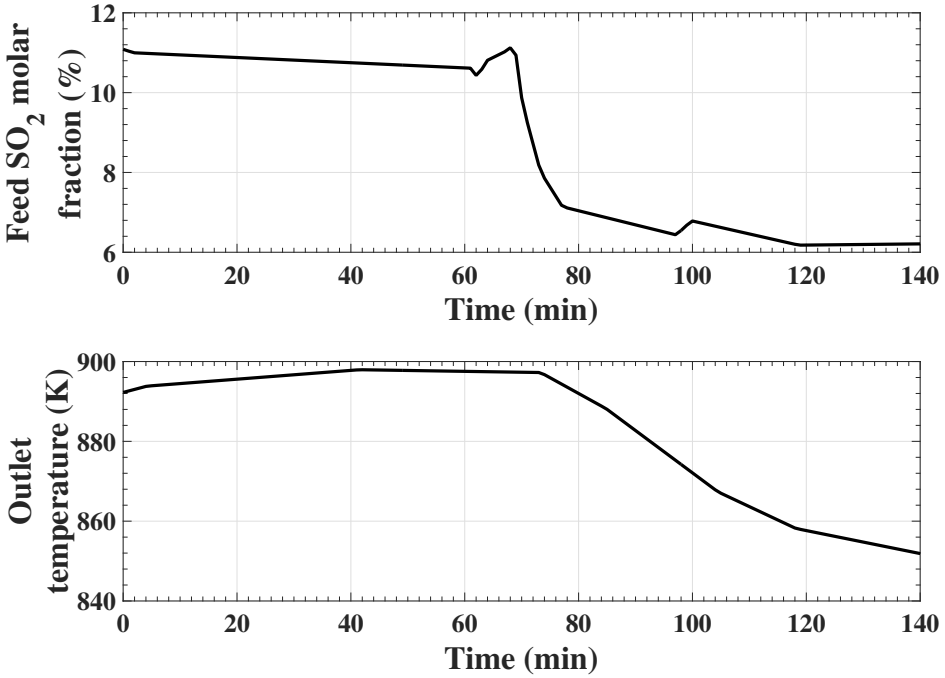


Figure 3.2: Dynamic evolvement of outlet temperature in response to a feed concentration decrease.

major disturbance for a converter stage is from $X_{SO_2}^{in}$. By examining a sequence of industrial measurement data with a major decrease of $X_{SO_2}^{in}$, dynamics of the outlet temperature $T$ in response to the decrease in $X_{SO_2}^{in}$ is displayed in Figure 3.2. The major decrease of $X_{SO_2}^{in}$ can be approximately taken as a step change and the response of output variable $T$ is then viewed as a step response. It is observed that the outlet temperature $T$ decreases as the feed fraction $X_{SO_2}^{in}$ decreases but it responds in a sluggish manner. For generality, another sequence of industrial data with both increase and decrease of $X_{SO_2}^{in}$ are examined in Figure 3.3. It shows that outlet temperature $T$ changes with feed concentration $X_{SO_2}^{in}$ with slow dynamics. Figure 3.2 and 3.3 show that the major variables $X_{SO_2}^{in}$ and $T$ in a converter stage do not vary simultaneously and the output $T$ varies with the input $X_{SO_2}^{in}$ in slow dynamics. The dynamic response of $T$ can be approximately taken as a first-order response. Due to significant difference in dynamic variation rate of $X_{SO_2}^{in}$ and $T$, it is not feasible to directly estimate the conversion ratio based

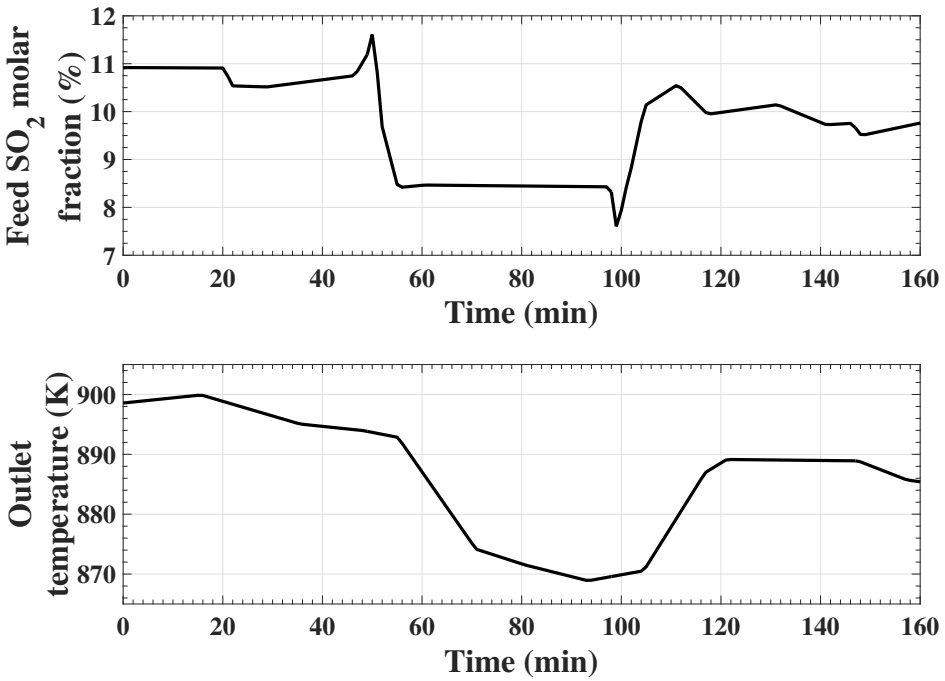


Figure 3.3: Dynamic evolvement of outlet temperature in response to feed concentration changes.

on the measured real-time data using the steady state expression in Equation (3.1) and some modifications are necessary.

Dynamic relation between $X_{SO_2}^{in}$ and $T$ can be further investigated by examining the correlation between two variables with different time delays. Figure 3.4 shows that outlet temperature $T$ is highly correlated with feed concentration $X_{SO_2}^{in}$ and the largest correlation between the two variables occurs at the delay time of 9 min. This confirms that variations of $T$ and $X_{SO_2}^{in}$ are unsynchronized, and $T$ responds to changes of $X_{SO_2}^{in}$ slowly.

The slow dynamics of outlet temperature is mainly due to large heat capacity of the catalyst bed in the converter. In a converter stage, the residence time of gas is short, typically 1-2 sec. When there is a decrease in $X_{SO_2}^{in}$, less reaction occurs and reduced reaction heat is generated. But the temperature of catalyst bed still remains at high temperature and starts to decrease slowly because of the reduced reaction heat. Due to heat transfer between the catalyst bed and

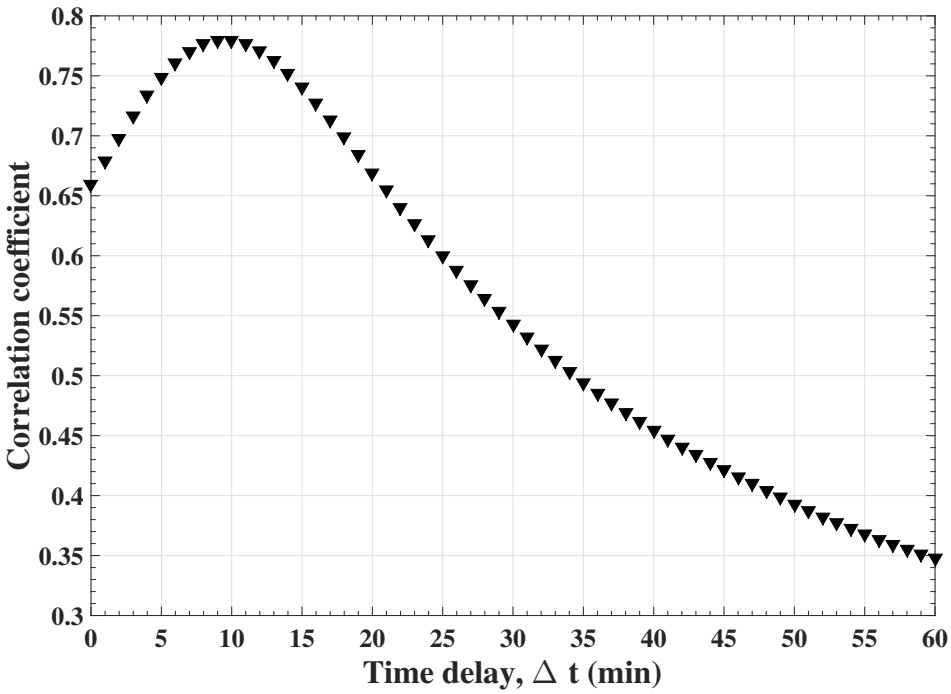


Figure 3.4: Correlation coefficient between $X^{in}(t)$ and $T(t + \Delta t)$ with different time shifts.

gas, gas temperature follows the temperature of catalyst bed and declines slowly.

### 3.1.3 Soft Sensors

The steady-state model described in Equation (3.1) can serve to estimate the conversion ratio of $SO_2$ if the involved variables are at steady state. From measured data examination described in the last subsection, available industrial measured variables are far from being at steady state, the input variable $X^{in}_{SO_2}$ and output variable $T$ are highly unsynchronized and the output response takes the form of a first-order format. In order to estimate the conversion ratio $\Phi$, we propose to synchronize the feed variables with the outlet variables using a filter. The conversion ratio can then be approximately estimated based on the synchronized variables. As shown in Figure 3.1, the proposed soft sensor consists of a filter and a modified steady-state model.

Different filters are available for this purpose. Data analysis in the last subsection indicates

that the response of output variable $T$ to step changes of the input can be approximated as a first-order response. It is thus reasonable to use a first-order exponential filter. This filter also has the advantage of simplicity for industrial implementation. By applying the first order exponential filter to the feed variables $X^{in}_{SO_2}$, the filtered feed molar fraction takes the form:

$$\tilde{X}^{in}_{SO_2}(j) = (1-\alpha)X^{in}_{SO_2}(j) + \alpha\tilde{X}^{in}_{SO_2}(j-1), \tag{3.3}$$

where $\tilde{X}^{in}_{SO_2}$ indicates the filtered feed molar fraction and $X^{in}_{SO_2}$ is the measured value, $\alpha$ is the filter parameter and $j$ is the sampling time. The filter parameter $\alpha$ is chosen such that the filtered signal $X^{in}_{SO_2}$ is synchronized with the outlet temperature. In this work, $\alpha$ is determined such that the correlation between the filtered signal $\tilde{X}^{in}_{SO_2}$ and $T$ reaches maximum at zero delay time, as shown in Figure 3.5. It is obtained that the filtered signal $\tilde{X}^{in}_{SO_2}$ and $T$ are synchronized when $\alpha = 0.95$. The obtained $\alpha$ value represents the dynamic information on the outlet temperature $T$ in response to the feed molar fraction $X^{in}_{SO_2}$.

After obtaining the filter parameter based on correlation of the two major variables, the filtered values for the feed variables can be calculated. Corresponding to the industrial data sequences shown in Figure 3.2 and 3.3, evolvements of the filtered signal $\tilde{X}^{in}_{SO_2}$ in comparison with measured outlet temperature $T$ are displayed in Figure 3.6 and 3.7, respectively. It can be seen that the filtered feed molar fraction varies in the similar rate as the outlet temperature and they can be considered to be dynamically synchronized. Since feed temperature $T^{in}$ is controlled to be at specified temperature, filtering of feed temperature $T^{in}$ is not as crucial as that $X^{in}_{SO_2}$. However, the collected inlet temperature measurement is relatively noisy and the signal needs to be smoothed out by a filter. In this work, the same first-order exponential filter in Equation (3.3) is also applied to the feed temperature $T^{in}$ to smooth out the noise, as shown in Figure 3.8.

Modification of Equation (3.1) by replacing $X^{in}_{SO_2}$ and $T^{in}$ with the filtered signals $\tilde{X}^{in}_{SO_2}$

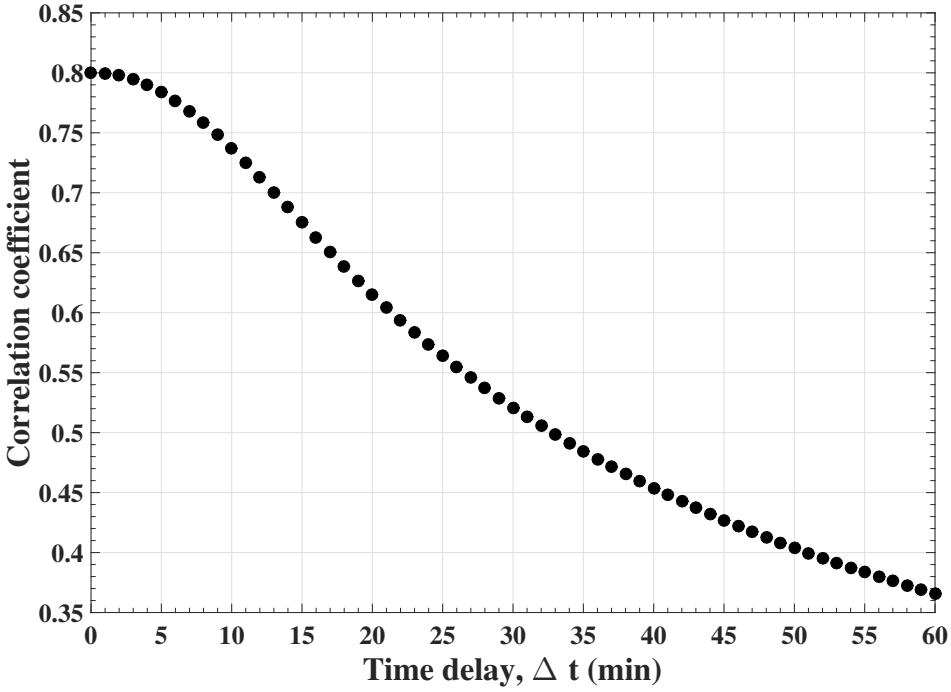


Figure 3.5: Correlation coefficient between the filtered $X^{in}(t)$ and $T(t + \Delta t)$ with different time shifts.

and $\tilde{T}^{in}$ leads to:

$$\tilde{\Phi} = \frac{(\tilde{X}^{in}_{SO_2} k_{SO_2} + X^{in}_{O_2} k_{O_2} + X^{in}_{SO_3} k_{SO_3} + X^{in}_{re} k_{N_2})(T - \tilde{T}^{in})}{[(k_{SO_2} + \frac{1}{2} k_{O_2} - k_{SO_3})T + (b_{SO_2} + \frac{1}{2} b_{O_2} - b_{SO_3})]\tilde{X}^{in}_{SO_2}}, \tag{3.4}$$

where the estimated $\Phi$ is denoted as $\tilde{\Phi}$. From Equation (3.4), the conversion ratio of $SO_2$ can be estimated from real-time measurement. With $\tilde{\Phi}$ obtained, outlet $SO_2$ molar fraction can also be derived from Equation (3.2) as:

$$\tilde{X}_{SO_2} = \frac{(1 - \tilde{\Phi})\tilde{X}^{in}_{SO_2}}{1 - \frac{1}{2}\tilde{\Phi}\tilde{X}^{in}_{SO_2}}. \tag{3.5}$$

With the filtered feed variables and measured temperature, conversion ratio and molar fraction of $SO_2$ out of the converter stage can be estimated using Equation (3.4) and (3.5). For the operations represented by Figure 3.2 when $SO_2$ feed molar fraction decreases, the estimated

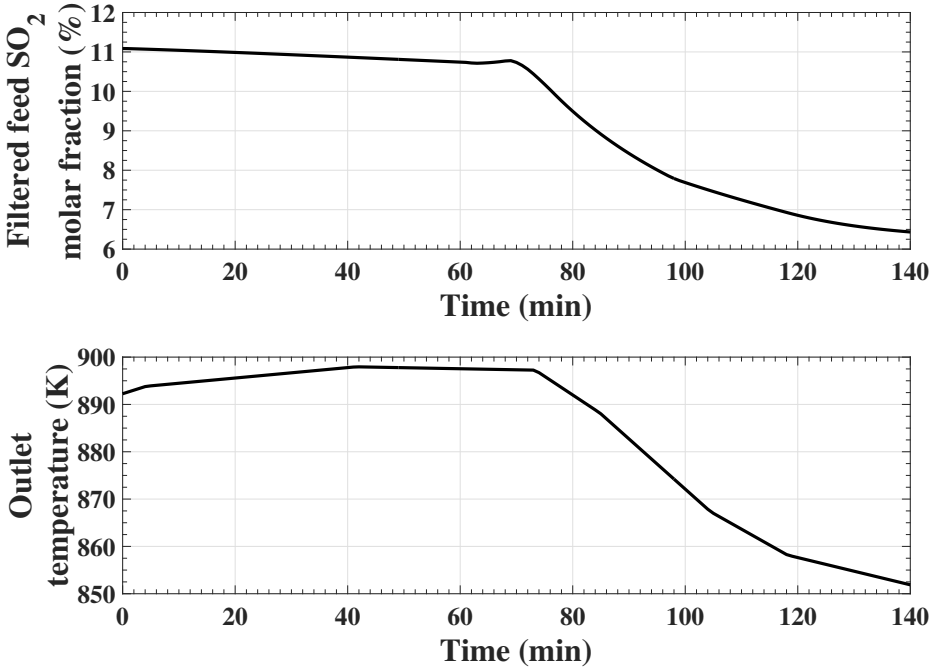


Figure 3.6: Comparison of dynamics of the filtered feed molar fraction and measured outlet temperature when there is a decrease in feed molar fraction.

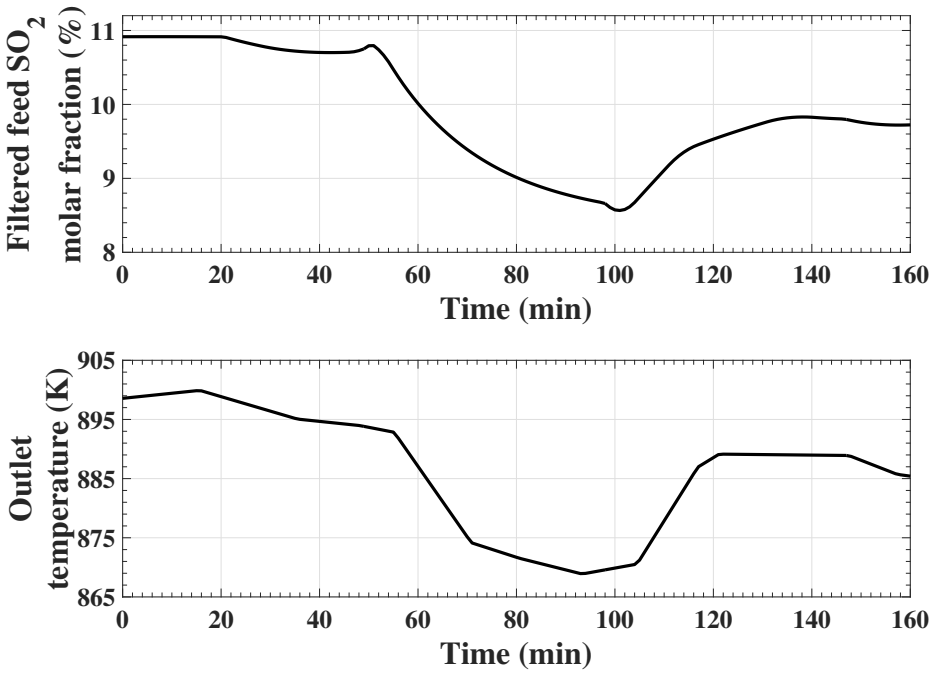


Figure 3.7: Comparison of dynamics of the filtered feed molar fraction and measured outlet temperature when there are changes in feed molar fraction.

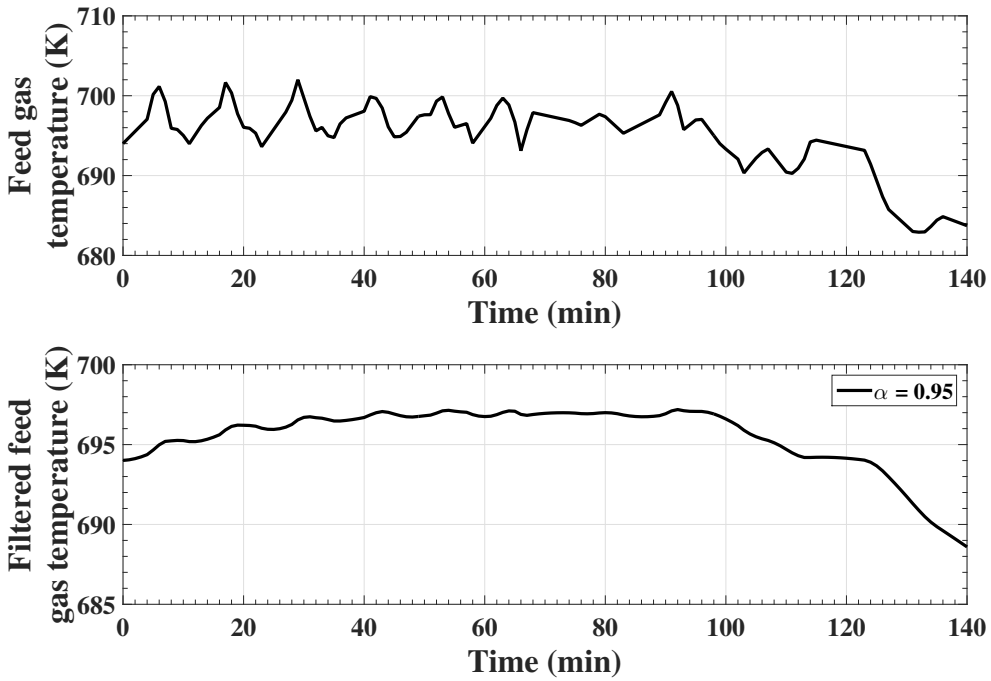


Figure 3.8: Feed temperature and filtered feed temperature corresponding to operation in Figure 3.2.

conversion ratio of $SO_2$ is shown in Figure 3.9. Maximum equilibrium limit is the maximum value of equilibrium conversion ratio calculated using Equation (2.24) among the related operating data points. It is observed that conversion ratio of $SO_2$ increases when $SO_2$ feed molar fraction decreases. The estimated conversion ratio does not violate the maximum limit, set by the equilibrium value at current operating conditions. Increase of the conversion ratio results from increased slope of heat-up path at lowered $SO_2$ inlet concentration, as illustrated in Figure 2.6. The fact that the corresponding equilibrium value of conversion ratio increases also contribute to increase of $SO_2$ conversion ratio. From Figure 3.9, the estimated outlet $SO_2$ concentration decreases significantly due to the decrease in $SO_2$ feed concentration as well as the increased conversion ratio.

Corresponding to industrial data in Figure 3.3, the estimated $SO_2$ conversion ratio and molar fraction are shown in Figure 3.10. The conversion ratio increases as $SO_2$ feed molar fraction

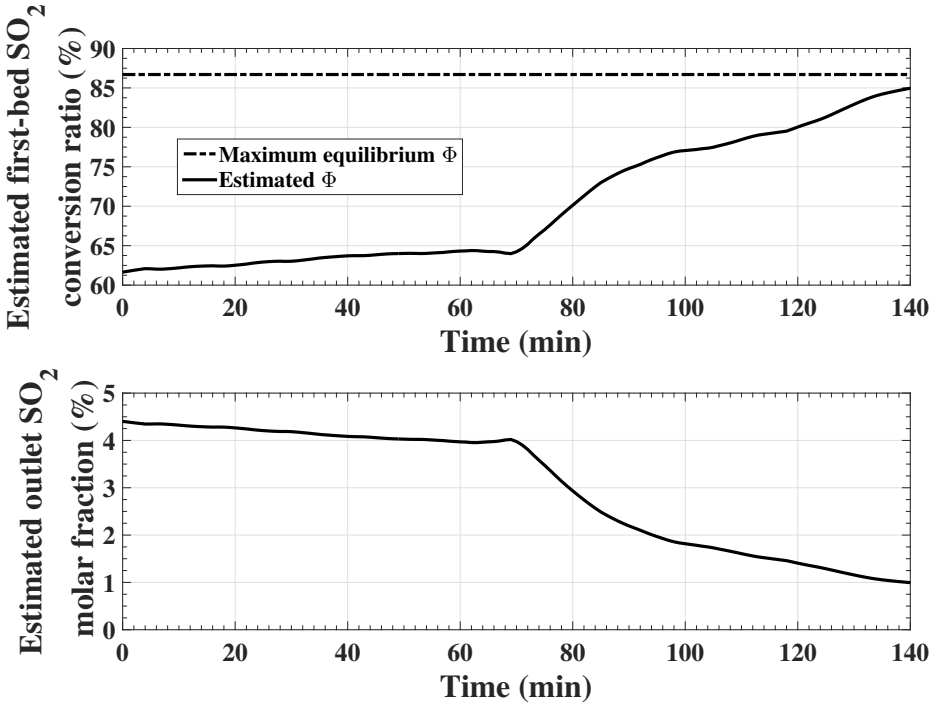


Figure 3.9: Estimated conversion ratio and molar fraction of $SO_2$ for a step decrease in $SO_2$ feed molar fraction as in Figure 3.2.

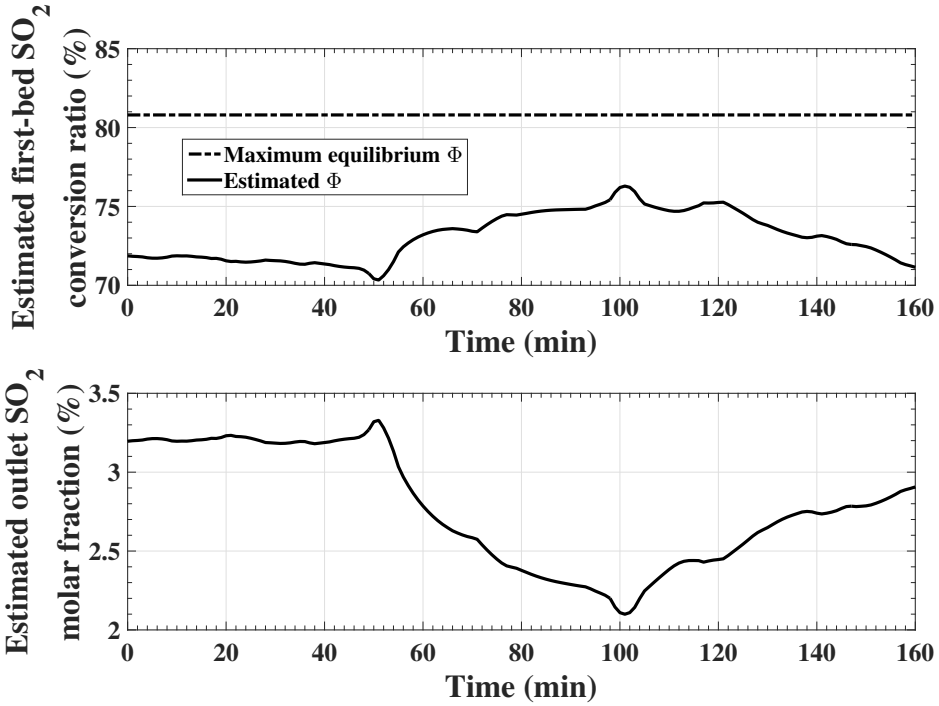


Figure 3.10: Estimated conversion ratio and molar fraction of $SO_2$ for step changes in $SO_2$ feed molar fraction as in Figure 3.3.

decreases while it decreases as $SO_2$ feed increases, as suggested by the first-bed heat-up path in Figure 2.6. The estimated $SO_2$ outlet molar fraction varies in the same direction as $SO_2$ feed molar fraction and it increases as $SO_2$ feed molar fraction increases, as discussed before for Figure 3.9.

The proposed soft sensor for $SO_2$ conversion ratio is compared with the estimate based solely on the steady-state model Equation (3.1). Figure 3.11 displays a comparison of the conversion ratio for the data with a step decrease of $SO_2$ feed molar fraction as in Figure 3.2. It is clear that the estimated conversion ratio based solely on the steady-state model violates the maximum equilibrium value when a sharp decrease in $SO_2$ feed molar fraction occurs. The proposed soft sensor generates an acceptable real-time estimate for $SO_2$ conversion ratio. Most available soft sensor approaches would not be applicable to this process because they usually require to derive model parameters from an available database with measured conversion ratio. Our proposed soft sensor provides a useful estimate on the important variable without requiring additional industrial measurement.

Based on the reliable steady-state model, the estimates of conversion ratio $\Phi$ and molar fraction $X_{SO_2}$ are expected to converge to their true steady-state value. Due to very short residence time of gas in the converter stage, it is expected that conversion ratio $\Phi$ and molar fraction $X_{SO_2}$ have a quick dynamic response to any changes in feed conditions. As the estimates of these variables heavily rely on temperature measurement, slow dynamics of temperature measurement limits the dynamics of the estimated variables and this may make them slower than that of the true values. Despite the slow dynamics, the inferred information for conversion ratio and outlet molar fraction is expected to track the true variation of these variables in reasonable closeness. They can provide useful monitoring on converter performance.

The proposed soft sensors can be used to estimate conversion ratio and molar fraction of $SO_2$ out of a converter stage. The estimated variables have not been validated with industrial

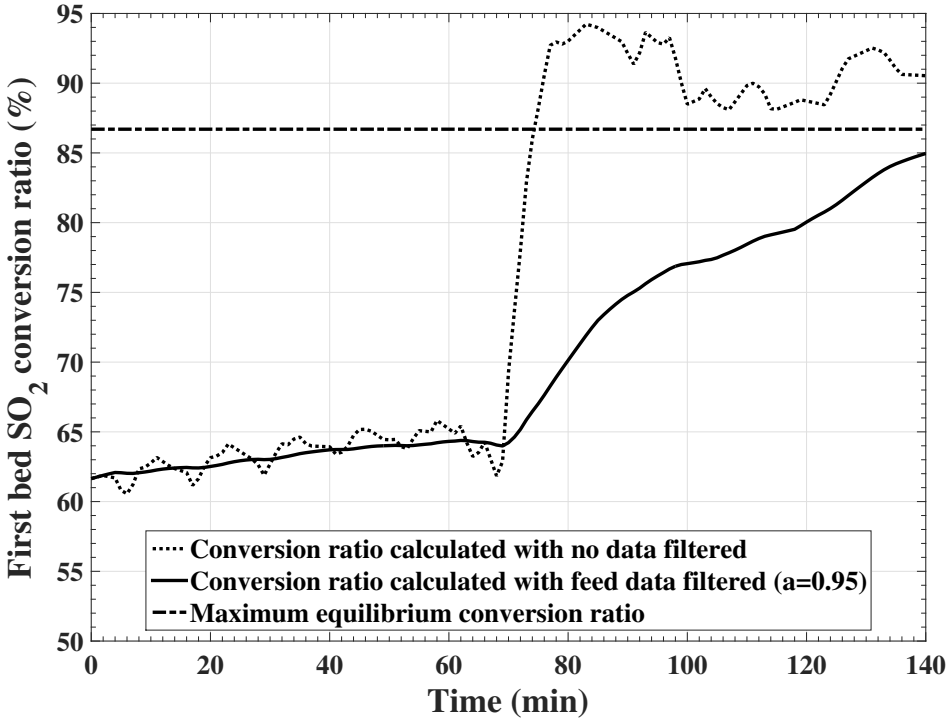


Figure 3.11: Comparison of $SO_2$ conversion ratio estimates for a step decrease in $SO_2$ feed molar fraction as in Figure 3.2.

data due to unavailability of related measurement. The soft sensors, however, are based on the reliable steady-state model with known parameters and real industrial operating data. It can be, therefore, expected to generate acceptable validity for the inferred information.

## 3.2 Summary

A catalytic converter oxidizing $SO_2$ into $SO_3$ is an essential component in a sulfuric acid plant. The outlet $SO_2$ concentration and $SO_2$ conversion ratio are important variables describing the performance of a $SO_2$ converter. In this chapter, soft sensors are proposed to estimate the conversion ratio and outlet molar fraction of $SO_2$ which are not usually measured in many smelters. Examination of industrial operating data indicates that outlet temperature of a converter stage varies dynamically with $SO_2$ feed molar fraction in a sluggish manner. The

two variables are highly correlated and the correlation coefficient reaches maximum at a delay time of 9 minutes. Application of a first-order exponential filter to $SO_2$ feed molar fraction leads to the filtered signal that is synchronized with the outlet temperature. A reliable steady-state model is developed for conversion ratio as a function of measured variables including temperature and feed molar fraction. By replacing the original feed variables with the filtered variables, the model generates useful estimation of the unmeasured variables.

# Chapter 4

# Dynamic Modelling of Sulfur Dioxide Converter Using ODE

This chapter aims to develop a dynamic model for the catalytic $SO_2$ converter in the acid plant of an industrial smelter such that the model can well reflect the industrial operation but be simple enough for the convenience of industrial applications. For the $SO_2$ converters in the smelters, conversion ratio of $SO_2$ is a very important variable commonly used as a performance indicator. In this chapter, $SO_2$ conversion ratio is defined for the individual stage relative to the $SO_2$ inlet into each stage as well as that relative to the feed $SO_2$ into the first stage of the converter. Relation between the two types of the conversion ratio is formulated. For industrial uses, a dynamic model is developed in the forms of both continuous ordinary differential equations (ODE) and finite difference equations. The extent of $SO_2$ oxidation in each stage is expressed by the calculated equilibrium conversion ratio multiplied by a parameter. The parameter is estimated from the industrial operating data and thus the obtained model can be readily adapted to different industrial converters with various catalyst bed conditions. Simulation results show that the obtained model fits well with the industrial data. Based on the model, process dynamics are investigated for the converter in an industrial smelter.

## 4.1 $SO_2$ Conversion Ratio

The $SO_2$ catalytic converter performance indicator, $SO_2$ conversion ratio has been defined in Equation (2.6) and described in Chapter 2. In its definition, $X^{in}_{SO_2}$ can be inlet $SO_2$ molar fraction to each bed or to the first bed of the converter. Depending on $X^{in}_{SO_2}$ being used, two types of $SO_2$ conversion ratio can be calculated for each bed:

(1) the **individual bed $SO_2$ conversion ratio** relative to the feed $SO_2$ into each bed if $X^{in}_{SO_2}$ indicates the $SO_2$ inlet concentration into the corresponding bed;

(2) the **overall converter $SO_2$ conversion ratio** for each bed relative to the feed $SO_2$ into the overall converter if $X^{in}_{SO_2}$ indicates the $SO_2$ inlet concentration to the first bed of the converter.

Based on the definition of these two types of $SO_2$ conversion ratio, the overall converter conversion ratio $\Phi_{t,k}$ relative to the feed $SO_2$ into the overall converter for each bed is related to the individual bed conversion ratio $\Phi_k$ relative to the feed $SO_2$ into the corresponding bed by the following expression:

$$\Phi_{t,k} = 1 - \prod_{j=1}^{k} (1 - \Phi_j), \tag{4.1}$$

where $k = 1, 2, 3, 4$ representing the four converter stages. The overall converter $SO_2$ conversion ratio $\Phi_{t,k}$ is usually referred to in the available literature (Davenport and King, 2006) and discussed in Chapter 2. However, the individual bed $SO_2$ conversion ratio $\Phi_k$ will be used for modelling in this chapter.

Chapter 2 introduces the equilibrium state by combining the reaction equilibrium curve with converter heat-up path. For equilibrium $SO_2$ conversion ratio of each bed $\Phi^E_k$, it can be obtained by solving Equations (2.23) and Equations (2.24) when the inlet conditions of each bed are applied, that is:

$$\begin{cases} \Phi_k^E = \dfrac{(X_{SO_2,k}^{in} k_{p,SO_2} + X_{O_2,k}^{in} k_{p,O_2} + X_{SO_3,k}^{in} k_{p,SO_3} + X_{re,k}^{in} k_{p,N_2})}{(-\Delta H) X_{SO_2,k}^{in}} (T_k^E - T_k^{in}); & (4.2) \\ T_k^E = \dfrac{-B_E}{A_E + R \cdot \ln \left[ \dfrac{X_{SO_3,k}^{in} + X_{SO_2,k}^{in} \Phi_k^E}{(1-\Phi_k^E) X_{SO_2,k}^{in}} \cdot \left( \dfrac{1 - \frac{1}{2} X_{SO_2,k}^{in} \Phi_k^E}{X_{O_2,k}^{in} - \frac{1}{2} X_{SO_2,k}^{in} \Phi_k^E} \right)^{\frac{1}{2}} \cdot P_{t,k}^{-\frac{1}{2}} \right]}. & (4.3) \end{cases}$$

For the industrial continuous operation, the actual $SO_2$ conversion ratio at the outlet of each bed should be ideally close to but slightly smaller than the equilibrium conversion ratio. In this chapter, the equilibrium conversion ratio is calculated from the above equations using the feed gas measurement, and the actual $SO_2$ conversion ratio is expressed as:

$$\Phi = \lambda \Phi^E, \tag{4.4}$$

where $\lambda$ is a parameter less than one. The value of $\lambda$ indicates how close the $SO_2$ conversion is to the equilibrium in a converter stage.

## 4.2 Dynamic Model Development

### 4.2.1 Continuous Dynamic Model Development

For the converter stage illustrated in Figure 2.1, the system is a distributed parameter system (DPS) as variables in a converter stage vary in both time and space, i.e., along the catalyst bed. A mechanistic model for DPS would naturally take the form of partial differential equations (PDE). For most industrial applications, however, an ordinary differential equation (ODE) model might be preferred for simplicity. In this section, a dynamic model for the converter in an industrial smelter is developed such that the model can fit well with industrial operations

and be convenient for industrial applications. For this purpose, it is assumed that:

(1) the value of variables at the outlet of the converter stage is approximately equal to that within the converter stage;

(2) the converter is considered to be adiabatic;

(3) temperature of the catalyst beds closely follows that of the gas.

Under these assumptions, a dynamic model can be developed based on mass and energy balances:

$$\frac{\rho_g V_g}{M_g}\frac{dX_{SO_2}}{dt} = \frac{\rho_g Q^{in}}{M_g}\left(X^{in}_{SO_2} - X_{SO_2}\right) - (1 - \frac{1}{2}X_{SO_2})r, \tag{4.5}$$

$$\left(\rho_g c_{p,g} V_g + \rho_{cat} c_{p,cat} V_{cat}\right)\frac{dT}{dt} = \rho_g c_{p,g} Q^{in}\left(T^{in} - T\right) + (-\Delta H)r, \tag{4.6}$$

where $r$ [mol/min] indicates the consumption rate of $SO_2$.

For the overall gas molecular weight, $M_g$, it is related with the gas compositions and can be evaluated by applying the Gibbs-Dalton's law (Shao et al., 2013):

$$M_g = \sum_i \left(X_i M_i\right), \tag{4.7}$$

where $i$ represents the gas components in the gas stream ($SO_2$, $O_2$, $SO_3$ and $N_2$). When the gas stream is considered to be ideal gas mixture, the gas density $\rho_g$ can be derived by:

$$\rho_g = \frac{P_t M_g}{RT}, \tag{4.8}$$

where $P_t$ is the total gas pressure. As for the heat capacity $c_{p,g}$ of the gas stream, it can be obtained as described in Section 5.3.2.

The reaction kinetics for $SO_2$ oxidation has been extensively studied and the available expressions for the reaction rate are mostly from the lab test results (Froment and Bischoff, 1979; Kiss et al., 2010). For industrial systems, the reaction rate could be different due to

different combinations of catalysts and packing patterns. The available kinetic expressions may not fit well with industrial systems or contain too many parameters that are hard to be estimated from industrial operating data. In developing a model that can fit well with different industrial converters, the model in Equation (4.6) should be further modified so that the model can be applicable even if the reaction kinetics is not available.

Considering the fact that $\rho_g \ll \rho_{cat}$, the dynamics of $X_{SO_2}$ in Equation (4.5) are negligible in comparison with those of $T$ in Equation (4.6), that is, Equation (4.5) can be approximated as:

$$0 \approx \frac{\rho_g Q^{in}}{M_g}\left(X^{in}_{SO_2} - X_{SO_2}\right) - (1 - \frac{1}{2}X_{SO_2})r, \tag{4.9}$$

and

$$r = \frac{\rho_g Q^{in}}{M_g} \cdot \frac{X^{in}_{SO_2} - X_{SO_2}}{1 - \frac{1}{2}X_{SO_2}}. \tag{4.10}$$

Using Equation (2.17), expression of reaction rate $r$ in (4.10) can be rewritten as:

$$r = \frac{\rho_g Q^{in}}{M_g}\Phi X^{in}_{SO_2}. \tag{4.11}$$

With the Equation (4.11) and the fact that $\rho_g \ll \rho_{cat}$, the model in Equation (4.6) is thus further simplified:

$$\frac{\rho_{cat} c_{p,cat} V_{cat}}{\rho_g c_{p,g} Q^{in}} \frac{dT}{dt} = T^{in} - T + X^{in}_{SO_2}\Phi \frac{-\Delta H}{c_{p,g} M_g}. \tag{4.12}$$

Substituting (4.4) to (4.12), the model can also be represented as:

$$\frac{\rho_{cat} c_{p,cat} V_{cat}}{\rho_g c_{p,g} Q^{in}} \frac{dT}{dt} = T^{in} - T + \lambda X^{in}_{SO_2}\Phi^E \frac{-\Delta H}{c_{p,g} M_g}, \tag{4.13}$$

where the equilibrium conversion ratio $\Phi^E$ can be computed with the given feed conditions through Equations (4.2) and (4.3). This model in (4.13) describes how gas temperature out of a converter stage evolves under given feed conditions. The parameter $\lambda$ needs to be estimated

from the industrial operating data and other parameters can be obtained based on the process information.

### 4.2.2 Discrete-Time Model

For parameter estimation and industrial applications, a discrete-time model based on Equation (4.13) is required. Defining

$$V_{sp} = \frac{\rho_{cat} c_{p,cat} V_{cat}}{\rho_g c_{p,g}}, \tag{4.14}$$

Equation (4.13) can be rearranged as

$$\frac{dT}{dt} + \frac{Q^{in}}{V_{sp}} T = \frac{Q^{in}}{V_{sp}} \left( T^{in} + \lambda X^{in}_{SO_2} \Phi^E \frac{-\Delta H}{c_{p,g} M_g} \right). \tag{4.15}$$

If $\exp\left(\frac{Q^{in}}{V_{sp}} t\right)$ is multiplied to both sides of Equation (4.15), it becomes

$$\frac{d}{dt}\left[ \exp\left(\frac{Q^{in}}{V_{sp}} t\right) T \right] = \exp\left(\frac{Q^{in}}{V_{sp}} t\right) \frac{Q^{in}}{V_{sp}} \left( T^{in} + \lambda X^{in}_{SO_2} \Phi^E \frac{-\Delta H}{c_{p,g} M_g} \right). \tag{4.16}$$

For calculation convenience, feed conditions are not considered time-varied over the short time period $\Delta t$. In this case, applying integration from $t$ to $t + \Delta t$ to Equation (4.16), yields:

$$\left[ \exp\left(\frac{Q^{in}}{V_{sp}} t\right) T \right] \Big|_t^{t+\Delta t} = \left( T^{in} + \lambda X^{in}_{SO_2} \Phi^E \frac{-\Delta H}{c_{p,g} M_g} \right) \left( \exp\left(\frac{Q^{in}}{V_{sp}} t\right) \Big|_t^{t+\Delta t} \right), \tag{4.17}$$

$$\begin{aligned} &\exp\left[\frac{Q^{in}}{V_{sp}} (t + \Delta t)\right] T(t + \Delta t) - \exp\left(\frac{Q^{in}}{V_{sp}} t\right) T(t) \\ &= \left( T^{in} + \lambda X^{in}_{SO_2} \Phi^E \frac{-\Delta H}{c_{p,g} M_g} \right) \left\{ \exp\left[\frac{Q^{in}}{V_{sp}} (t + \Delta t)\right] - \exp\left(\frac{Q^{in}}{V_{sp}} t\right) \right\}. \end{aligned} \tag{4.18}$$

After rearrangement, a model regarding outlet temperature is derived:

$$\begin{aligned} T(t + \Delta t) &= \exp\left(-\frac{Q^{in}}{V_{sp}} \Delta t\right) T(t) \\ &+ \left[1 - \exp\left(-\frac{Q^{in}}{V_{sp}} \Delta t\right)\right] \left( T^{in} + \lambda X^{in}_{SO_2} \Phi^E \frac{-\Delta H}{c_{p,g} M_g} \right), \end{aligned} \tag{4.19}$$

that is,

$$
\begin{aligned}
T_k\left(j+1\right) &= \exp\left(-\frac{Q_k^{in}(j)}{V_{sp,k}(j)}\Delta t\right) T_k\left(j\right) \\
&+ \left[1-\exp\left(-\frac{Q_k^{in}(j)}{V_{sp,k}(j)}\Delta t\right)\right]\left[T_k^{in}(j)+\lambda_k X_{SO_2,k}^{in}(j)\Phi_k^E(j)\frac{-\Delta H}{c_{p,g}M_g}\right],
\end{aligned}
\tag{4.20}
$$

where $j$ indicates the sampling time and $k = 1, 2, 3, 4$ representing the four converter stages. The discrete-time model in (4.20) is convenient for parameter estimation and model validation from the industrial discrete-time data. From the developed models, it can be seen that process dynamics for the gas temperature is dominantly affected by the term $V_{sp}/Q^{in}$ - the larger term implying the slower dynamics.

With given feed conditions for each stage, model in (4.13) and (4.20) can be used to predict the gas temperature variations for the converter stages. The needed feed conditions include feed gas temperature, gas composition and flowrate. In industrial practices, inlet gas temperatures for all stages are often measured. For the feed compositions of the first stage, gas concentration of $SO_2$ is usually available, $SO_3$ molar concentration is assumed zero, and oxygen concentration can be assumed to be proportionally related with $SO_2$ concentration according to (Davenport and King, 2006). For the second, third and forth stages, however, feed compositions are often not measured online and information may not be available. It is thus necessary to estimate the inlet gas compositions for these later stages. Due to the fact that the gas compositions remain the same through heat exchangers between the first three converter stages (as shown in Figure 1.2), feed gas concentration of the second and third beds is equal to the outlet gas concentration from the preceding beds, i.e.,

$$
X_{i,k}^{in} = X_{i,k-1}, \quad (k = 2, 3, \text{ and } i = \text{SO}_2, \text{O}_2, \text{SO}_3, \text{re}). \tag{4.21}
$$

Equation (4.21) is not applicable to the fourth stage as the gas needs to pass an interpass $SO_3$ absorption tower after the third stage. If $SO_3$ is assumed to be completely removed in the

absorption tower, feed concentration of the last bed can be written as:

$$X_{i,4}^{in} = \frac{X_{i,3}}{1 - X_{SO_3,3}}, \quad (i = \text{SO}_2, \text{O}_2, \text{re}) \tag{4.22}$$

$$X_{SO_3,4}^{in} = 0. \tag{4.23}$$

With the assumption of negligible dynamics on gas compositions in a converter stage, steady-state models on the catalytic converter stage, Equations (2.13 - 2.16), can be used to provide the estimates for the outlet gas molar fractions for the $k$-th stage if the parameter $\lambda$ for the stage is known:

$$X_{SO_2,k} = \frac{(1 - \lambda_k \Phi_k^E) X_{SO_2,k}^{in}}{1 - \frac{1}{2}\lambda_k \Phi_k^E X_{SO_2,k}^{in}}, \tag{4.24}$$

$$X_{O_2,k} = \frac{X_{O_2}^{in} - \frac{1}{2}\lambda_k \Phi_k^E X_{SO_2,k}^{in}}{1 - \frac{1}{2}\lambda_k \Phi_k^E X_{SO_2,k}^{in}}, \tag{4.25}$$

$$X_{SO_3,k} = \frac{X_{SO_3,k}^{in} + \lambda_k \Phi_k^E X_{SO_2,k}^{in}}{1 - \frac{1}{2}\lambda_k \Phi_k^E X_{SO_2,k}^{in}}, \tag{4.26}$$

$$X_{re,k} = \frac{1 - X_{SO_2,k}^{in} - X_{O_2,k}^{in} - X_{SO_3,k}^{in}}{1 - \frac{1}{2}\lambda_k \Phi_k^E X_{SO_2,k}^{in}}. \tag{4.27}$$

The volume gas flowrate for the first stage is usually measured. Based on reaction (1.2), there is one half mole loss in the total gas molar amount with every mole of $SO_2$ converted. the outlet molar flowrate $N_k$ for the $k$-th stage can thus be described as:

$$N_k = \left(1 - \frac{1}{2}\lambda_k \Phi_k^E X_{SO_2,k}^{in}\right) N_k^{in}, \tag{4.28}$$

where

$$N_k^{in} = \frac{P_k^{in} Q_k^{in}}{R T_k^{in}}, \tag{4.29}$$

$$N_k = \frac{P_k Q_k}{R T_k}, \tag{4.30}$$

if the ideal gas law is applied. Therefore, the volume flowrates of the second and third beds are derived as:

$$Q_k^{in} = \left(1 - \frac{1}{2}\lambda_{k-1}\Phi_{k-1}^{E} X_{SO_2,k-1}^{in}\right) \frac{T_k^{in} P_{k-1}^{in} Q_{k-1}^{in}}{T_{k-1}^{in} P_k^{in}}, \tag{4.31}$$

where $k = 2, 3$. For the fourth bed, with a complete $SO_3$ removal by the intermediate absorption tower, its feed flowrate is:

$$Q_4^{in} = (1 - X_{SO_3,3}) \left(1 - \frac{1}{2}\lambda_3 \Phi_3^{E} X_{SO_2,3}^{in}\right) \frac{T_4^{in} P_3^{in} Q_3^{in}}{T_3^{in} P_4^{in}}. \tag{4.32}$$

With the given and estimated gas feed conditions for each bed, temperature and $SO_2$ concentration (or conversion ratio) for the gas out of each bed can be predicted from the above modelling equations (4.13) and (4.20).

## 4.3 Parameter Estimation

A dynamic model is developed for converter stages in the previous section. For the model to reflect an industrial operation, the parameter $\lambda$ needs to be estimated for each catalyst bed from the industrial operating data. In this chapter, it is assumed that $\lambda$ is a constant value for each stage. The parameter $\lambda_k$ is estimated by minimizing the following objective function:

$$\min_{\lambda_k} J_k = \min_{\lambda_k} \sum_j \left[\hat{T}_k(j) - T_k(j)\right]^2, \quad (k = 1, 2, 3, 4), \tag{4.33}$$

where $T_k$ is the measured temperature from industrial and $\hat{T}_k(j)$ is the prediction derived using Equation (4.20) when inlet industrial data are applied:

$$\hat{T}_k(1) = T_k(1), \tag{4.34}$$

$$\hat{T}_k\,(j+1) = \exp\left(-\frac{Q_k^{in}(j)}{V_{sp,k}(j)}\Delta t\right) T_k\,(j) + \left[1-\exp\left(-\frac{Q_k^{in}(j)}{V_{sp,k}(j)}\Delta t\right)\right]\left[T_k^{in}(j) + \lambda_k X_{SO_2,k}^{in}(j)\Phi_k^E(j)\frac{-\Delta H}{c_{p,g}M_g}\right], \quad (j=1,2,3,\cdots). \tag{4.35}$$

Industrial operating data with a sampling time of 1 min are collected and used for estimation of $\lambda_k$. Based on half a month's industrial data, $\lambda_k$ values are selected from 0 to 1, and the optimal $\lambda_k$ is obtained when minimum of the objective function (4.33) is achieved respectively for each bed. The estimated optimal $\lambda_k$ is listed in Table 4.1. The value of $\lambda_k$ provides a relative indication on how close the reaction reaches to the equilibrium in each stage. From Table 4.1, the reaction in the first three stages reaches close to the equilibrium. A recursive estimation may also be used if the system experiences some slow changes or $\lambda_k$ values need to be updated for varying operating conditions.

Table 4.1: Optimal parameter $\lambda_k$ estimated from collected industrial data

| Stages of converter, $k$ | Parameter $\lambda_k$ |
|---|---|
| 1 | 0.99 |
| 2 | 0.96 |
| 3 | 0.96 |
| 4 | 0.30 |

## 4.4 Model Validation

With the estimated $\lambda_k$ in Table 4.1, outlet temperature of the each converter stage can be predicted using Equation (4.20) with the measured feed conditions. With one-month industrial

operating data, half of the data are used for parameter estimation and the other half for model validation.

Figure 4.1 shows two periods of one-day measured and predicted outlet temperatures for the four stages of the $SO_2$ converter in an industrial smelter. It is observed that variations of the predicted temperature matches the measurement well for all four stages. The model predicted temperature is able to track the major variations of measurement. Besides, one period of data when feed $SO_2$ experiences step drop and increase are displayed in Figure 4.2. In the face of inlet $SO_2$ step changes, temperature prediction follows the measurement tightly and performs the same gradual changes. The close match between the model predicted and measured temperature shows that the developed model with the estimated parameter is valid in describing the industrial system.

In predicting the outlet temperature for each stage from the model, the outlet $SO_2$ molar fraction and the conversion ratio need to be estimated from Equations (2.17) and (4.24). These two variables are not measured online but estimation of them provides an additional monitoring for the process. Figure 4.3 shows the estimated $SO_2$ outlet molar fraction and the conversion ratio for the same period as in Figure 4.1(a). By comparing the $SO_2$ outlet concentrations and $SO_2$ conversion ratios with the first-bed inlet, it is noticed that the first-bed $SO_2$ feed concentration has significant effects on the two estimated output variables. Despite the large variations in the $SO_2$ feed concentration, $SO_2$ outlet concentrations out of the third and forth stages are significantly reduced with small variations.

## 4.5 Dynamic Simulation

With the developed model, system dynamics can be studied by examining the effects of input variables. The process parameters used for dynamic simulations of the $SO_2$ converter are listed in Table 4.2. Based on the given process parameters and the parameter $\lambda$ estimated from the industrial operating data, effects of the input variables, including $SO_2$ feed concentration,

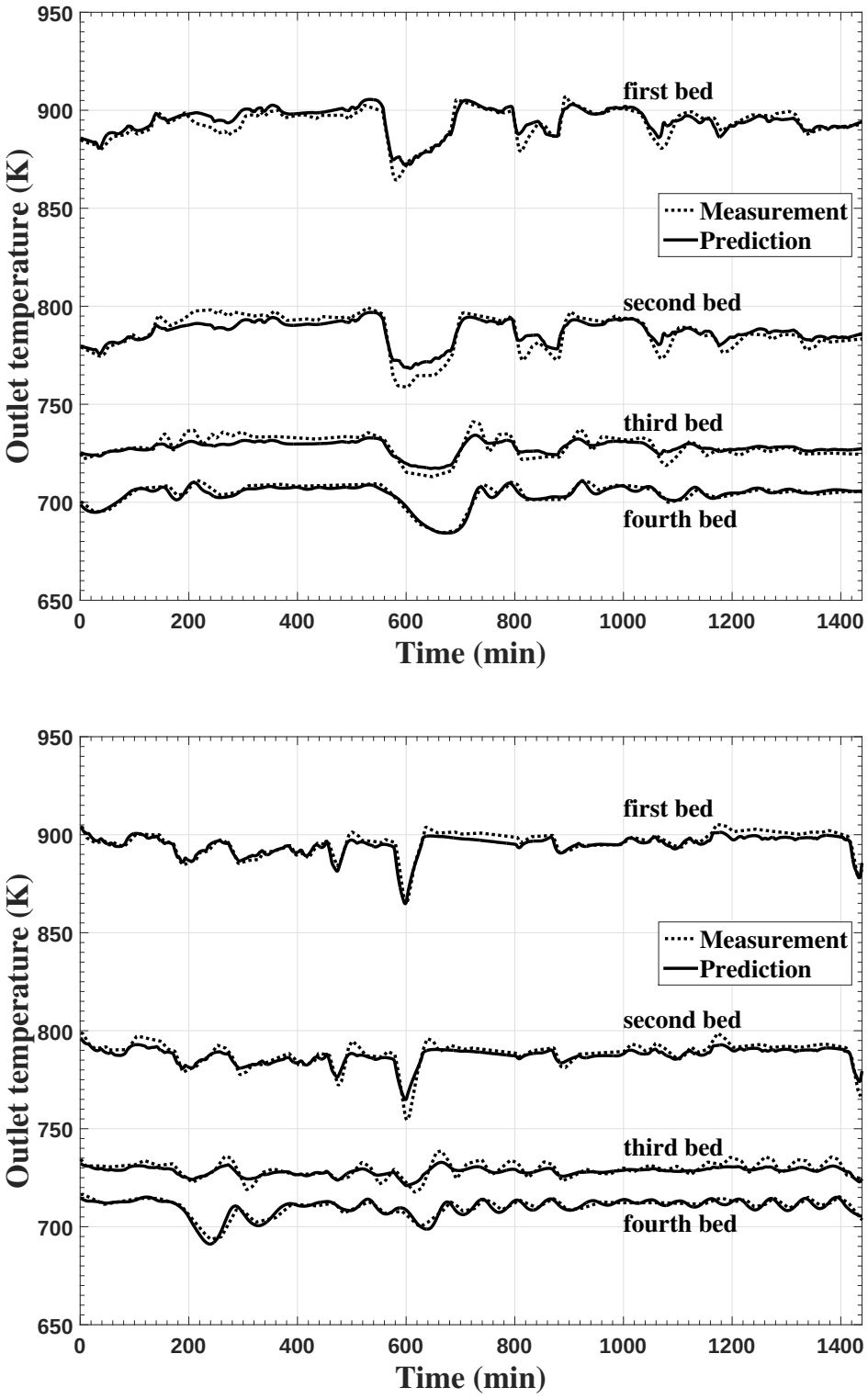


Figure 4.1: Two periods of one-day measured and predicted outlet temperature comparison of the four-bed $SO_2$ converter

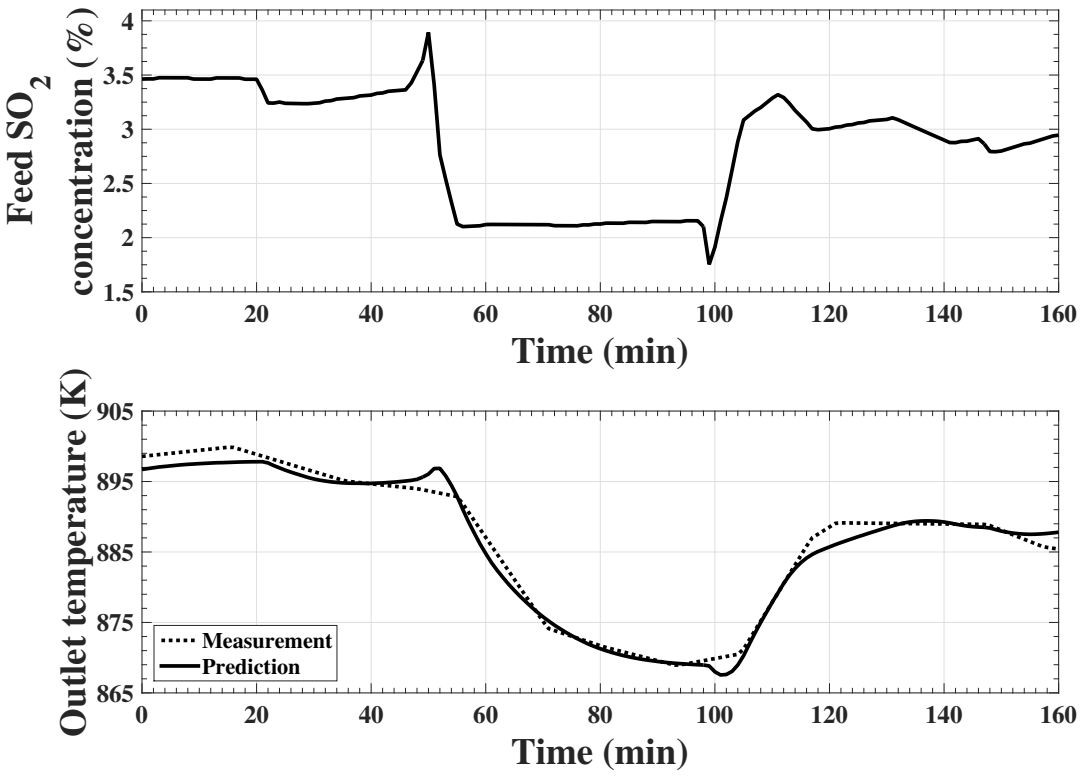


Figure 4.2: Comparison of the first-bed measured and predicted outlet temperature in response to inlet $SO_2$ changes

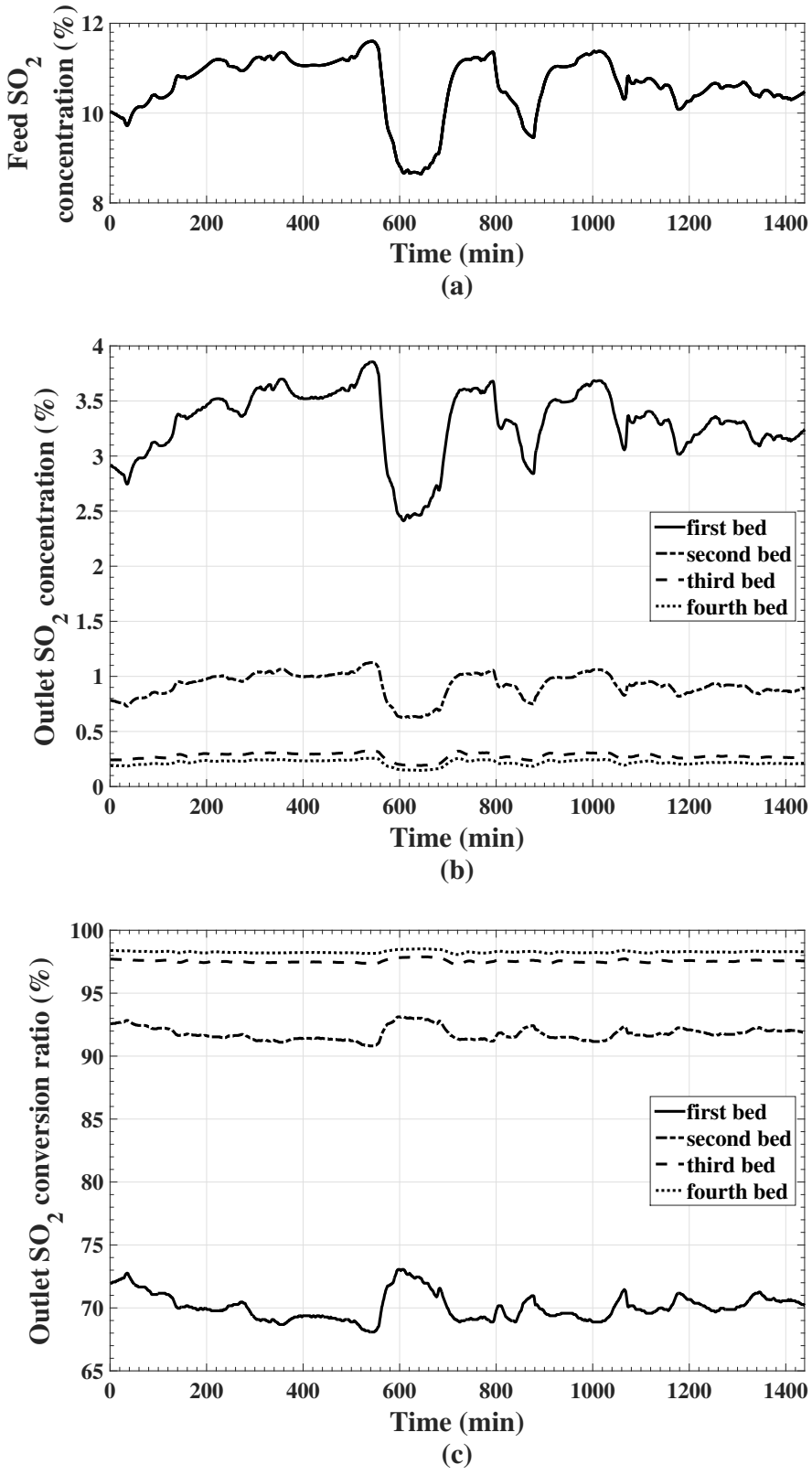


Figure 4.3: Outlet $SO_2$ concentration and overall $SO_2$ conversion ratio estimation after filtering the first-bed feed $SO_2$ concentration

flowrate and the feed gas temperature, are investigated.

Table 4.2: Initial conditions and process parameters for dynamic simulations

| Initial conditions | | Process parameters | |
|---|---|---|---|
| $X^{in}_{SO_2,1}$ | 10 % | $V_1$ | 80 $m^3$ |
| $X^{in}_{O_2,1}$ | 11 %[a] | $V_2$ | 96 $m^3$ |
| $X^{in}_{SO_3,1}$ | 0 % | $V_3$ | 125 $m^3$ |
| $T^{in}$ | 660 K[b] | $V_4$ | 120 $m^3$ |
| $P_{t,1}$ | 1.4 atm | $\rho_{cat,1}$ | 412 kg/$m^3$ |
| $P_{t,2}$ | 1.3 atm | $\rho_{cat,2}$ | 398 kg/$m^3$ |
| $P_{t,3}$ | 1.2 atm | $\rho_{cat,3}$ | 370 kg/$m^3$ |
| $P_{t,4}$ | 1.1 atm | $\rho_{cat,4}$ | 420 kg/$m^3$ |
| $Q^{in}_1$ | 194 $km^3$/hr | $c_{p,cat}$ | 830 J/(kg·K) |

[a] First-bed inlet $O_2$ concentration is assumed to be $1.1X^{in}_{SO_2,1}$ (Davenport and King, 2006).
[b] Inlet temperature for all stages is assumed to be the same for simulation simplicity.

$SO_2$ feed concentration to the converter is an important disturbance input variable for the converter in a smelter. A smelter generates offgas laden with $SO_2$ and the gas is fed to an acid plant for $SO_2$ reduction. The offgas from the smelter may have large variations in $SO_2$ concentration, which significantly raises the operational challenge for the acid plant in a smelter in comparison with that using sulfur burning as its source gas. The effect of $SO_2$ concentration in the feed gas on the system dynamics of the converter is investigated by examining the step response of the outlet temperature. Figure 4.4 displays the outlet temperature evolvements of the four beds when the first-bed inlet $SO_2$ molar fraction has a step increase from 10% to 11%. It is observed that $SO_2$ feed concentration in the source gas affects the outlet gas temperature for all four stages and temperatures increase with the $SO_2$ feed concentration. It is thus important to control the feed concentration to be within a proper range so that over-heating of the catalyst beds can be avoided while maintaining an efficient $SO_2$ conversion. From Figure 4.4, the temperature increment resulting from the $SO_2$ feed concentration increase is the largest for the first bed and the increment reduces for the second bed, and only small temperature increment is observed for the third and forth beds. This implies that most $SO_2$ in the offgas is converted in the first two stages, and only small amount of $SO_2$ conversions occur in the third

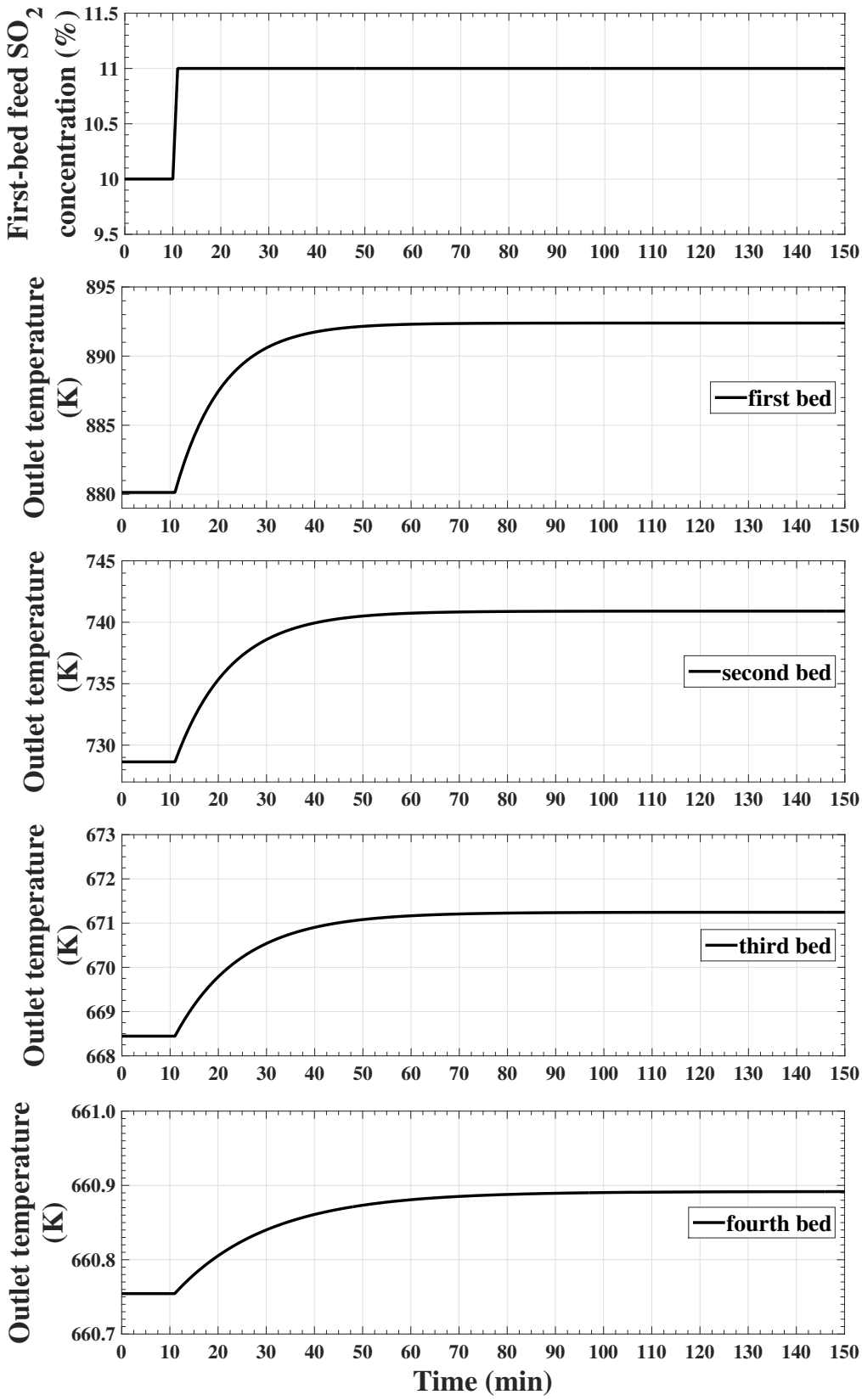


Figure 4.4: Dynamic simulation on outlet temperatures of four catalyst beds in response to a step change on first-bed inlet $SO_2$ concentration

and fourth stages.

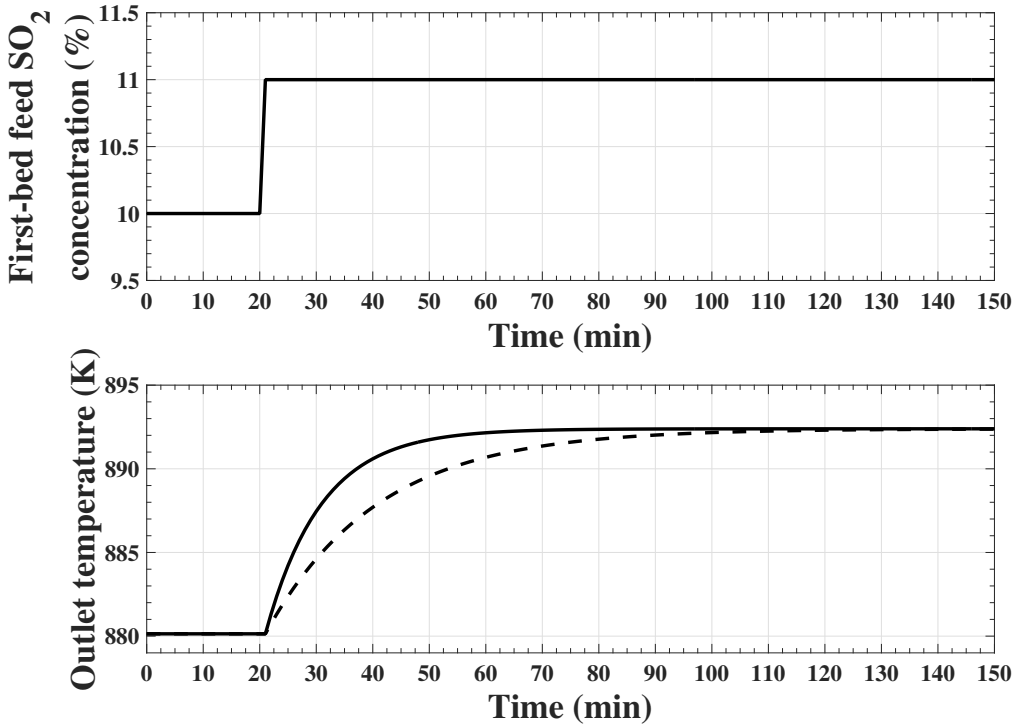


Figure 4.5: Dynamic simulation on first-bed outlet temperature in response to a step change on the first-bed inlet $SO_2$ concentration under different flowrates

In Figure 4.4, the gas temperatures for the four beds respond to the step change in $SO_2$ feed concentration in a slow dynamic manner. As the gas passes through the series of stages, the temperature responses become not only diminished but also more sluggish. Despite the very short residence time of gas in each stage, the system has relatively large time constants leading to slower dynamic response. As described in Equation (4.20), the time constant is determined by $(\rho_{cat} c_{p,cat} V_{cat}) \,/\, (\rho_g c_{p,g} Q^{in})$ and the gas flowrate plays the key role in the time constant. Figure 4.5 shows the first-bed outlet temperatures under different gas flowrates when a step change in $X^{in}_{SO_2,1}$ occurs. A slower response in the outlet temperature is observed when the flowrate decreases. As the gas passes through the catalyst stages, temperature response becomes slower due to the additive effects of time constant in the previous stages. In addition, flowrate decreases along the catalyst beds with $SO_2$ conversion and this further slows down the

temperature response. Figure 4.5 indicates that the gas flowrate affects how fast the temperature responds but does not affect the final steady state temperature value.

$SO_2$ concentration in the feed gas affects outlet temperature in a slow dynamic manner, but its effect on $SO_2$ conversion or $SO_2$ outlet concentration is fast such that their dynamics can be negligible due to the very short residence time of the off-gas in the converter stages. Figure 4.6 shows the effects of $SO_2$ feed concentration on outlet $SO_2$ concentration, $SO_2$ conversion ratio and outlet temperature, respectively. From Figure 4.6(a), it can be seen that outlet $SO_2$ concentrations for the four beds increase as $SO_2$ feed concentration increases, but the steady-state gain of outlet concentration to feed concentration is much less than 1 (around 0.5 for the first bed and much less for other beds), i.e., for every 1% increment in the feed concentration, there is much less than 1% increment in the outlet concentration. This implies that larger amount of $SO_2$ is converted in the stage as $SO_2$ feed concentration increases and high $SO_2$ concentration favors $SO_2$ conversion. From Figure 4.6(c), outlet temperature increases as $SO_2$ feed concentration increases. This further confirms that more $SO_2$ conversion occurs in the reaction and larger amount of heat is generated with increased $SO_2$ feed concentration. Despite more $SO_2$ conversion for larger $SO_2$ feed concentration, the $SO_2$ conversion ratio decreases as feed concentration increases, as shown in Figure 4.6(b). This is due to the larger value in the denominator of Equation (2.17) for larger feed concentration. From Figure 4.6(a) and Figure 4.6(b), lower $SO_2$ feed concentration leads to less $SO_2$ conversion but larger $SO_2$ conversion ratio. This is valid only when the system is in the normal operation and $SO_2$ feed concentration is in the required desirable range. The model may need to be modified by re-estimating the parameter $\lambda$ if very low $SO_2$ feed concentration occurs as it may result in very slow reaction and, consequently, smaller $SO_2$ conversion and conversion ratio. If it happens, a new $\lambda$ value needs to be estimated from the industrial data under the new conditions.

Inlet temperature to each bed of the converter is regulated to ensure efficient $SO_2$ conversion. Figure 4.7 shows the steady-state outlet $SO_2$ concentration, overall $SO_2$ conversion ratio and

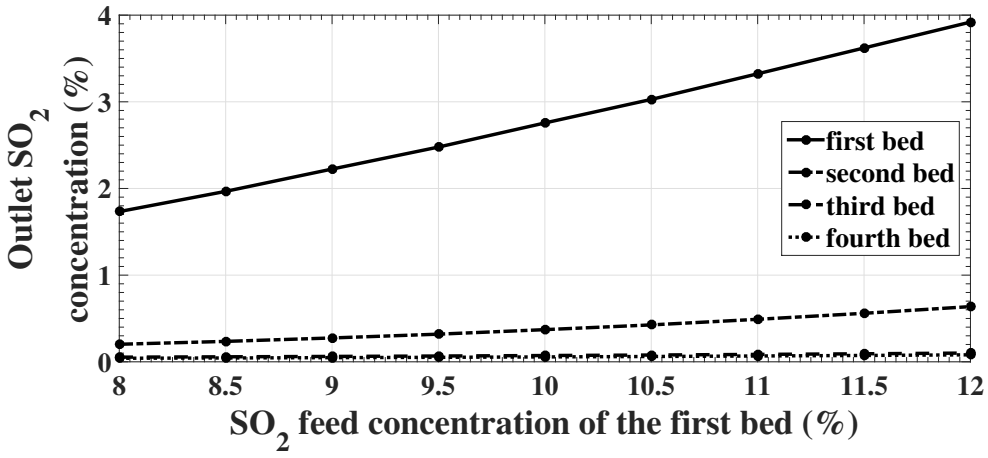


(a)

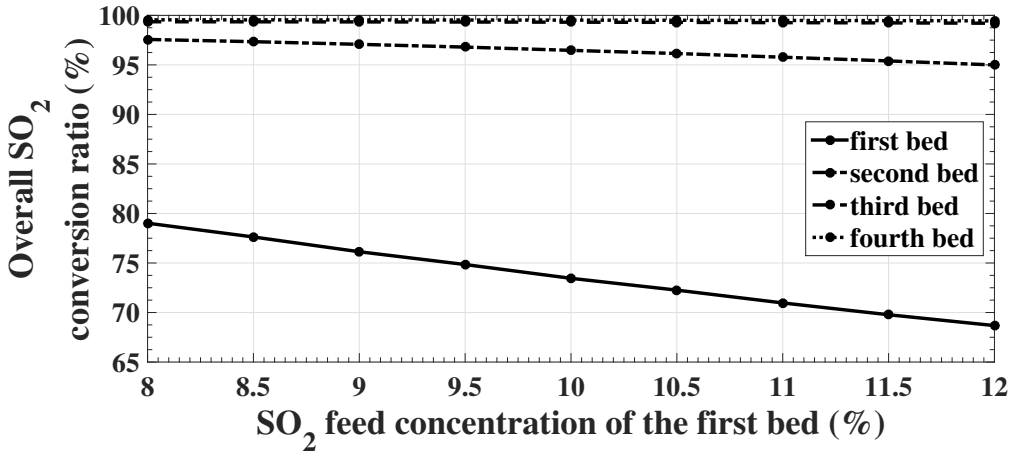


(b)

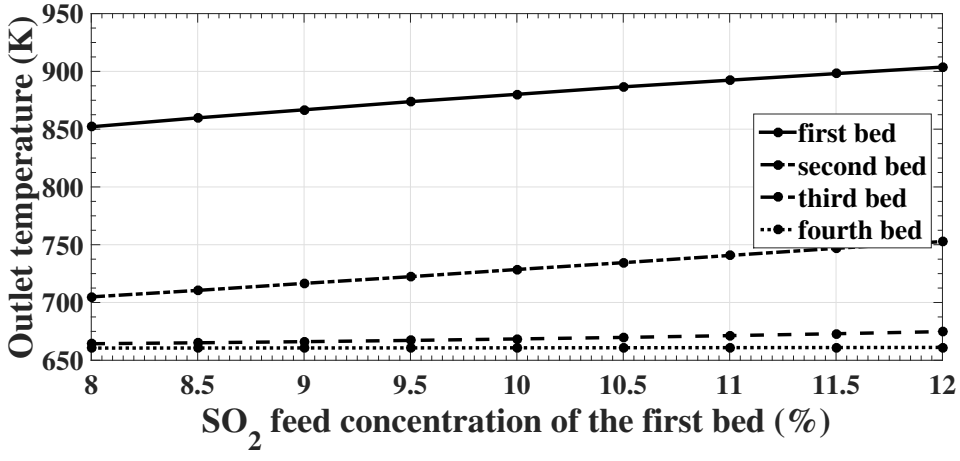


(c)

Figure 4.6: Outlet $SO_2$ concentrations, overall $SO_2$ conversion ratios and outlet temperature under different feed $SO_2$ concentrations

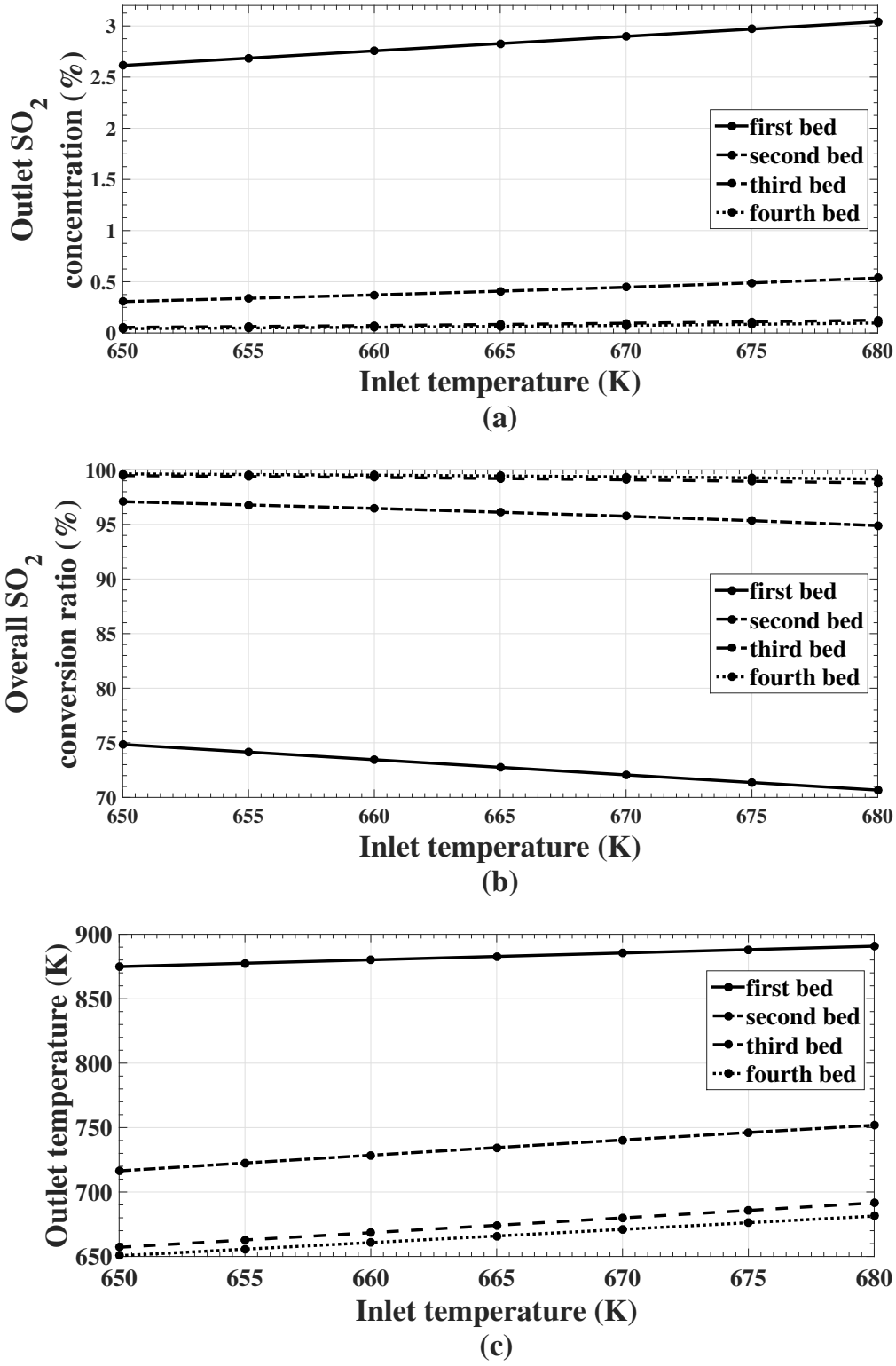


Figure 4.7: Outlet $SO_2$ concentrations, overall $SO_2$ conversion ratios and outlet temperature under different feed temperatures

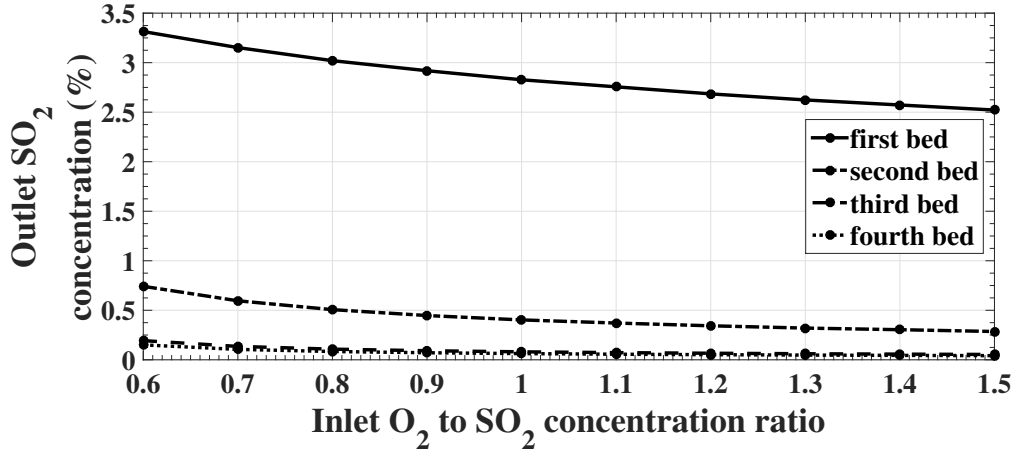


(a)

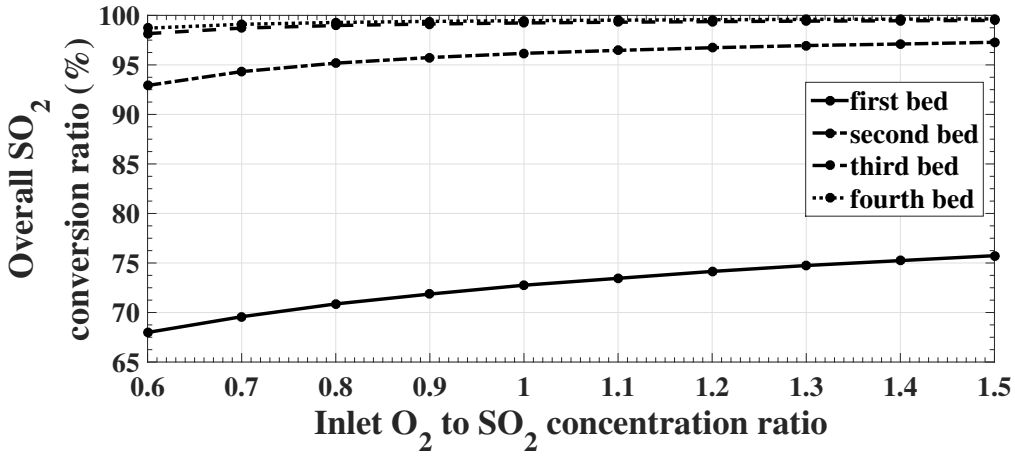


(b)

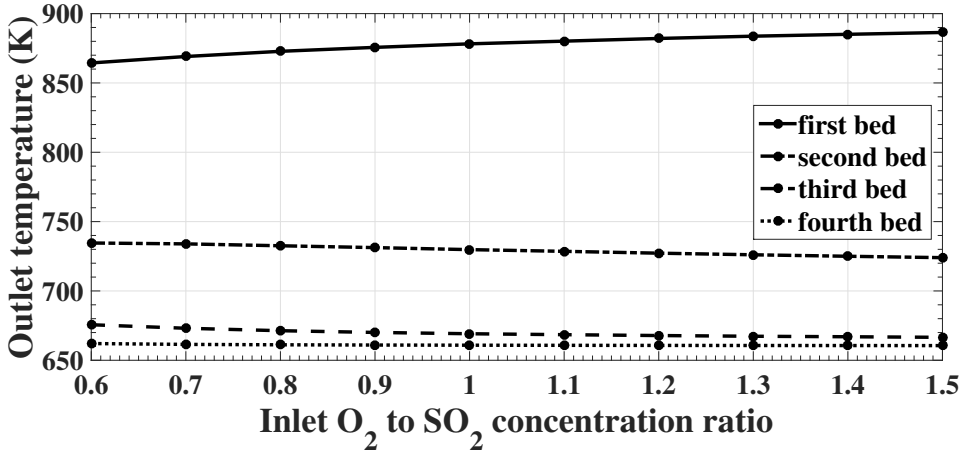


(c)

Figure 4.8: Outlet $SO_2$ concentrations, overall $SO_2$ conversion ratios and outlet temperature under different inlet $O_2$ to $SO_2$ concentration ratios

outlet temperature, respectively, under different inlet temperatures. It is noticed that as inlet temperature decreases, outlet $SO_2$ concentration declines, i.e., more $SO_2$ is converted and higher conversion ratio is achieved. The simulation indicates that lower inlet temperature is desirable for higher $SO_2$ conversion. The lowest inlet temperature is, however, limited by the ignition temperature of the catalyst, for example, $\sim$635 K for $V_2O_5$-$K_2SO_4$ based catalyst. A Cs-promoted catalyst substituting $K_2SO_4$ with $Cs_2SO_4$ has been found being able to provide a lower ignition temperature, $\sim$595 K (Schlesinger et al., 2011). Due to its high cost, the Cs-promoted catalyst is used only in certain beds or mixed with the $K_2SO_4$-based one to improve the $SO_2$ conversion. From Figure 4.7(c), outlet temperature increases with inlet temperature. The steady-state gain of outlet temperature from inlet temperature is less than one, i.e., for every degree increment in inlet temperature there is less than one degree increment in outlet temperature. In the normal industrial operation, it is critical to regulate the inlet temperature to each bed, especially the first bed, such that gas temperature is above the ignition temperature of the catalyst but is not too high to cause permanent damage on the catalyst.

Oxygen is necessary for $SO_2$ oxidation in the reaction (1.2). Oxygen has to be provided sufficiently to ensure efficient oxidization of $SO_2$. The feed $O_2$ concentration is usually not measured in industrial smelters. The effect of $O_2$ to $SO_2$ concentration ratio on the steady-state performance of the system is investigated via simulation, as shown in Figure 4.8. It can be seen that higher feed $O_2$ to $SO_2$ concentration ratio favors $SO_2$ oxidation and thus leads to lower outlet $SO_2$ concentration and larger $SO_2$ conversion ratio. The temperature also increases with higher feed $O_2$ to $SO_2$ concentration ratio due to more reaction heat generated. The effect of increasing feed $O_2$ to $SO_2$ concentration ratio is more significant for the first two stages and when the concentration ratio is smaller. When the ratio is greater than $\sim 1.3$, the effect becomes less noticeable. Excessive $O_2$ supply beyond some point in the feed gas may not generate considerable benefit in $SO_2$ oxidization.

## 4.6 Summary

In this chapter, a dynamic model of the catalytic $SO_2$ converter in an industrial smelter is developed based on mass and energy conservations. The developed model uses the $SO_2$ conversion ratios as a key variable, which has high industrial relevance in the smelters. In contrast to the existing models, the proposed model in this paper does not require reaction kinetics knowledge or kinetics parameters and thus can be useful when accurate kinetics information is not available. Comparison of model predicted temperature with the industrial operating data indicates that the derived model is valid in describing the industrial system.

Based on the developed model, simulations are performed to investigate the process dynamics and effects of process input variables. Results indicate that gas temperature out of the converter stages has slow dynamics and gas flowrate is the key variable affecting the dynamics. Examinations on the steady-state effect of input variables show that more $SO_2$ conversion occurs with higher $SO_2$ feed concentration but $SO_2$ conversion ratio decreases. When gas inlet temperature is above the catalyst's ignition point, $SO_2$ conversion decreases with increasing temperature.

The obtained model contains a parameter that is easy to be estimated from industrial operating data and can thus be adapted to describe a variety of $SO_2$ converters under different operating conditions. The developed model provides a necessary foundation for process optimization and enhanced control development for industrial smelters.

# Chapter 5

# Two-Phase Dynamic Modelling of Sulfur Dioxide Converter Using PDE

Dynamic modelling of the $SO_2$ converters has been conducted in extensive literatures (Gosiewski, 1993; Kiss et al., 2010; Sørensen et al., 2015). However, the difference of the temperature and/or gas concentrations between gas flow and catalyst is often neglected in the existing models.

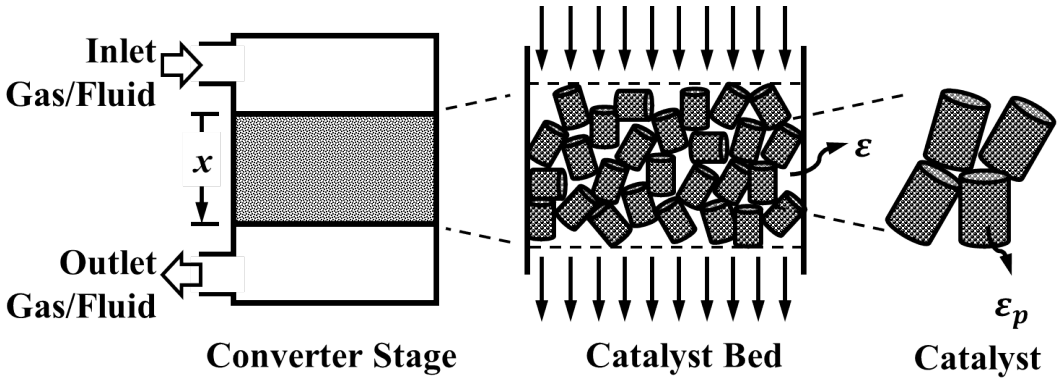


Figure 5.1: Schematic diagram of the catalyst particle packing inside a $SO_2$ converter stage

For a catalytic $SO_2$ converter, catalyst particles are packed loosely with space between each other, as displayed in Figure 5.1. Catalyst particles are not pure solid. Numerous pores exist

within each particle. When the gas flows through the catalyst bed, gas fills in the space between particles as well as within particles. For the gas inside the particles, it usually performs in a different way from that outside the particles. Therefore, in this chapter, the substances in the converter bed are considered as two phases: fluid and solid phases. Detailed dynamic modelling is carried out on both phases using respective mass and energy conservations. With two-phase substances considered, the dynamic model is able to incorporate the temperature and gas concentration for both fluid and solid phases, and be used to investigate the interactions between the two phases.

The new dynamic model is established as a set of partial differential equations (PDE), which describe the behaviours of the $SO_2$ converter with time and space. Simulations are performed to examine the variable spatial profiles and investigate the effects of inlet variables. Process behaviour was studied when dramatic $SO_2$ supply changes occur, i.e., the inlet $SO_2$ is cut off for a period of time and then the $SO_2$ supply restores. The dynamics of outlet temperature for the two situations are explored in detail from simulation results.

In the two-phase dynamic modelling, assumptions are made as follows:

(1) converter is considered to be adiabatic;

(2) porosity is assumed to be uniform throughout each converter stage;

(3) gas density and temperature variations in the radial direction are not considered;

(4) porosity of the catalyst bed is assumed to represent the void ratio of the cross-sectional area;

(5) chemical reaction in the fluid phase can be neglected;

(6) gas flow and diffusion effects are negligible in mass conservation modelling;

(7) energy convection is neglected in catalyst energy conservation;

(8) Darcy velocity is assumed to be spatially constant inside the converter.

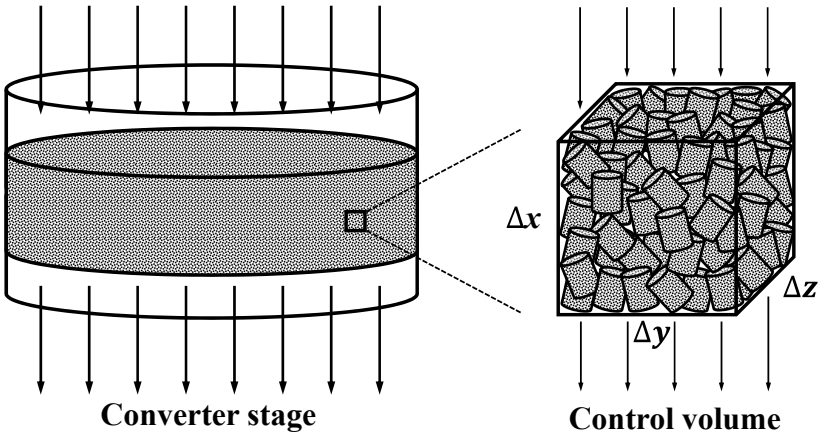


Figure 5.2: A converter stage and an infinitesimal control volume

## 5.1 Mass Conservation

For the mass conservation of a converter stage, an infinitesimal control volume is considered, as showed in Figure 5.2. Inside the control volume with dimensions $\Delta x \times \Delta y \times \Delta z$, gas mixture with multi-components (for example, $SO_2$, $O_2$, and $SO_3$ in this thesis) passes through. In the catalyst bed, gas components exist not only in the moving gas mixture between catalyst particles, but also within the catalyst particles. The gas components in the moving gas mixture are denoted as "fluid phase" and those inside catalyst particles are "solid phase".

For a multi-component gas mixture, the density of a given component (represented by subscript $i$) in the fluid (or catalyst) is defined as the mass of component $i$ per unit volume of the fluid-phase (or solid-phase) mixture, that is,

$$\rho_{f,i} = \frac{\text{Mass of fluid-phase component } i}{\text{Volume of the fluid-phase mixture}}; \tag{5.1}$$

$$\rho_{s,i} = \frac{\text{Mass of solid-phase component } i}{\text{Volume of the solid-phase mixture}}, \tag{5.2}$$

and the total density of the fluid-phase (or solid-phase) mixture is the total mass of the fluid-phase (or solid-phase) mixture in the fluid-phase (or solid-phase) volume:

$$\begin{aligned}\rho_f &= \frac{\text{Mass of fluid-phase mixture}}{\text{Volume of the fluid-phase mixture}} = \frac{\sum_i \text{Mass of fluid-phase component } i}{\text{Volume of the fluid-phase mixture}} \\ &= \sum_i \rho_{f,i};\end{aligned} \tag{5.3}$$

$$\begin{aligned}\rho_s &= \frac{\text{Mass of solid-phase mixture}}{\text{Volume of the solid-phase mixture}} = \frac{\sum_i \text{Mass of solid-phase component } i}{\text{Volume of the solid-phase mixture}} \\ &= \sum_i \rho_{s,i};\end{aligned} \tag{5.4}$$

Apart from density, mass concentration can be expressed by molar concentration as well. For the fluid-phase component $i$, its molar concentration is defined as the number of moles of $i$ existing per unit volume of the fluid mixture. It is known that one mole of any components has a mass equal to its molecular weight. Therefore, molar concentration of fluid-phase component $i$, by definition, is:

$$\begin{aligned}C_{f,i} &= \frac{\text{Number of moles of fluid-phase component } i}{\text{Volume of the fluid-phase mixture}} \\ &= \frac{\{\text{Mass of fluid-phase component } i\}/\{\text{Molecular weight of } i\}}{\text{Volume of the fluid-phase mixture}} \\ &= \frac{\rho_{f,i}}{M_i},\end{aligned} \tag{5.5}$$

where $M$ [g/mol] denotes the molecular weight. Solid-phase molar concentration is expressed similarly as:

$$C_{s,i} = \frac{\rho_{s,i}}{M_i}. \tag{5.6}$$

### 5.1.1 Fluid-Phase Mass Conservation

In the control volume shown in Figure 5.2, when the fluid-phase is considered, the mass balance of component $i$ can be stated as follows:

$$\begin{bmatrix}\text{net rate of mass}\\ \text{accumulation of fluid-}\\ \text{phase } i \text{ in control volume}\end{bmatrix} = \begin{bmatrix}\text{rate of mass}\\ \text{influx of fluid-phase}\\ i \text{ to control volume}\end{bmatrix} - \begin{bmatrix}\text{rate of mass}\\ \text{efflux of fluid-phase}\\ i \text{ from control volume}\end{bmatrix} + \begin{bmatrix}\text{rate of mass transfer}\\ \text{of } i \text{ from solid phase}\\ \text{to fluid phase in control volume}\end{bmatrix} + \begin{bmatrix}\text{rate of chemical}\\ \text{production of fluid-phase}\\ i \text{ in control volume}\end{bmatrix}. \tag{5.7}$$

If the total volume of the control volume is expressed as $V_{cv}$, which equals to $(\Delta x \Delta y \Delta z)$, the volumes of fluid-phase $V_f$ and solid-phase $V_s$ mixtures are:

$$V_{cv} = V_f + V_s, \tag{5.8}$$

$$V_f = \varepsilon V_{cv} = \varepsilon \Delta x \Delta y \Delta z, \tag{5.9}$$

$$V_s = (1-\varepsilon) V_{cv} = (1-\varepsilon) \Delta x \Delta y \Delta z, \tag{5.10}$$

where $\varepsilon$ denotes the porosity of the catalyst bed. For simplicity, the density and temperature variations in the radial direction are not considered in this two-phase dynamic modelling, since the radial dispersion becomes negligible during normal industrial operations (Mann et al., 1986; Gosiewski, 1993). Therefore, both concentration and temperature gradients are taken into account only in the gas flow direction $x$. If the porosity of the catalyst bed is assumed to represent the void ratio of the cross-sectional area, the cross-sectional areas $S_{cs}$ of both phases perpendicular to $x$ in the control volume can be simply expressed as:

$$S_{cs,f} = \frac{V_f}{\Delta x} = \varepsilon \Delta y \Delta z, \tag{5.11}$$

$$S_{cs,s} = \frac{V_s}{\Delta x} = (1-\varepsilon) \Delta y \Delta z. \tag{5.12}$$

In Equation (5.7), the net rate of mass accumulation of fluid-phase $i$ within the control volume is given as:

$$\begin{aligned}\left[\begin{array}{c}\text{net rate of mass accumulation}\\ \text{of fluid-phase } i \text{ in control volume}\end{array}\right] &= \frac{\Delta\rho_{f,i}}{\Delta t}\cdot V_f \\ &= \varepsilon\frac{\Delta\rho_{f,i}}{\Delta t}\cdot(\Delta x\Delta y\Delta z)\,.\end{aligned} \tag{5.13}$$

The rates of mass influx of $i$ to the control volume and efflux from the control volume are:

$$\left[\begin{array}{c}\text{rate of mass influx of}\\ \text{fluid-phase } i \text{ to control volume}\end{array}\right] = \left(\rho_{f,i}v_i|_x\right)\cdot(\varepsilon\Delta y\Delta z)\,, \tag{5.14}$$

$$\left[\begin{array}{c}\text{rate of mass efflux of}\\ \text{fluid-phase } i \text{ from control volume}\end{array}\right] = \left(\rho_{f,i}v_i|_{x+\Delta x}\right)\cdot(\varepsilon\Delta y\Delta z)\,, \tag{5.15}$$

where $v_i$ stands for the absolute velocity of component $i$ relative to stationary coordinate axes.

The mass flux of component $i$ relative to the average velocity $v$ of the fluid-phase gas mixture is defined as mass diffusion $j_i$ (kg/(m$^2$·sec)). According to an empirical relation postulated by Fick (Fick, 1855), this mass flux takes the form as:

$$j_i = -D_i\nabla\rho_{f,i}, \tag{5.16}$$

where $D_i$ [m$^2$/sec] is the mass diffusivity or diffusion coefficient of component $i$ through the fluid mixture. Besides, the mass flux of component $i$ to the average velocity can also be expressed as (Lam, 2006; Welty et al., 2008):

$$j_i = \rho_{f,i}\left(v_i - v\right). \tag{5.17}$$

Equating Equations (5.16) and (5.17), it yields:

$$\rho_{f,i}v_i = -D_i\frac{\partial\rho_{f,i}}{\partial x} + \rho_{f,i}v. \tag{5.18}$$

The mass transfer between fluid- and solid-phase $i$ takes place due to their mass concentration difference. Written in a way analogous to Newton's law of cooling (Welty et al., 2008), the mass flux of $i$, $j_i^*$ [kg/(m$^2$·sec)], caused by fluid-solid phase density difference has the following expression:

$$j_i^* = \beta_i(\rho_{s,i} - \rho_{f,i}), \tag{5.19}$$

where $\beta$ [m/sec] is defined as the mass transfer coefficient. Actually, $j_i^*$ represents the mass of component $i$ passes through a unit contact area between fluid and catalyst particle per given increment of time due to the density difference between fluid and solid phases. When solid-phase density of $i$ is higher than the fluid-phase one, $j_i^*$ is positive and transfer of component $i$ goes from solid phase to fluid phase. A negative $j_i^*$ represents that component $i$ is transferring from the fluid phase to solid phase. With Equation (5.19), rate of mass transfer of $i$ from solid phase in (5.7) is derived as:

$$\left[\begin{array}{c}\text{rate of mass transfer of } i \text{ from} \\ \text{solid phase to fluid phase in control volume}\end{array}\right] = j_i^* \cdot \frac{S_p}{V_p} \cdot V_s, \tag{5.20}$$

where $V_p$ is the volume of one catalyst particle and $S_p$ is the contact surface of fluid with one catalyst particle. If a specific area $a_p$ [1/m] is introduced as:

$$a_p = \frac{S_p}{V_p}, \tag{5.21}$$

Equation (5.20) becomes:

$$\begin{aligned}\left[\begin{array}{c}\text{rate of mass transfer of } i \text{ from} \\ \text{solid phase to fluid phase in control volume}\end{array}\right] &= j_i^* \cdot a_p \cdot V_s \\ &= (1-\varepsilon)\beta_i a_p(\rho_{s,i} - \rho_{f,i}) \cdot \Delta x \Delta y \Delta z.\end{aligned} \tag{5.22}$$

For the concerned reaction (1.2), catalyst is necessary and essential, and thus the chemical

reaction in the fluid-phase can be neglected (Bousri et al., 2012):

$$\begin{bmatrix}\text{rate of chemical production of}\\ \text{fluid-phase } i \text{ in control volume}\end{bmatrix} = 0. \tag{5.23}$$

When Equations (5.13-5.15), (5.22) and (5.23) are substituted into Equation (5.7), it yields:

$$\begin{aligned}\frac{\Delta\rho_{f,i}}{\Delta t}\cdot(\varepsilon\Delta x\Delta y\Delta z) = \left(\rho_{f,i}v_i\big|_x\right)\cdot(\varepsilon\Delta y\Delta z) - \left(\rho_{f,i}v_i\big|_{x+\Delta x}\right)\cdot(\varepsilon\Delta y\Delta z)\\ + (1-\varepsilon)\beta_i a_p(\rho_{s,i}-\rho_{f,i})\cdot\Delta x\Delta y\Delta z.\end{aligned} \tag{5.24}$$

Diving by $(\Delta x\Delta y\Delta z)$, mass conservation of fluid-phase $i$ becomes:

$$\varepsilon\frac{\Delta\rho_{f,i}}{\Delta t} = \varepsilon\frac{\rho_{f,i}v_i\big|_x - \rho_{f,i}v_i\big|_{x+\Delta x}}{\Delta x} + (1-\varepsilon)\beta_i a_p(\rho_{s,i}-\rho_{f,i}). \tag{5.25}$$

Evaluated in the limit as $\Delta x$ and $\Delta t$ approach zero, it gives:

$$\varepsilon\frac{\partial\rho_{f,i}}{\partial t} = -\varepsilon\frac{\partial(\rho_{f,i}v_i)}{\partial x} + (1-\varepsilon)\beta_i a_p(\rho_{s,i}-\rho_{f,i}). \tag{5.26}$$

Substituting Equation (5.18) into (5.26), one has the fluid-phase mass conservation regarding density written as:

$$\begin{aligned}\varepsilon\frac{\partial\rho_{f,i}}{\partial t} &= -\varepsilon\frac{\partial}{\partial x}\left(-D_i\frac{\partial\rho_{f,i}}{\partial x} + \rho_{f,i}v\right) + (1-\varepsilon)\beta_i a_p(\rho_{s,i}-\rho_{f,i})\\ &= \varepsilon D_i\frac{\partial}{\partial x}\left(\frac{\partial\rho_{f,i}}{\partial x}\right) - \varepsilon v\frac{\partial(\rho_{f,i})}{\partial x} + (1-\varepsilon)\beta_i a_p(\rho_{s,i}-\rho_{f,i}).\end{aligned} \tag{5.27}$$

Converting the fluid-phase mass balance in Equation (5.27) into the one in terms of molar concentration by using Equations (5.5) and (5.6), we can have the corresponding molar concentration expression:

$$\varepsilon\frac{\partial C_{f,i}}{\partial t} = \varepsilon D_i\frac{\partial}{\partial x}\left(\frac{\partial C_{f,i}}{\partial x}\right) - \varepsilon v\frac{\partial(C_{f,i})}{\partial x} + (1-\varepsilon)\beta_i a_p(C_{s,i}-C_{f,i}). \tag{5.28}$$

### 5.1.2 Solid-Phase Mass Conservation

For the mass conservation of solid-phase mixture inside catalyst particles, the gas flow and diffusion effects are usually negligible in dynamic modelling (Shahamiri and Wierzba, 2011; Bousri et al., 2012). Therefore, the general expression of mass balance of solid-phase component $i$ may be stated as:

$$\begin{bmatrix}\text{net rate of mass}\\ \text{accumulation of solid-}\\ \text{phase } i \text{ in control volume}\end{bmatrix} = \begin{bmatrix}\text{rate of mass transfer}\\ \text{of } i \text{ from fluid phase}\\ \text{to solid phase in control volume}\end{bmatrix} + \begin{bmatrix}\text{rate of chemical}\\ \text{production of solid-phase}\\ i \text{ in control volume}\end{bmatrix}. \tag{5.29}$$

Similarly as Equations (5.13), (5.22) and (5.23), three terms in Equation (5.29) can be expressed respectively as:

$$\begin{aligned}&\begin{bmatrix}\text{net rate of mass accumulation}\\ \text{of solid-phase } i \text{ in control volume}\end{bmatrix}\\ =&\frac{\Delta\rho_{s,i}}{\Delta t}\cdot V_s\\ =&(1-\varepsilon)\frac{\Delta\rho_{s,i}}{\Delta t}\cdot\Delta x\Delta y\Delta z,\end{aligned} \tag{5.30}$$

$$\begin{aligned}&\begin{bmatrix}\text{rate of mass transfer of } i \text{ from}\\ \text{fluid phase to solid phase in control volume}\end{bmatrix}\\ =&(1-\varepsilon)\beta_i a_p(\rho_{f,i}-\rho_{s,i})\cdot\Delta x\Delta y\Delta z,\end{aligned} \tag{5.31}$$

$$\begin{aligned}&\begin{bmatrix}\text{rate of chemical production of}\\ \text{solid-phase } i \text{ in control volume}\end{bmatrix}\\ =&R_{s,i}\left(\rho_{cat}V_s\right)\\ =&(1-\varepsilon)R_{s,i}\rho_{cat}\cdot\Delta x\Delta y\Delta z.\end{aligned} \tag{5.32}$$

Here $R_{s,i}$ [kg/(kg-cat·sec)] is the chemical production rate of gas component $i$ with the help of one unit mass of catalyst.

Substituting Equations (5.30-5.32) into Equation (5.29), it gives:

$$\begin{aligned}&(1-\varepsilon)\,\frac{\Delta\rho_{s,i}}{\Delta t}\cdot\Delta x\Delta y\Delta z\\ =&(1-\varepsilon)\beta_i a_p(\rho_{f,i}-\rho_{s,i})\cdot\Delta x\Delta y\Delta z+(1-\varepsilon)R_{s,i}\rho_{cat}\cdot\Delta x\Delta y\Delta z.\end{aligned}\tag{5.33}$$

Diving by $(1-\varepsilon)\,\Delta x\Delta y\Delta z$ and applying evaluation in the limit when $\Delta x$, $\Delta y$, $\Delta z$ and $\Delta t$ approach zero, we have:

$$\frac{\partial\rho_{s,i}}{\partial t}=\beta_i a_p(\rho_{f,i}-\rho_{s,i})+R_{s,i}\rho_{cat}.\tag{5.34}$$

Expressed by molar concentrations with Equations (5.5) and (5.6), the differential equation of solid-phase mass balance regarding component $i$ can be written as:

$$\frac{\partial C_{s,i}}{\partial t}=\beta_i a_p(C_{f,i}-C_{s,i})+r_{s,i}\rho_{cat},\tag{5.35}$$

where $r_{s,i}$ [mol/(kg-cat·sec)] is related to $R_{s,i}$ via:

$$r_{s,i}=R_{s,i}\cdot M_i.\tag{5.36}$$

## 5.2 Energy Conservation

### 5.2.1 Fluid-Phase Energy Conservation

Considering the control volume in Figure 5.2, energy balance of the fluid-phase mixture can be given as:

$$\begin{bmatrix}\text{net rate of energy}\\ \text{accumulation of fluid phase}\\ \text{in control volume}\end{bmatrix} = \begin{bmatrix}\text{rate of energy}\\ \text{influx of fluid phase}\\ \text{to control volume}\end{bmatrix} - \begin{bmatrix}\text{rate of energy}\\ \text{efflux of fluid phase}\\ \text{from control volume}\end{bmatrix} + \begin{bmatrix}\text{rate of heat transfer}\\ \text{from solid phase to fluid}\\ \text{phase in control volume}\end{bmatrix} + \begin{bmatrix}\text{rate of chemical reaction}\\ \text{heat release to fluid}\\ \text{phase in control volume}\end{bmatrix} \tag{5.37}$$

If fluid-phase temperature change is $\Delta T_f$ for a given time increment $\Delta t$, the net rate of energy accumulation of fluid phase in the control volume is expressed as:

$$\begin{aligned}\begin{bmatrix}\text{net rate of energy accumulation}\\ \text{of fluid phase in control volume}\end{bmatrix} &= \rho_f V_f c_{p,f} \frac{\Delta T_f}{\Delta t} \\ &= \varepsilon \rho_f c_{p,f} \frac{\Delta T_f}{\Delta t} \cdot \Delta x \Delta y \Delta z,\end{aligned} \tag{5.38}$$

where $c_{p,f}$ [J/(kg·K)] is the heat capacity of the fluid-phase mixture.

When fluid-phase gas mixture is assumed to flow in only $x$ direction, the energy influx and efflux of fluid phase include the energy transfer due to fluid flow across the void part of control surface $\varepsilon \Delta y \Delta z$ and conduction effect in the fluid-phase gas. According the Fourier's law concerning heat conduction, the conductive heat flux $\dot{q}_f$ [J/(m$^2$·sec)] can be stated by the temperature gradient as (Janna, 1999):

$$\dot{q}_f = -k_f \frac{\partial T_f}{\partial x}, \tag{5.39}$$

where $k_f$ [J/(m·K·sec)] is the thermal conductivity of fluid-phase mixture. Therefore, the rate

of energy influx of fluid phase minus the rate of energy efflux is obtained as follows:

$$\begin{aligned}
&\begin{bmatrix}\text{rate of energy influx of}\\ \text{fluid phase to control volume}\end{bmatrix} - \begin{bmatrix}\text{rate of energy efflux of}\\ \text{fluid phase from control volume}\end{bmatrix}\\
=&\underbrace{\rho_f c_{p,f} v \left(T_f|_x - T_f|_{x+\Delta x}\right)\cdot(\varepsilon\Delta y\Delta z)}_{\text{energy transfer due to fluid flow}} + \underbrace{\left(\dot{q}_f|_x - \dot{q}_f|_{x+\Delta x}\right)\cdot(\varepsilon\Delta y\Delta z)}_{\text{conductive effect}}\\
=&\rho_f c_{p,f} v \left(T_f|_x - T_f|_{x+\Delta x}\right)\cdot(\varepsilon\Delta y\Delta z) + \left[\left(-k_f\frac{\partial T_f}{\partial x}\right)\Big|_x - \left(-k_f\frac{\partial T_f}{\partial x}\right)\Big|_{x+\Delta x}\right]\cdot(\varepsilon\Delta y\Delta z)\,.
\end{aligned} \tag{5.40}$$

Energy transfer between solid and fluid phases occurs due to the existence of temperature difference. For fluid flowing through porous catalyst bed, the heat flux $\dot{q}_f^*$ [J/(m$^2$·sec)] is used to represent the energy exchange through a unit contact area between fluid and catalyst particle per given increment of time as a result of heat transfer. Based on Newton's law of cooling, $\dot{q}_f^*$ takes the form as (Janna, 1999):

$$\dot{q}_f^* = h\left(T_s - T_f\right), \tag{5.41}$$

where $h$ [J/(m$^2$·K·sec)] is the heat transfer coefficient. In this case, the heat transfer rate from solid phase to fluid phase in control volume is derived as:

$$\begin{aligned}
\begin{bmatrix}\text{rate of heat transfer from solid}\\ \text{phase to fluid phase in control volume}\end{bmatrix} &= \dot{q}_f^*\cdot\frac{S_p}{V_p}\cdot V_s\\
&= \dot{q}_f^*\cdot a_p\cdot V_s\\
&= (1-\varepsilon)h a_p\left(T_s - T_f\right)\cdot\Delta x\Delta y\Delta z.
\end{aligned} \tag{5.42}$$

Since reaction (1.2) requires the presence of catalyst, the chemical reaction within the fluid phase is not considered here, and then we have:

$$\begin{bmatrix}\text{rate of chemical reaction heat release}\\ \text{to fluid phase in control volume}\end{bmatrix} = 0. \tag{5.43}$$

Substituting Equations (5.38), (5.40), (5.42) and (5.43) into (5.37), we obtain:

$$\begin{aligned}\varepsilon\rho_f c_{p,f}\frac{\Delta T_f}{\Delta t}\cdot\Delta x\Delta y\Delta z = {} & \rho_f c_{p,f} v\left(T_f|_x - T_f|_{x+\Delta x}\right)\cdot(\varepsilon\Delta y\Delta z)\\ & + \left[\left(-k_f\frac{\partial T_f}{\partial x}\right)\Big|_x - \left(-k_f\frac{\partial T_f}{\partial x}\right)\Big|_{x+\Delta x}\right]\cdot(\varepsilon\Delta y\Delta z)\\ & + (1-\varepsilon)ha_p\left(T_s - T_f\right)\cdot\Delta x\Delta y\Delta z.\end{aligned} \tag{5.44}$$

If Equation (5.44) is divided by $\Delta x\Delta y\Delta z$ and evaluated when $\Delta x$, $\Delta y$, $\Delta z$ and $\Delta t$ approach zero, it yields:

$$\varepsilon\rho_f c_{p,f}\frac{\partial T_f}{\partial t} = \varepsilon k_f\frac{\partial}{\partial x}\left(\frac{\partial T_f}{\partial x}\right) - \varepsilon\rho_f c_{p,f} v\frac{\partial T_f}{\partial x} + (1-\varepsilon)ha_p\left(T_s - T_f\right). \tag{5.45}$$

### 5.2.2 Solid-Phase Energy Conservation

The energy balance for the solid phase holds a similar expression to the fluid phase and is given as:

$$\begin{aligned}\begin{bmatrix}\text{net rate of energy}\\ \text{accumulation of solid phase}\\ \text{in control volume}\end{bmatrix} = {} & \begin{bmatrix}\text{rate of energy}\\ \text{influx of solid phase}\\ \text{to control volume}\end{bmatrix} - \begin{bmatrix}\text{rate of energy}\\ \text{efflux of solid phase}\\ \text{from control volume}\end{bmatrix}\\ & + \begin{bmatrix}\text{rate of heat}\\ \text{transfer from fluid phase to}\\ \text{solid phase in control volume}\end{bmatrix}\\ & + \begin{bmatrix}\text{rate of chemical reaction}\\ \text{heat release to solid}\\ \text{phase in control volume}\end{bmatrix}.\end{aligned} \tag{5.46}$$

For the terms in (5.46), they can be expressed as:

$$\begin{aligned}
&\begin{bmatrix}\text{net rate of energy accumulation}\\ \text{of solid phase in control volume}\end{bmatrix}\\
=&\rho_{cat} V_s c_{p,cat} \cdot \frac{\Delta T_s}{\Delta t}\\
=&(1-\varepsilon)\rho_{cat} c_{p,cat} \frac{\Delta T_s}{\Delta t} \cdot \Delta x \Delta y \Delta z,
\end{aligned} \tag{5.47}$$

$$\begin{aligned}
&\begin{bmatrix}\text{rate of energy influx of}\\ \text{solid phase to control volume}\end{bmatrix} - \begin{bmatrix}\text{rate of energy efflux of}\\ \text{solid phase from control volume}\end{bmatrix}\\
=&\underbrace{\left(\dot{q}_s|_x - \dot{q}_s|_{x+\Delta x}\right) \cdot (1-\varepsilon)\,\Delta y \Delta z}_{\text{conductive effect}}\\
=&(1-\varepsilon)\left[\left(-k_{cat}\frac{\partial T_s}{\partial x}\right)\Big|_x - \left(-k_{cat}\frac{\partial T_s}{\partial x}\right)\Big|_{x+\Delta x}\right] \cdot \Delta y \Delta z,
\end{aligned} \tag{5.48}$$

$$\begin{aligned}
&\begin{bmatrix}\text{rate of convective heat transfer from fluid}\\ \text{phase to solid phase in control volume}\end{bmatrix}\\
=&\dot{q}_s^* \cdot \frac{S_p}{V_p} \cdot V_s\\
=&\dot{q}_s^* \cdot a_p \cdot V_s\\
=&(1-\varepsilon) h a_p \left(T_f - T_s\right) \cdot \Delta x \Delta y \Delta z,
\end{aligned} \tag{5.49}$$

$$\begin{aligned}
&\begin{bmatrix}\text{rate of chemical reaction heat release}\\ \text{to solid phase in control volume}\end{bmatrix}\\
=&r_h \cdot (\rho_{cat} V_s)\\
=&(1-\varepsilon) r_h \rho_{cat} \cdot \Delta x \Delta y \Delta z,
\end{aligned} \tag{5.50}$$

where $r_h$ (J/(kg-cat·sec)) denotes the energy release rate by the catalytic chemical reaction. Note that Equation (5.48) excludes the energy flux by gas flow, because the average solid-phase gas flow velocity is assumed zero.

Substituting Equations (5.47-5.50) into (5.46), it gives:

$$\begin{aligned}
&(1-\varepsilon)\rho_{cat}c_{p,cat}\frac{\Delta T_s}{\Delta t}\cdot\Delta x\Delta y\Delta z \\
=&(1-\varepsilon)\left[\left(-k_{cat}\frac{\partial T_s}{\partial x}\right)\Big|_x-\left(-k_{cat}\frac{\partial T_s}{\partial x}\right)\Big|_{x+\Delta x}\right]\cdot\Delta y\Delta z \\
&+(1-\varepsilon)ha_p\left(T_f-T_s\right)\cdot\Delta x\Delta y\Delta z \\
&+(1-\varepsilon)r_h\rho_{cat}\cdot\Delta x\Delta y\Delta z.
\end{aligned} \tag{5.51}$$

After being divided by $(1-\varepsilon)\,\Delta x\Delta y\Delta z$ and evaluated in the limit when $\Delta x$, $\Delta y$, $\Delta z$ and $\Delta t$ approach zero, a partial differential equation for solid-phase energy conservation is obtained:

$$\rho_{cat}c_{p,cat}\frac{\partial T_s}{\partial t}=k_{cat}\frac{\partial}{\partial x}\left(\frac{\partial T_s}{\partial x}\right)+ha_p\left(T_f-T_s\right)+r_h\rho_{cat} \tag{5.52}$$

## 5.3 Two-Phase Dynamic Modelling

### 5.3.1 Two-Phase Model for $SO_2$ Converter

Combining the differential relationship developed above, the overall two-phase dynamic model for the $SO_2$ converter is summarized as follows:

energy conservations:

$$\varepsilon\rho_f c_{p,f}\cdot\frac{\partial T_f}{\partial t}=\varepsilon k_f\frac{\partial}{\partial x}\left(\frac{\partial T_f}{\partial x}\right)-\varepsilon\rho_f c_{p,f}v\cdot\frac{\partial T_f}{\partial x}+(1-\varepsilon)ha_p\left(T_s-T_f\right), \tag{5.53}$$

$$\rho_{cat}c_{p,cat}\cdot\frac{\partial T_s}{\partial t}=k_{cat}\frac{\partial}{\partial x}\left(\frac{\partial T_s}{\partial x}\right)+ha_p\left(T_f-T_s\right)+r_h\rho_{cat}, \tag{5.54}$$

fluid-phase mass conservations:

$$\begin{aligned}\varepsilon\frac{\partial C_{f,SO_2}}{\partial t} =&\varepsilon D_{SO_2}\frac{\partial}{\partial x}\left(\frac{\partial C_{f,SO_2}}{\partial x}\right) - \varepsilon v\cdot\frac{\partial C_{f,SO_2}}{\partial x}\\ &+(1-\varepsilon)\beta_{SO_2}a_p(C_{s,SO_2}-C_{f,SO_2}),\end{aligned} \tag{5.55}$$

$$\begin{aligned}\varepsilon\frac{\partial C_{f,O_2}}{\partial t} =&\varepsilon D_{O_2}\frac{\partial}{\partial x}\left(\frac{\partial C_{f,O_2}}{\partial x}\right) - \varepsilon v\cdot\frac{\partial C_{f,O_2}}{\partial x}\\ &+(1-\varepsilon)\beta_{O_2}a_p(C_{s,O_2}-C_{f,O_2}),\end{aligned} \tag{5.56}$$

$$\begin{aligned}\varepsilon\frac{\partial C_{f,SO_3}}{\partial t} =&\varepsilon D_{SO_3}\frac{\partial}{\partial x}\left(\frac{\partial C_{f,SO_3}}{\partial x}\right) - \varepsilon v\cdot\frac{\partial C_{f,SO_3}}{\partial x}\\ &+(1-\varepsilon)\beta_{SO_3}a_p(C_{s,SO_3}-C_{f,SO_3}),\end{aligned} \tag{5.57}$$

solid-phase mass conservations:

$$\frac{\partial C_{s,SO_2}}{\partial t} = \beta_{SO_2}a_p(C_{f,SO_2}-C_{s,SO_2}) + r_{s,SO_2}\rho_{cat}, \tag{5.58}$$

$$\frac{\partial C_{s,O_2}}{\partial t} = \beta_{O_2}a_p(C_{f,O_2}-C_{s,O_2}) + r_{s,O_2}\rho_{cat}, \tag{5.59}$$

$$\frac{\partial C_{s,SO_3}}{\partial t} = \beta_{SO_3}a_p(C_{f,SO_3}-C_{s,SO_3}) + r_{s,SO_3}\rho_{cat}. \tag{5.60}$$

and the following boundary conditions will be applied at the inlet and outlet in our simulations: at the inlet $x = 0$:

$$T_f(t, x = 0) = T^{in}(t), \tag{5.61}$$

$$T_s(t, x = 0) = T^{in}(t), \tag{5.62}$$

$$C_{f,i}(t, x = 0) = C_i^{in}(t) \tag{5.63}$$

at the outlet $x = x_{max}$:

$$\left.\frac{\partial T_f}{\partial x}\right|_{x=x_{max}} = 0, \tag{5.64}$$

$$\left.\frac{\partial T_s}{\partial x}\right|_{x=x_{max}} = 0, \tag{5.65}$$

$$\left.\frac{\partial C_{f,i}}{\partial x}\right|_{x=x_{max}} = 0, \tag{5.66}$$

$$\left.\frac{\partial C_{s,i}}{\partial x}\right|_{x=x_{max}} = 0, \tag{5.67}$$

where $i$ represents different gas components, $SO_2$, $O_2$ and $SO_3$.

### Average Fluid Velocity

With the first-bed inlet volume flowrate $Q^{in}$ measured and collected from the smelter, the Darcy velocity $u$ can be calculated as:

$$u = \frac{Q^{in}}{\pi \left(D_C/2\right)^2}, \tag{5.68}$$

where $D_C$ [m] is the diameter of the catalytic converter. The average fluid velocity $v$ relates with the Darcy velocity $u$ by the porosity as:

$$v = \frac{u}{\varepsilon}. \tag{5.69}$$

### Spatial Pressure

Darcy's law describes the relation between gas pressure gradient and flowrate (Darcy, 1856; Holst and Aziz, 1972; Amhalhel and Furmanski, 1997):

$$u = -\frac{\kappa}{\mu_f}\frac{\partial P}{\partial x}, \tag{5.70}$$

where $\kappa$ [m$^2$] represents Darcy permeability and $\mu_f$ [Pa·sec] is the fluid viscosity. If the Darcy velocity $u$ is assumed spatially constant in the converter, then pressure inside the converter stage can be given as:

$$P(x) = P(0) - u\frac{\kappa}{\mu_f}x. \tag{5.71}$$

Equation (5.71) suggests that gas pressure decreases when gas flows along the $x$-direction.

### 5.3.2 Properties and Parameters

In the derived dynamic model from Equations (5.53) to (5.60) and (5.71), several parameters are included and they should be determined for the next calculations.

#### Darcy Permeability

If the catalyst particles are considered to be spherical, Darcy permeability has the expression as follows (Richardson et al., 2013):

$$\kappa = 0.0055\frac{\varepsilon^3 d_p}{(1-\varepsilon)^2}, \qquad [\text{m}^2] \tag{5.72}$$

where $d_p$ [m] is the catalyst particle diameter.

#### Viscosity

For fluid viscosity, its values of different gas components can be calculated by the following empirical equation (Liessmann et al., 1995; Coker, 2007):

$$\mu = A_\mu + B_\mu T + C_\mu T^2, \qquad [\text{Pa·sec}] \tag{5.73}$$

with the empirical coefficients given in Table 5.1. The viscosity of the gas mixture can then be obtained by:

$$\mu_f = \sum_i \left(X_i \mu_i\right), \qquad (i = \mathrm{SO_2}, \mathrm{O_2}, \mathrm{SO_3}, \mathrm{N_2}) \tag{5.74}$$

where $X$ is the molar fraction of different gas components.

Table 5.1: Empirical coefficients for different gas components regarding gas viscosity

| Gas Components | $A_\mu$ | $B_\mu$ | $C_\mu$ | $T_{min}$ [K] | $T_{max}$ [K] |
|---|---|---|---|---|---|
| $SO_2$ | -1.1103$\times10^{-6}$ | 5.02$\times10^{-8}$ | -1.08$\times10^{-11}$ | 200 | 1000 |
| $O_2$ | 4.4224$\times10^{-6}$ | 5.62$\times10^{-8}$ | -1.13$\times10^{-11}$ | 150 | 1500 |
| $SO_3$ | -5.4$\times10^{-7}$ | 4.76$\times10^{-8}$ | -6$\times10^{-12}$ | 273 | 1200 |
| $N_2$ | 4.2606$\times10^{-6}$ | 4.75$\times10^{-8}$ | -9.88$\times10^{-12}$ | 150 | 1500 |

Notes: $T_{min}$ and $T_{max}$ indicate the minimum and maximum of the applicable temperature.

### Catalyst Density

Catalyst beds inside a catalytic $SO_2$ converter may be composed of different amount and types of vanadium-based catalyst. The bulk density of the catalyst beds and the bed thickness are obtained from the producer in Table 5.2.

Table 5.2: Bulk density of the catalyst beds

| Stages of Converter | Average Bulk Density [kg/m$^3$] | Catalyst Bed Thickness [inches] |
|---|---|---|
| 1 | 411.61 | 25.8 |
| 2 | 397.67 | 30.9 |
| 3 | 370.00 | 40.3 |

### Thermal Conductivity Coefficient

For the gas thermal conductivity coefficient $k_f$ of different gas components, an empirical expression is given by Coker (Coker, 2007):

$$k_f = A_k + B_k \cdot T + C_k \cdot T^2, \qquad \text{[W/(m·K)]} \tag{5.75}$$

where $A_k$, $B_k$ and $C_k$ are empirical coefficients and vary for different gas components. For $SO_2$, $O_2$, $SO_3$ and $N_2$, their empirical coefficients are listed in Table 5.3 (Liessmann et al., 1995; Coker, 2007). With the thermal conductivity of individual gas components derived, the thermal conductivity of the gas mixture can be calculated by:

$$k_f = \sum_i (X_i k_{f,i}) \,. \qquad (i = \mathrm{SO_2, O_2, SO_3, N_2}) \tag{5.76}$$

Table 5.3: Empirical coefficients for different gas components regarding thermal conductivity

| Gas Components | $A_k$ | $B_k$ | $C_k$ | $T_{min}$ [K] | $T_{max}$ [K] |
|---|---|---|---|---|---|
| $SO_2$ | -0.00394 | $4.4847\times10^{-5}$ | $2.1066\times10^{-9}$ | 198 | 1000 |
| $O_2$ | 0.00121 | $8.6157\times10^{-5}$ | $-1.3346\times10^{-8}$ | 80 | 1500 |
| $SO_3$ | -0.00791 | $5.9685\times10^{-5}$ | $-3.0238\times10^{-9}$ | 273 | 1200 |
| $N_2$ | 0.00309 | $7.5930\times10^{-5}$ | $-1.1014\times10^{-8}$ | 78 | 1500 |

Notes: $T_{min}$ and $T_{max}$ indicate the minimum and maximum of the applicable temperature.

According to the manufacture information regarding the catalyst, silicon dioxide ($SiO_2$) is the majority of catalyst compositions (up to 70%). Therefore, the thermal conductivity of catalyst $k_{cat}$ would be represented by that of $SiO_2$, 0.15 W/(m·K) as of fine dry sand (Hamdhan and Clarke, 2010).

### Heat Capacity

When gas pressure remains constant or barely changes, heat capacity of gas varies with the temperature. The National Institute of Standard and Technology (NIST) of the United States provides an empirical expression relating the the heat capacity with temperature based on collected experiment data (NIST-$SO_2$; NIST-$O_2$; NIST-$SO_3$; NIST-$N_2$)

$$k_p = A_p + B_p \cdot T_{cp} + C_p \cdot T_{cp}^2 + D_p \cdot T_{cp}^3 + \frac{E_p}{T_{cp}^2}, \qquad \text{[J/(mol·K)]} \tag{5.77}$$

where $k_p$ is the molar heat capacity, $T_{cp}$ is defined as $T/1000$ while $A_p$, $B_p$, $C_p$, $D_p$ and $E_p$ are empirical coefficients. For the gas components $SO_2$, $O_2$, $SO_3$ and $N_2$, the values of the empirical coefficients are given in Table 5.4 (Chase, 1998). The heat capacity of the gas mixture is then obtained via:

$$k_p = \sum_i \left(X_i k_{p,i}\right). \qquad (i = \mathrm{SO_2},\ \mathrm{O_2},\ \mathrm{SO_3},\ \mathrm{N_2}) \tag{5.78}$$

As for the heat capacity $c_p$ [J/(kg·K)] regarding per mass, it can be derived by the following equation:

$$c_p = \frac{k_p}{M} \tag{5.79}$$

Table 5.4: Empirical coefficients for different gas components regarding heat capacity

| Gas Components | $A_p$ | $B_p$ | $C_p$ | $D_p$ | $E_p$ | $T_{min}$ [K] | $T_{max}$ [K] |
|---|---|---|---|---|---|---|---|
| $SO_2$ | 21.43049 | 74.35094 | -57.75217 | 16.35534 | 0.086731 | 298 | 1200 |
| $O_2$ | 30.03235 | 8.772972 | -3.988133 | 0.788313 | -0.741599 | 700 | 2000 |
| $SO_3$ | 24.02503 | 119.4607 | -94.38686 | 26.96237 | -0.117517 | 298 | 1200 |
| $N_2$ | 19.50583 | 19.88705 | -8.598535 | 1.369784 | 0.527601 | 500 | 2000 |

Notes: $T_{min}$ and $T_{max}$ indicate the minimum and maximum of the applicable temperature.

For the catalyst, its heat capacity $c_{p,cat}$ is assumed the same as that of its majority component $SiO_2$ with the value of 800 [J/(kg·K)] (Hamdhan and Clarke, 2010).

### Heat Transfer Coefficient

When the catalyst particles are assumed to be identical spheres, the heat transfer coefficient and specific area are given as (Amiri and Vafai, 1994; Amhalhel and Furmanski, 1997):

$$h = k_f \left[2 + 1.1 Pr^{1/3} \left(\rho_f v \frac{d_p}{\mu_f}\right)^{0.6}\right] / d_p, \tag{5.80}$$

$$a_p = 6/d_p, \tag{5.81}$$

where $d_p$ [m] represents the particle diameter, $\mu_f$ denotes the viscosity of the fluid mixture and $Pr$ is the Prandtl number with the following expression:

$$Pr = \frac{\mu_f c_{p,f}}{k_f}. \tag{5.82}$$

**Diffusion Coefficient**

For a binary gas mixture with components $a$ and $b$, diffusion coefficient has an expression given below (Thirumaleshwar, 2009):

$$D_{ab} = 0.0043 \cdot \frac{T^{3/2}}{P_t \left(V_{m,a}^{1/3} + V_{m,b}^{1/3}\right)^2} \cdot \left(\frac{1}{M_a} + \frac{1}{M_b}\right)^{1/2}, \qquad [\text{cm}^2/\text{sec}] \tag{5.83}$$

where $V_{m,a}$ and $V_{m,b}$ are molar volumes of components $a$ and $b$ at normal boiling points, respectively, with a unit of [cm$^3$/mol]. If fluid-phase gas mixture is assumed to be air, the diffusion coefficients of $SO_2$, $O_2$, $SO_3$ and $N_2$ can be derived with the given molar weight and molar volume in Table 5.5 (Thirumaleshwar, 2009).

Table 5.5: Molar weights and molar volumes for different gas components

| Gas Components | Molecular Weight [g/mol] | Molar Volumes [cm$^3$/mol] |
|---|---|---|
| Air | 29 | 29.89 |
| $SO_2$ | 64 | 44.78 |
| $O_2$ | 32 | 25.63 |
| $SO_3$ | 48 | 20.10 |
| $N_2$ | 28 | 31.20 |

**Mass Transfer Coefficient**

If the catalyst particle is considered to be spherical, mass transfer coefficient of gas component $i$ takes the form as (Gupta and Thodos, 1963; Welty et al., 2008):

$$\beta_i = \frac{2.06v}{\varepsilon Re^{0.575} Sc^{2/3}}, \tag{5.84}$$

where the Reynolds number $Re$ and Schmidt number $Sc$ are obtained by:

$$Re = \frac{\rho_{f,i} d_p v}{\mu_{f,i}},$$
$$Sc = \frac{\mu_{f,i}}{\rho_{f,i} D_i}.$$

### 5.3.3 Reaction Rate

Reaction rate is the most important variable for dynamic modelling of the catalytic $SO_2$ converter. It determines the source terms $r_h$ in energy conservation (5.54) and $r_{s,i}$ in mass balances (5.58)-(5.60). For reaction (1.2), its reaction rate, namely the rate of $SO_2$ production, has been studied by Froment and Bischoff (Froment and Bischoff, 1979) and the results have been used in the literatures (Kiss et al., 2010; Nouri and Ouederni, 2013):

$$r_{SO_2} = -K_1 \frac{X_{s,SO_2} X_{s,O_2} - \frac{1}{K_E} X_{s,SO_3} X_{s,O_2}^{1/2} P_t^{-1/2}}{22.414(P_t^{-1} + K_2 X_{s,SO_2} + K_3 X_{s,SO_3})^2}, \qquad \text{[kmol/(kg-cat·hr)]} \tag{5.85}$$

where $K_1$, $K_E$, $K_2$, $K_3$ are empirical parameters related with temperature, and the following relations have been proposed (Froment and Bischoff, 1979; Kiss et al., 2010):

$$K_E = \exp\left(-10.68 + \frac{11300.0}{T}\right) \qquad [1/\text{atm}^{1/2}]$$

$$K_1 = 2.1125 \times 10^5 \cdot \exp\left(-\frac{3599.78}{T}\right) \qquad [\text{kmol/(kg-cat}\cdot\text{atm}^2\cdot\text{hr)}]$$

$$K_2 = 14.641 \qquad [\text{atm}^{-1}]$$

$$K_3 = 6.5775 \qquad [\text{atm}^{-1}]$$

With $r_{SO_2}$ obtained, the source terms $r_h$ and $r_{s,i}$ are then expressed as:

$$r_h = r_{SO_2}\Delta H, \tag{5.86}$$

$$r_{s,SO_2} = r_{SO_2}, \tag{5.87}$$

$$r_{s,O_2} = \frac{1}{2} r_{SO_2}, \tag{5.88}$$

$$r_{s,SO_3} = -r_{SO_2}, \tag{5.89}$$

where $\Delta H = -98$ kJ/mol, is the heat released with every mole of $SO_2$ consumed by reaction (1.2).

## 5.4 Dynamic Simulation

For dynamic simulation, the derived two-phase models in Equations (5.53-5.60) are discretized with time and space using finite difference method. Following the boundary conditions in Equations (5.61-5.67), simulations are carried out on these discretized equations with given inlet conditions.

**Spatial Variation Profiles**

The detailed two-phase dynamic model can be used to describe the spatial and temporal variations of temperature and concentrations inside every stage of the $SO_2$ converter under given feed conditions. With the feed conditions provided in Table 5.6, the spatial variations of temperature and $SO_2$ concentration within the first three converter stages are given in Figure 5.3. The reaction rates and $SO_2$ conversion ratios are shown in Figure 5.4.

Table 5.6: Feed conditions for spatial variation simulations

| Feed Concentrations[(a)] | | Other Feed Variables | |
|---|---|---|---|
| $X^{in}_{SO_2,1}$ | 10% | $T^{in}$ | 700 K[(c)] |
| $X^{in}_{O_2,1}$ | 11% | $Q^{in}_1$ | 50 $m^3$/sec[(b)] |
| $X^{in}_{SO_3,1}$ | 0% | $P^{in}$ | 1.4 atm |

Notes:
(a) Feed concentrations of the second and third beds follow Equation (4.21);
(b) Feed flowrates of the second and third beds follow Equation (4.31);
(c) Inlet temperature of all beds equals to 700 K.

In Figures 5.3 and 5.4, simulation results show that the spatial variations of both temperature and concentrations mainly occur in the top 10% layer of the catalyst beds, indicating that most the $SO_2$ conversion in these beds happens in the top layer of the catalyst beds. From Figure 5.3(c) and (d), it is observed that the solid-phase $SO_2$ concentration is noticeably lower than that of fluid phase in the top layer of catalyst bed. This difference results from the assumption that the reaction happens in the solid-phase gas mixture. Figure 5.4(a) tells that the $SO_2$ oxidation reaction starts when the gas touches the catalyst beds and slows down with temperature increasing and $SO_2$ concentration decreasing. From the $SO_2$ conversion ratio displayed in Figure 5.4(b), about 90% of $SO_2$ is oxidized into $SO_3$ in the first two converter stages. With a low concentration of $SO_2$ entering the third bed, the third-bed spatial profiles of temperature, $SO_2$ concentration, reaction rate, as well as conversion ratio present less variations in contrast to those of the first two beds.

Figure 5.5 compares the simulated outlet $SO_2$ concentration and conversion ratio with those

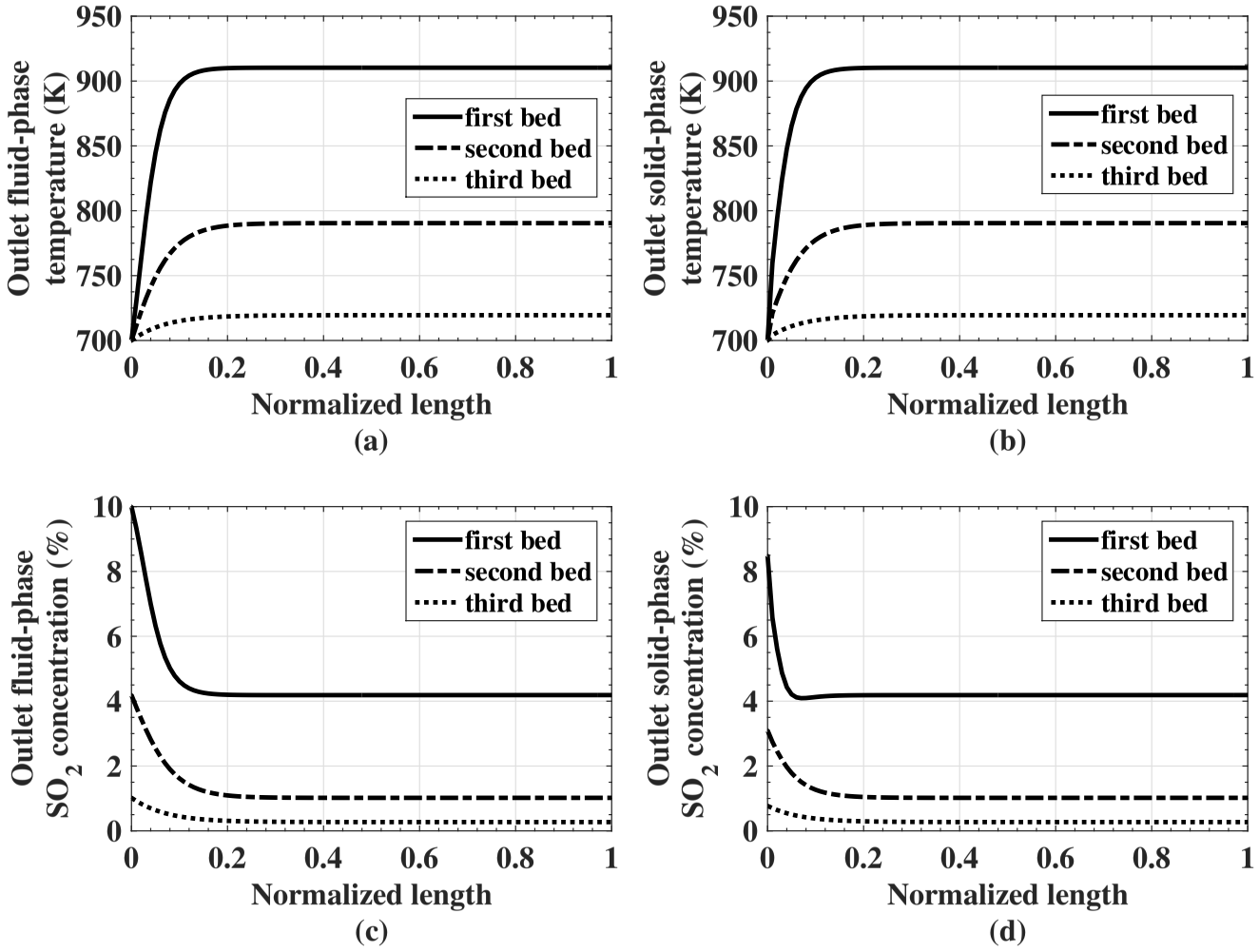


Figure 5.3: Simulated spatial variation profiles of fluid- and solid-phase outlet temperatures and $SO_2$ concentrations

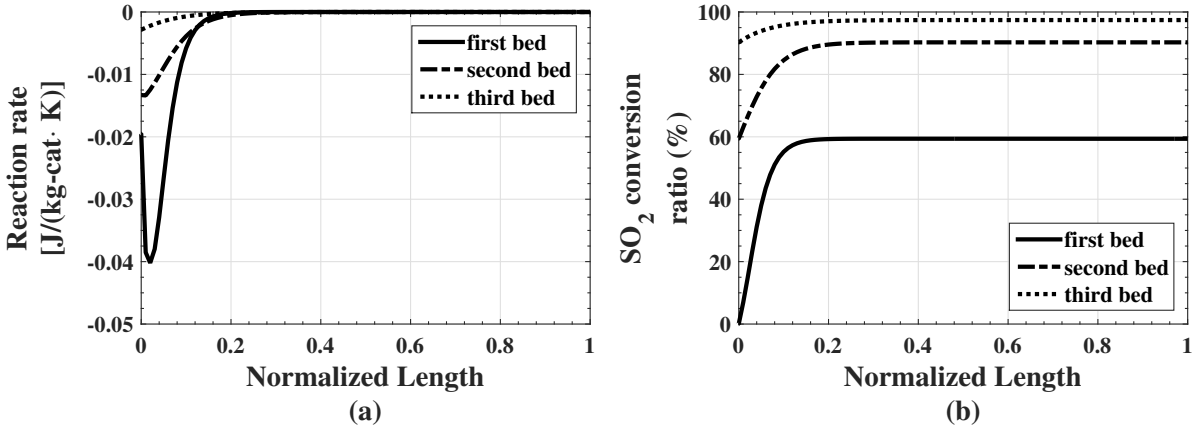


Figure 5.4: Simulated spatial profiles of steady-state reaction rate and $SO_2$ conversion ratio

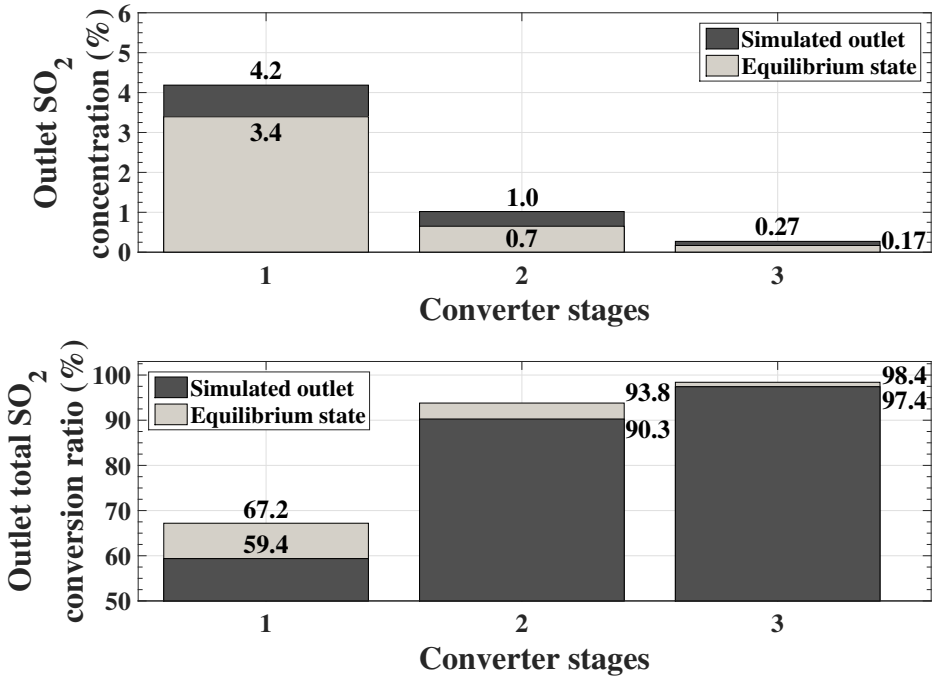


Figure 5.5: Comparison of simulated and equilibrium outlet $SO_2$ concentration and conversion ratio

from the equilibrium state under the same feed conditions. The comparison shows that the simulated operation gives a lower $SO_2$ conversion and higher outlet $SO_2$ concentration than the equilibrium state predicts, which agrees with the discussion in Section 2.3 that industrial conversion cannot exceed the equilibrium one. Besides, the difference between simulated and equilibrium outlet $SO_2$ concentration and conversion ratio is getting smaller in the consecutive stages. It suggests that the multi-stage structure of the $SO_2$ converter is expected to not only encourage more $SO_2$ conversion, but allow the operation to get closer to the equilibrium state, the theoretical maximum conversion of the converter.

**Feed $SO_2$ Cut-off and Restoration Simulation**

Based on the observations from the industrial operations and the developed dynamic model, the variations in outlet variables usually result from the changes in inlet gas temperature and/or $SO_2$ concentration. From the schematic diagram of a sulfuric acid plant in Figure 1.2, the inlet gas temperature of every converter stage is adjusted through external heat exchangers by manipulating by-pass valves. Sudden increases or decreases of inlet gas temperature barely happen if proper valve control is applied. On the other hand, the gas entering a sulfuric acid plant comes from multiple up-stream sources in an industrial smelter, for example, from furnaces, roasters and/or Pierce-Smith converters. As a result, the $SO_2$ concentration entering the acid plant may experience dramatic changes and causes challenges in acid plant operations. Based on the developed two-phase dynamic model, simulations are performed to explore the process performance when dramatic changes in $SO_2$ source gas occurs. The process is examined when inlet $SO_2$ is cut off for a period of time and then restores. For these simulations, the feed conditions are given in Table 5.7.

Figure 5.6 displays the spatial profiles of temperature and $SO_2$ concentration of both phases after inlet $SO_2$ is cut off. In Figures 5.6(c) and (d), $SO_2$ concentrations along the catalyst bed quickly drop to zero in the first minute after $SO_2$ is cut off. Once the $SO_2$ fraction gets lower or even becomes zero, reaction stops and no heat will be generated. Therefore, when

Table 5.7: Feed conditions for $SO_2$ cut-off and restoring simulations

| Feed Variables | $SO_2$ Cut-off | $SO_2$ Restoring |
|---|---|---|
| $X^{in}_{SO_2}$ | $10\% \rightarrow 0$ | $0 \rightarrow 10\%$ |
| $X^{in}_{O_2}$ | $11\% \rightarrow 12.22\%$ | $12.22\% \rightarrow 11\%$ |
| $X^{in}_{SO_3}$ | 0 | 0 |
| $T^{in}$ | 700 K | 700 K |
| $Q^{in}$ | 50 $m^3$/sec | 50 $m^3$/sec |
| $P^{in}$ | 1.4 atm | 1.4 atm |

Note: The ratio $X^{in}_{O_2}/X^{in}_{re}$ equals to $11/79 = 0.139$ during both $SO_2$ cut-off and restoring cases.

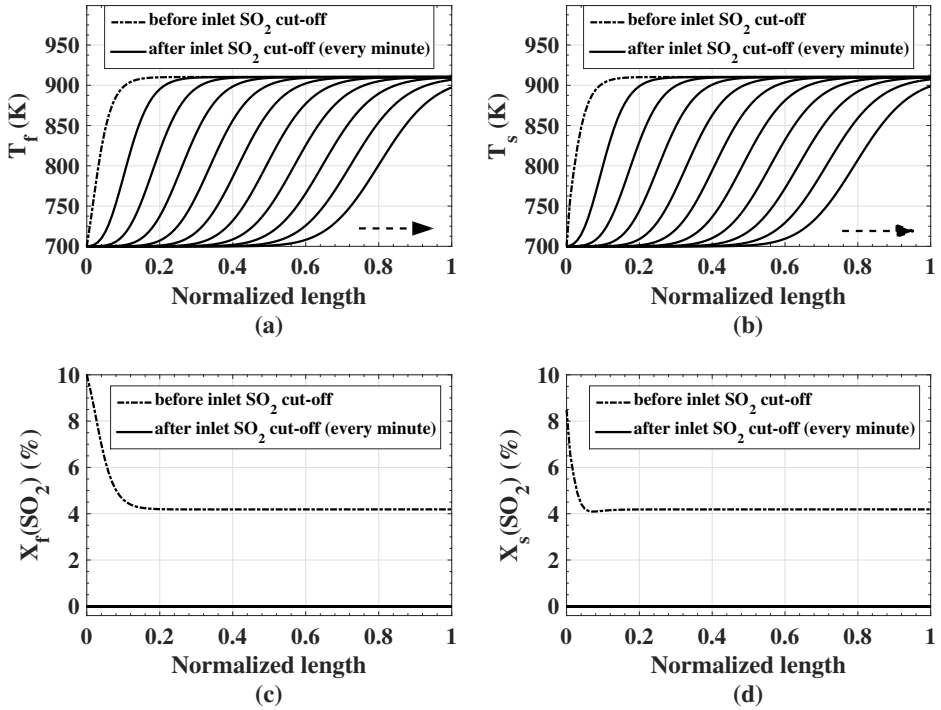


Figure 5.6: Spatial profiles of fluid- and solid-phase temperature and $SO_2$ concentration after inlet $SO_2$ cut-off

the $SO_2$ supply stops, the converter stage can be considered as a cooling process where the catalyst bed is being cooled down by the inlet cold gas. From Figure 5.6(a) and (b), fluid and solid temperatures have similar dynamics. Arrows in these two sub-figures indicate the shifting direction of the temperature waves for every minute. At the exit, temperature drop will not be noticed until 9 minutes after the inlet $SO_2$ cut-off.

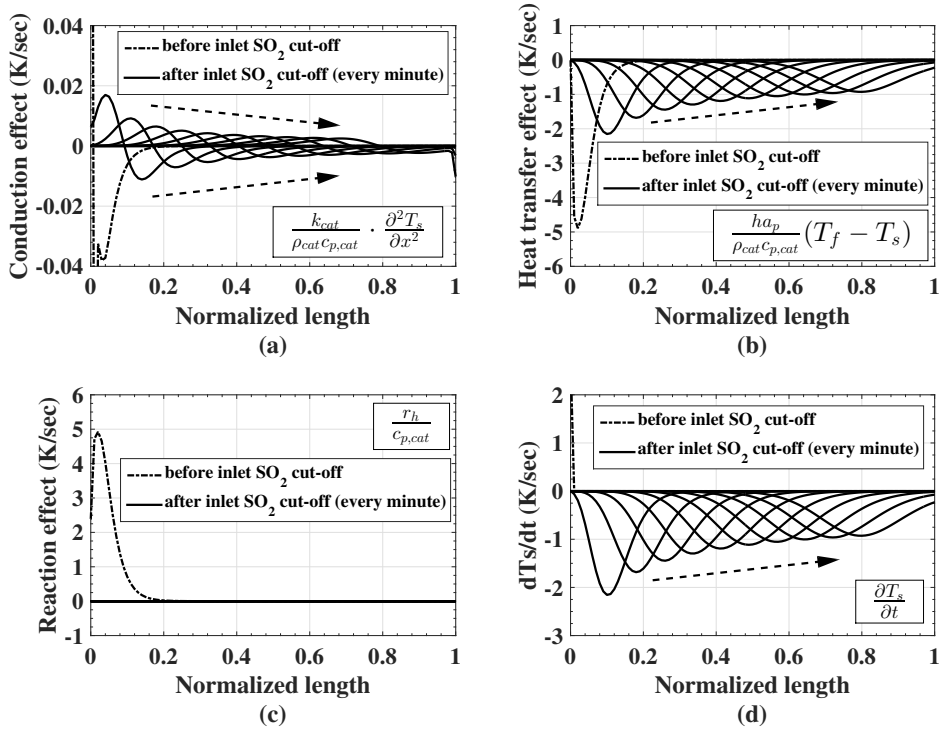


Figure 5.7: Detailed spatial profiles of individual energy terms on solid-phase temperature dynamics after inlet $SO_2$ cut-off

Detailed spatial profiles regarding the effects of individual terms in the energy equations on the solid- and fluid-phase temperature dynamics after the $SO_2$ cut-off are provided in Figures 5.7 and 5.8, respectively. For the variation profiles of solid-phase temperature in Figure 5.7(c), reaction stops with no $SO_2$ supply. Comparing to the heat transfer effect in Figure 5.7(b), energy related to conduction in Figure 5.7(a) within the catalyst is small and could be neglected. The decrease of catalyst temperature is mainly determined by the heat transfer to the fluid-phase gas flow. This is evident from the similar variation in Figures 5.7(b) and (d). Figure 5.7(b) also

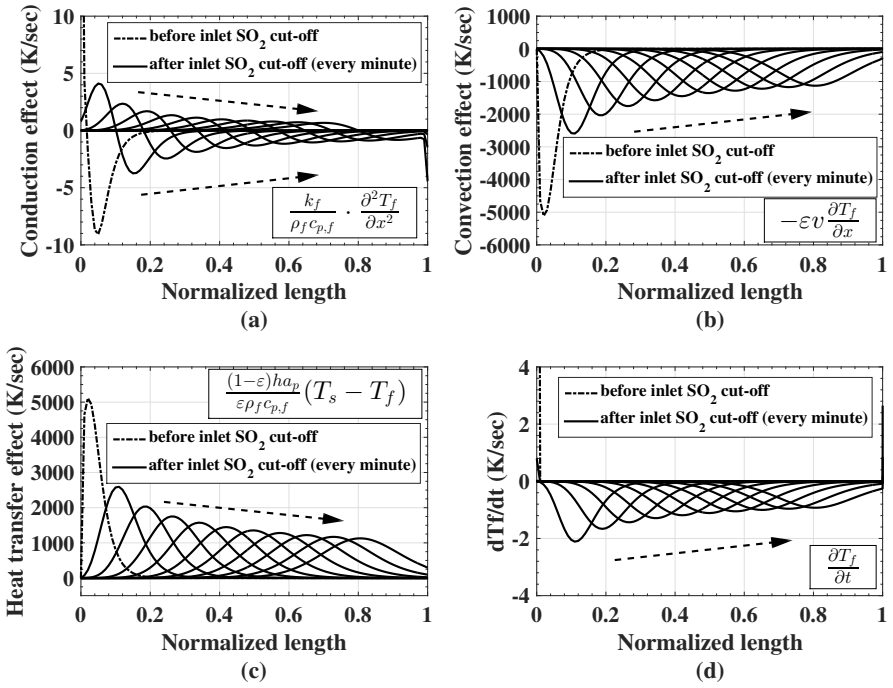


Figure 5.8: Detailed spatial profiles of individual energy terms on fluid-phase temperature dynamics after inlet $SO_2$ cut-off

indicates that the effect resulting from the heat loss to the fluid decays with time. In Figure 5.8, the fluid-phase energy effect due to conduction is found negligible, and the temperature variation is mainly determined by the convection by the gas flow and the heat received from the catalyst. The effects of the heat transfer and convection get weaker and weaker with time.

With $SO_2$ supply being cut-off for a period of time, the $SO_2$ is let to restore to the normal operation. Spatial profiles of fluid- and solid-phase temperatures and $SO_2$ concentrations when $SO_2$ supply restores are presented in Figure 5.9. It can be seen that $SO_2$ concentration inside the converter gradually increases with the temperature due to restoration of the chemical reaction, which is different from the case when $SO_2$ inlet is suspended and the concentration rapidly diminishes as shown in Figure 5.6(c) and 5.6(d). From Figure 5.9(a) and 5.9(b), the temperature of the top layer of catalyst builds up first and the outlet temperature starts to increase after 4 minutes. Comparing with the 9 minute delay in Figure 5.6(a), outlet temperature has a quicker

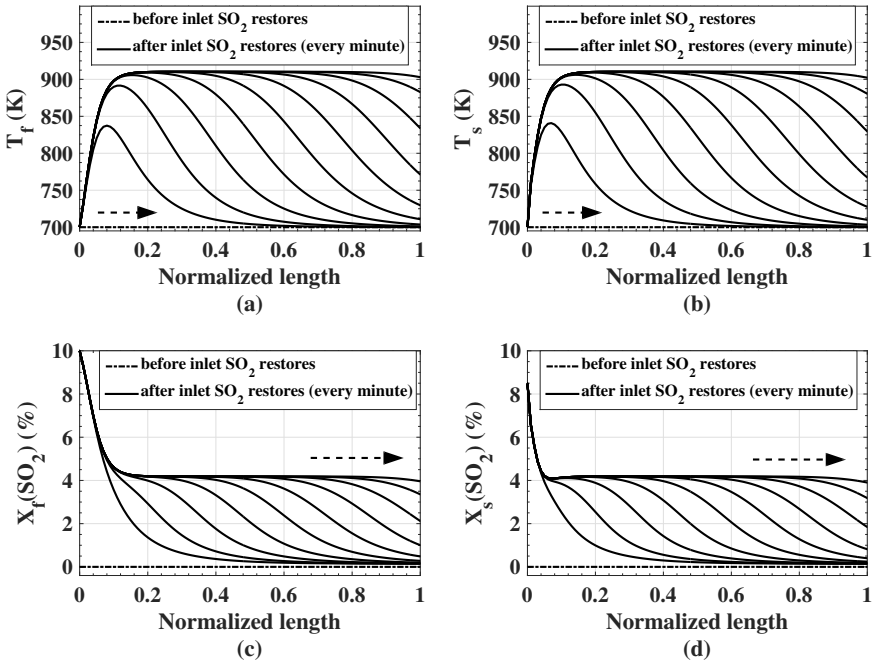


Figure 5.9: Spatial profiles of fluid- and solid-phase temperature and $SO_2$ concentration after inlet $SO_2$ restoration

response to the $SO_2$ restoration. In addition, the temperature waves in Figure 5.6(a) and 5.6(b) are tigher than those in Figure 5.9(a) and 5.9(b), which indicates that outlet temperature has a faster response and shorter dynamics for $SO_2$ restoration.

Figures 5.10 and 5.11 display the spatial profiles of the effects of individual terms in the energy equations on solid- and fluid-phase temperature dynamics during the $SO_2$ restoration. From Figure 5.10(c), reaction happens fast and intensely in the top 10% layer of the catalyst as the inlet $SO_2$ concentration restores. With most $SO_2$ consumed, reaction gets slower in the remaining part of catalyst. The intensive reaction heats up the corresponding top layer of catalyst and energy is released into fluid-phase gas by heat transfer. From Figure 5.11(b) and (c), it is observed that the fluid-phase gas flow picks up the heat from the top catalyst, and gradually releases it back to the downstream part of catalyst. Unlike the decaying heat transfer effects in Figures 5.7 and 5.8, the heat transfer of the top layer of catalyst remains significant due to the continuous reaction. The strong heat transfer means more energy is released from catalyst to

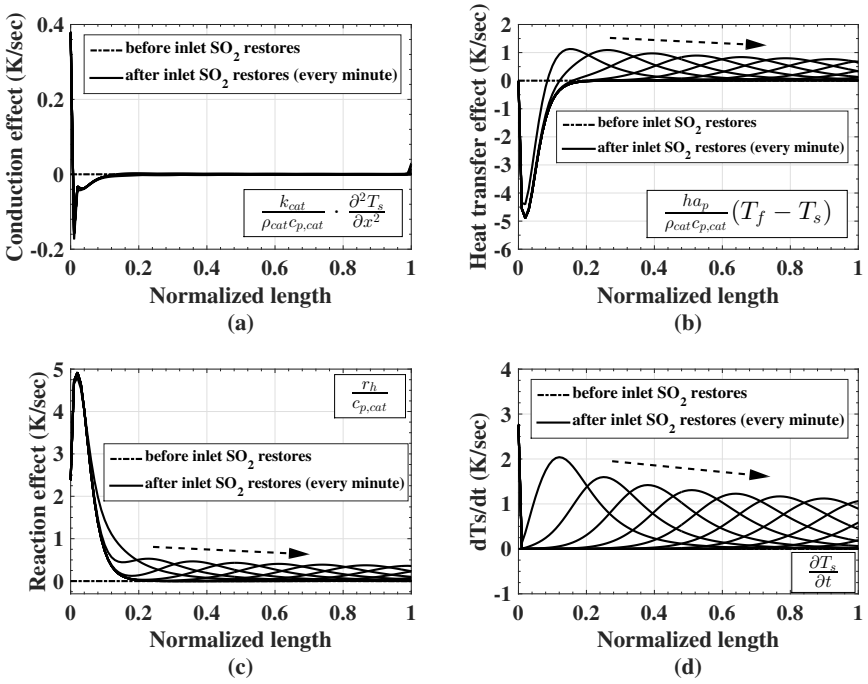


Figure 5.10: Detailed spatial profiles of individual energy terms on solid-phase temperature dynamics after inlet $SO_2$ restoration

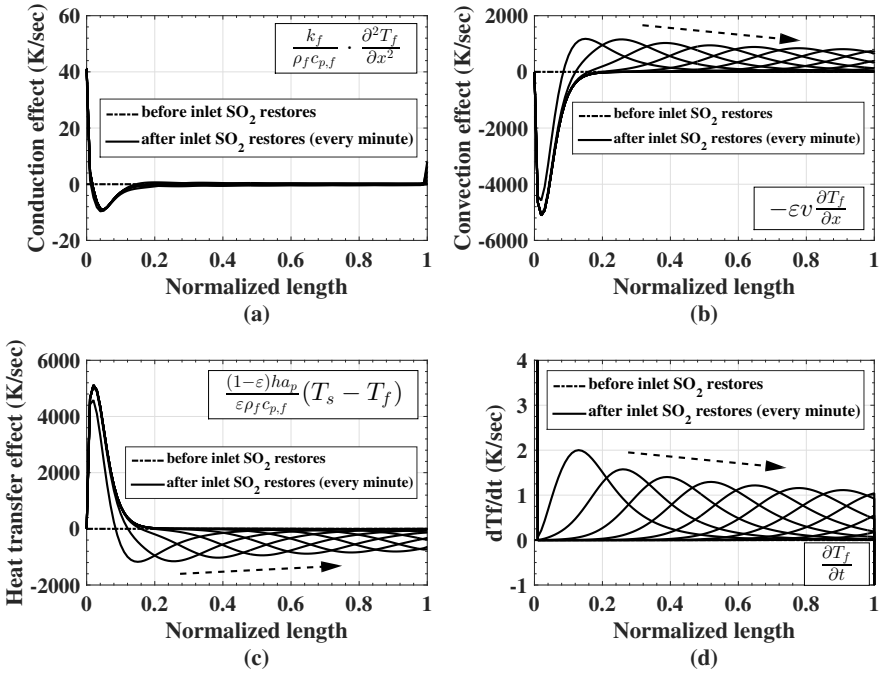


Figure 5.11: Detailed spatial profiles of individual energy terms on fluid-phase temperature dynamics after inlet $SO_2$ restoration

fluid gas. With the steadily heat supply carried down by the gas stream, the downstream catalyst heats up gradually.

We next explore the underlying mechanism for the different responding dynamics of the system to the $SO_2$ cut-off and restoring cases. Figure 5.12 shows the outlet gas temperature variations for the $SO_2$ cut-off and restoring cases. The inlet $SO_2$ concentration is cut off and restores at $t = 0$ in both cases. It is noticed that the outlet gas temperature responds to the $SO_2$ restoration quicker than to the $SO_2$ cut-off. It takes about 4 minutes for outlet temperature to start responding to the $SO_2$ step increase, while 9 minutes delay is observed on the outlet temperature after inlet $SO_2$ stops. In addition, the new steady state of outlet temperature takes a longer time to be reached when the system is experiencing the inlet $SO_2$ cut-off.

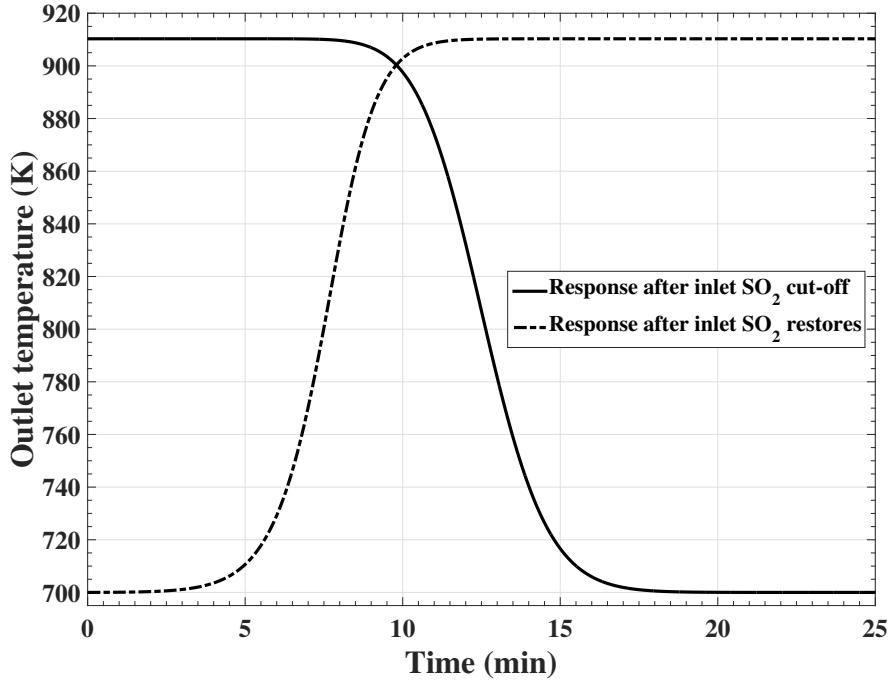


Figure 5.12: Simulated outlet temperature profiles during inlet $SO_2$ cut-off and restoring cases

As previously mentioned, when the supply of $SO_2$ is suspended at the inlet, the catalyst bed cools down mainly due to the heat loss to the continuous inlet cool gas flow. The heat loss flux

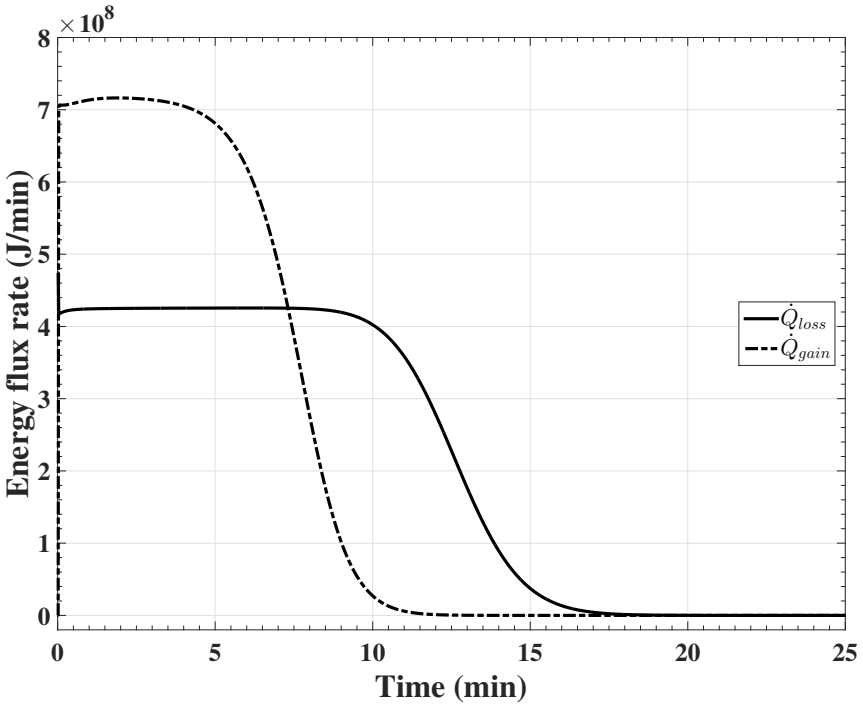


Figure 5.13: Heat loss flux rate of the catalyst bed after inlet $SO_2$ cut-off and heat gain flux rate of the catalyst bed after inlet $SO_2$ restoration

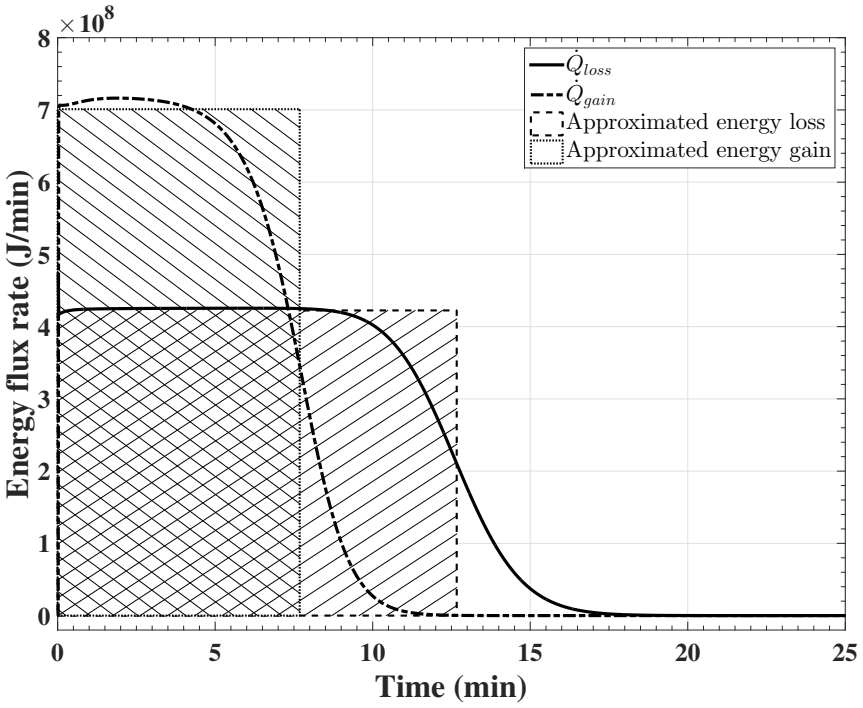


Figure 5.14: Approximated total heat loss of the catalyst bed after inlet $SO_2$ cut-off and approximated total heat gain of the catalyst bed after inlet $SO_2$ restoration

rate $\dot{Q}_{loss}$ [J/sec] of the catalyst bed can be expressed as:

$$\begin{aligned}
\dot{Q}_{loss}(t) &= \underbrace{\int_{V_s} -k_{cat}\frac{\partial^2 T_s(t)}{\partial x^2} dV}_{\text{due to conduction}} + \underbrace{\int_{V_s} h(t)a_p \left[T_s(t) - T_f(t)\right] dV}_{\text{due to heat transfer between gas and catalyst bed}} \\
&\approx \sum_{j=0}^{n_x} \left[ -k_{cat}\frac{\partial T_s(t, j\Delta x)^2}{dx^2} \cdot (1-\varepsilon)\Delta x \cdot \pi \frac{D_C^2}{4} \right] \\
&+ \sum_{j=0}^{n_x} \left[ h(t, j\Delta x)a_p(T_s(t, j\Delta x) - T_f(t, j\Delta x)) \cdot (1-\varepsilon)\Delta x \cdot \pi \frac{D_C^2}{4} \right] \\
&= (1-\varepsilon)x_{max}\pi\frac{D_C^2}{4}(-k_{cat}) \sum_{j=0}^{n_x} \left[ \frac{\partial T_s(t, j\Delta x)^2}{dx^2} \right] \\
&+ (1-\varepsilon)x_{max}\pi\frac{D_C^2}{4}a_p \sum_{j=0}^{n_x} \left[ h(t, j\Delta x)(T_s(t, j\Delta x) - T_f(t, j\Delta x)) \right], \qquad (5.90)
\end{aligned}$$

where $n_x$ represents the number of grid points along the bed thickness that we used in the finite difference calculations. On the other hand, when the $SO_2$ supply restores, the catalyst bed is heated up mainly due to the chemical reaction along with the heat transfer to the gas. In this case, the heat gain flux rate $\dot{Q}_{gain}$ [J/sec] of the catalyst bed is derived as follows:

$$\begin{aligned}
\dot{Q}_{gain}(t) &= \underbrace{\int_{V_s} k_{cat}\frac{\partial^2 T_s(t)}{\partial x^2} dV}_{\text{due to conduction}} + \underbrace{\int_{V_s} r_h(t)\rho_{cat} dV}_{\text{due to chemical reaction}} - \underbrace{\int_{V_s} h(t)a_p \left[T_s(t) - T_f(t)\right] dV}_{\text{due to heat transfer between gas and catalyst bed}} \\
&\approx \sum_{j=0}^{n_x} \left[ k_{cat}\frac{\partial T_s(t, j\Delta x)^2}{dx^2} \cdot (1-\varepsilon)\Delta x \cdot \pi \frac{D_C^2}{4} \right] \\
&+ \sum_{j=0}^{n_x} \left[ r_h(t, j\Delta x)\rho_{cat} \cdot (1-\varepsilon)\Delta x \cdot \pi \frac{D_C^2}{4} \right] \\
&- \sum_{j=0}^{n_x} \left[ h(t, j\Delta x)a_p(T_s(t, j\Delta x) - T_f(t, j\Delta x)) \cdot (1-\varepsilon)\Delta x \cdot \pi \frac{D_C^2}{4} \right] \\
&= (1-\varepsilon)x_{max}\pi\frac{D_C^2}{4}k_{cat} \sum_{j=0}^{n_x} \left[ \frac{\partial T_s(t, j\Delta x)^2}{dx^2} \right] + (1-\varepsilon)\rho_{cat}x_{max}\pi\frac{D_C^2}{4} \sum_{j=0}^{n_x} \left[ r_h(t, j\Delta x) \right] \\
&- (1-\varepsilon)x_{max}\pi\frac{D_C^2}{4}a_p \sum_{j=0}^{n_x} \left[ h(t, j\Delta x)(T_s(t, j\Delta x) - T_f(t, j\Delta x)) \right]. \qquad (5.91)
\end{aligned}$$

In the previous simulations, both $\dot{Q}_{loss}$ and $\dot{Q}_{gain}$ are available and they are shown in Figure 5.13. Comparison of the two cases of heat flux rate indicates that the catalyst bed obtains the heat faster in $SO_2$ restoration than its losing heat when $SO_2$ supply stops. For the catalyst bed, the total heat loss during $SO_2$ cut-off and the total heat gain during $SO_2$ restoration should be equal. If the time of losing heat or gaining heat is approximated when the middle value between the maximum and minimum rates is reached, the total heat loss and heat gain in these two cases can be shown as the areas with diagonal-lines in Figure 5.14. As the rate of heat gain is higher in the $SO_2$ restoring case, the time for catalyst bed to reach the steady state is shorter than the case during $SO_2$ cut-off. The heat flux rates shown in Figure 5.13 verify that temperature has a faster response and shorter dynamics to the $SO_2$ build-up. After 10 minutes, the heat loss flux rate curve gradually declines to zero because both gas and catalyst bed are cooled to the same temperature as the inlet gas flow. After the inlet $SO_2$ restores and a new steady state of the system is reached, the heat gain rate of the catalyst bed becomes zero.

Figure 5.15 displays two periods of first-bed industrial data of outlet gas temperature when sudden changes of inlet $SO_2$ concentration occur. Exit gas temperature gradually decreases as the inlet $SO_2$ concentration decreases. When the $SO_2$ concentration restores, outlet gas temperature follows. It is observed that response time of outlet temperature is different when the system encounters $SO_2$ concentration decrease and increase. Exit temperature displays a slower change when there is a sudden drop of $SO_2$ concentration. The simulation results in Figure 5.12 are different from the data shown in Figure 5.15 because the industrial data are the results of all the inlet variable variations, including flowrate and inlet temperature. Despite the difference between the simulated data and industrial data, our model could be helpful to understand the complex behaviours of the $SO_2$ converter.

**Effects of Inlet Flowrate and Temperature**

Flowrate and inlet temperature are two important input variables and simulations are carried out to investigate the effects of inlet temperature and flowrate changes. The state achieved with the

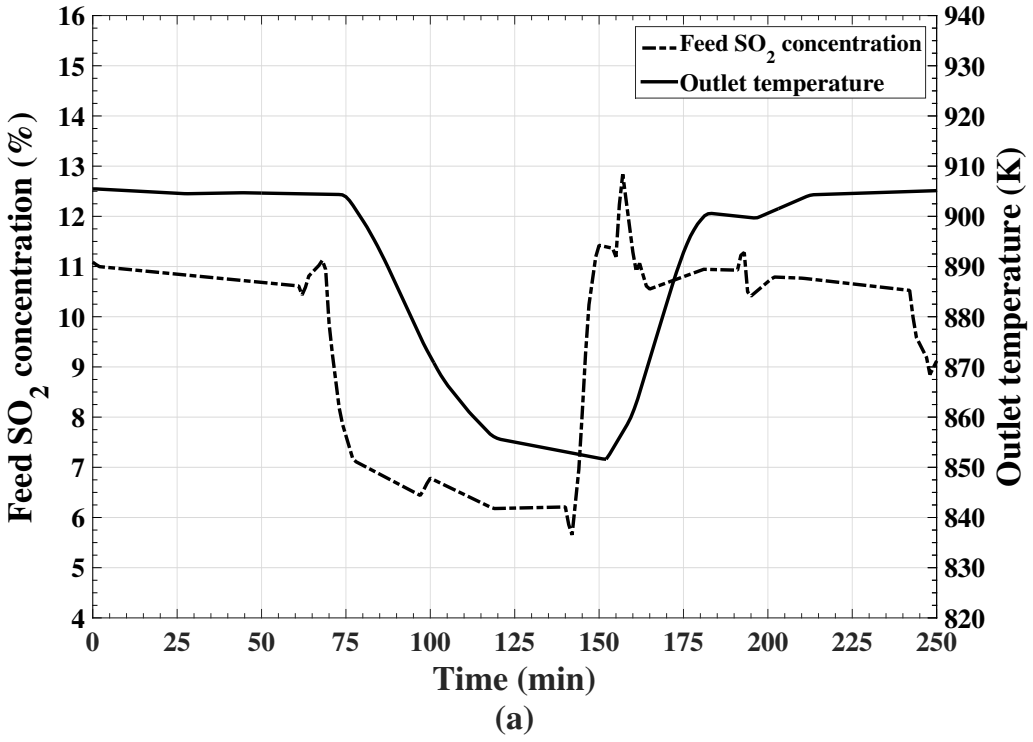


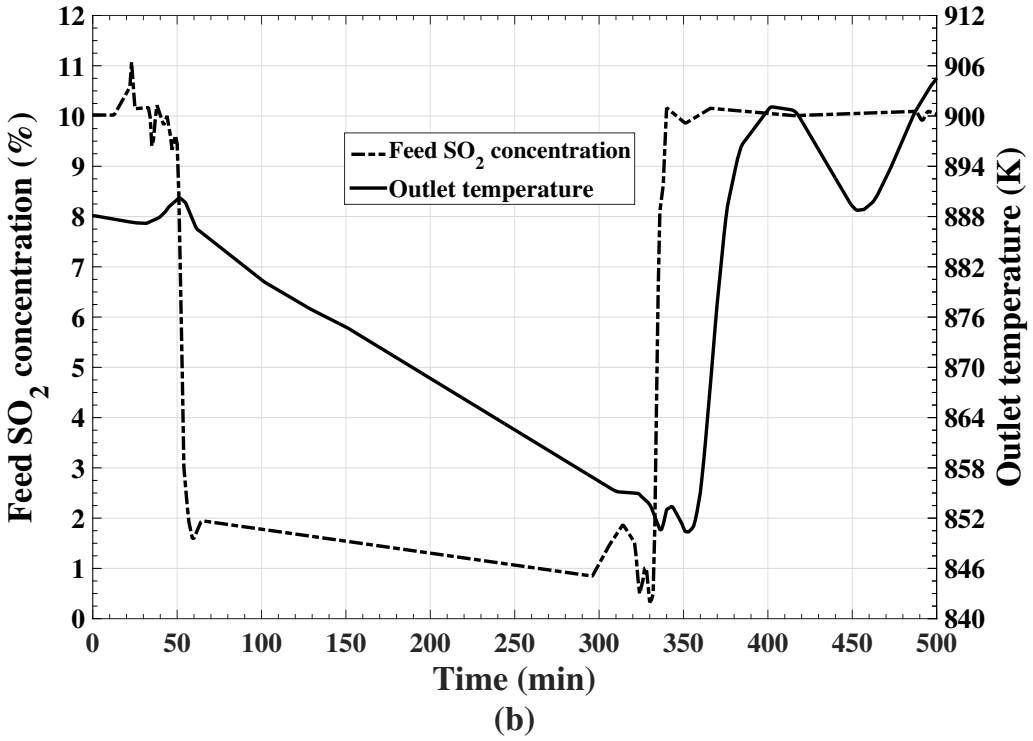


Figure 5.15: Two sets of selected data of feed $SO_2$ concentration and first-bed outlet temperature showing the system response to $SO_2$ changes

feed conditions in Table 5.6 is used as the initial condition for simulation.

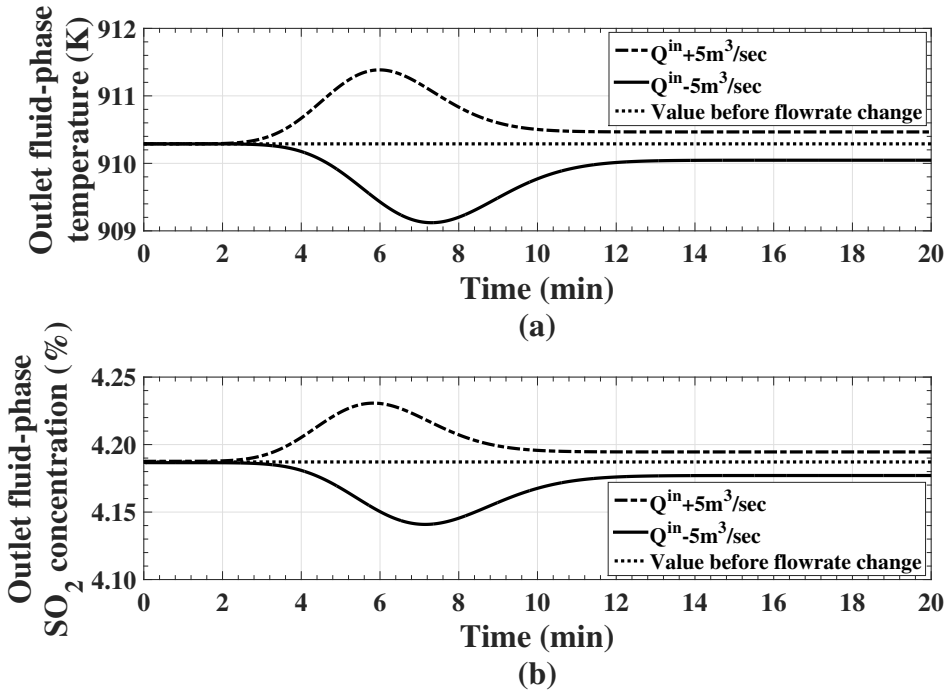


Figure 5.16: Simulated outlet temperature and $SO_2$ concentration in response to inlet flowrate changes

When $\pm 10\%$ (i.e. $\pm 5$ $m^3$/sec) step changes in the flowrate are applied to the steady state in the first-bed converter, variations of outlet temperature and $SO_2$ concentration with time are shown in Figure 5.16. As inlet flowrate increases, both outlet temperature and $SO_2$ concentration increase and reach a new steady state. However, it is noticed that the differences between the old and new steady states are not significant (less than 0.5K in temperature and 0.02% in $SO_2$ concentration), and they probably would be neglected for industrial operations. From Figure 5.16, although the flowrate does not have significant impact on the stead-state values, it causes quite noticeable disturbances on the outlet variables. The dynamics of the disturbances is slower with slower flowrate.

For $SO_2$ conversion, a proper flowrate is required to ensure sufficient residence time for the chemical reaction in the converter. Figures 5.3 and 5.5 indicate that the outlet state of the

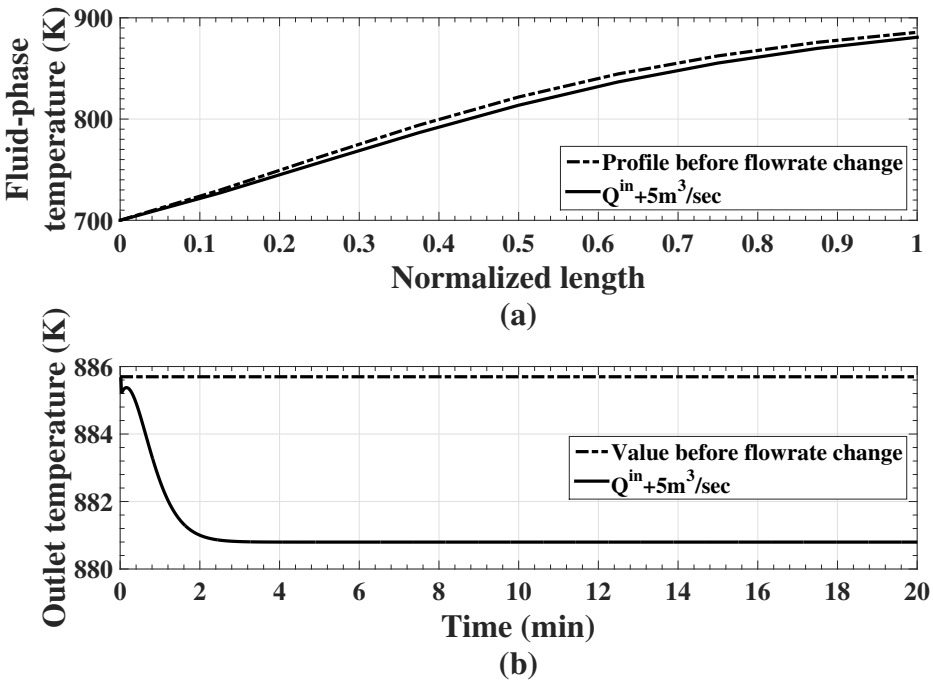


Figure 5.17: Fluid-phase temperature spatial profile and outlet temperature variation with time in response to inlet flowrate changes when outlet state is far from equilibrium

system is close to the chemical reaction equilibrium under the conditions given in Tables 5.2 and 5.6. The residence time of the gas through the catalyst bed depends on the flowrate and the amount of catalyst. If the system is operated under a fast flowrate or with a small amount of catalyst, the outlet gas state could be far from the equilibrium of reaction. Figure 5.17 shows fluid-phase temperature spatial profile and outlet temperature variation with time in the case if only 1/10 of catalyst is installed inside the first bed comparing to the case in Table 5.2. It is noticed that the outlet state in Figure 5.17(a) is farther away from the equilibrium than the case shown in Figure 5.3(a) due to insufficient residence time. In Figure 5.17, when inlet flowrate has a 5 $m^3$/sec increase, a noticeable 5K decrease at the outlet temperature is observed because of less reaction time and $SO_2$ conversion. In the situation when residence time is too short for chemical reaction, changes in inlet flowrate could have significant effects on the system outlet variables. Therefore, in order to reduce the effects of flowrate on the outlet variables, gas flow

should be maintained such that there is enough time for chemical reaction by providing a proper flowrate and adequate catalyst.

Effects of inlet gas temperature on the outlet temperature and $SO_2$ concentration are explored for the first-bed converter by introducing $\pm$10K step changes, as shown in Figure 5.18. Simulation results indicate that both outlet temperature and $SO_2$ concentration increase to a new steady state in response to a step increase of inlet temperature, and lower exit temperature and concentration are observed at the new steady state when inlet temperature drops. It is noticed that a change in the inlet temperature does not lead to a change in the outlet temperature with the same amount. A 10K change in inlet temperature causes only $\sim$5 K change at the outlet. This difference is mainly caused by the constraint of reaction equilibrium and can be noticed in Figure 2.5 as well. In industrial smelters, inlet temperature is usually adjusted to maintain a satisfactory performance of the $SO_2$ converter.

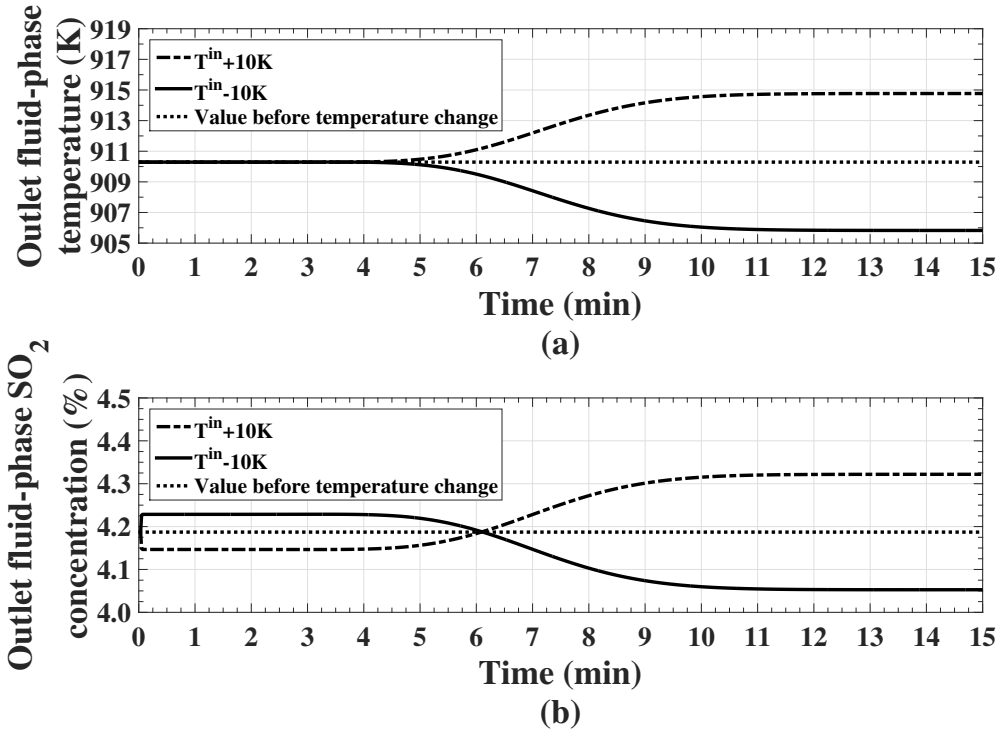


Figure 5.18: Simulated outlet temperature and $SO_2$ concentration in response to inlet temperature changes

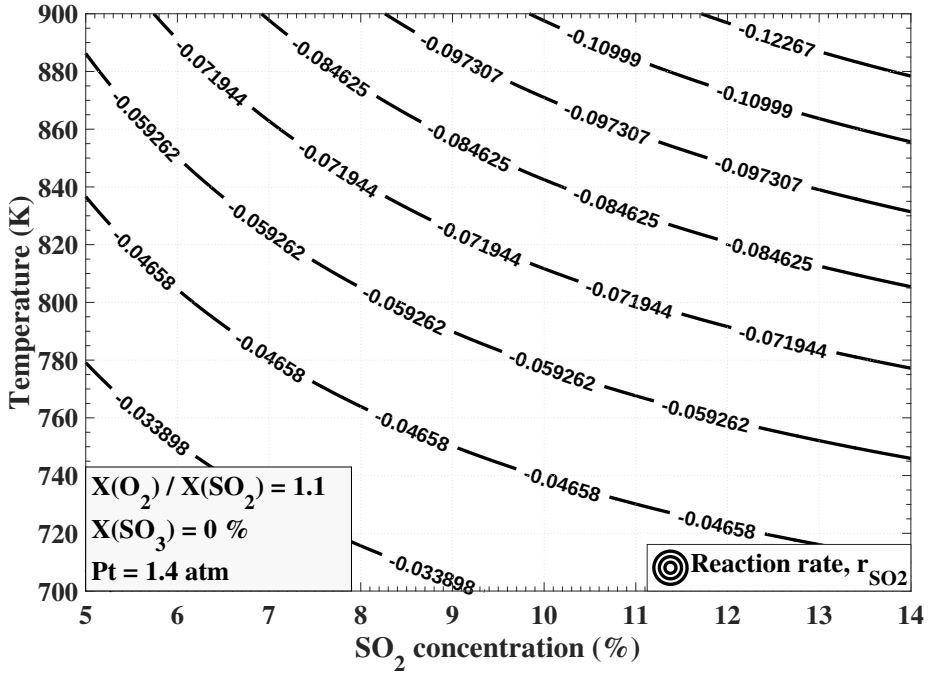


Figure 5.19: Reaction rate contour plot under different $SO_2$ concentrations and temperatures

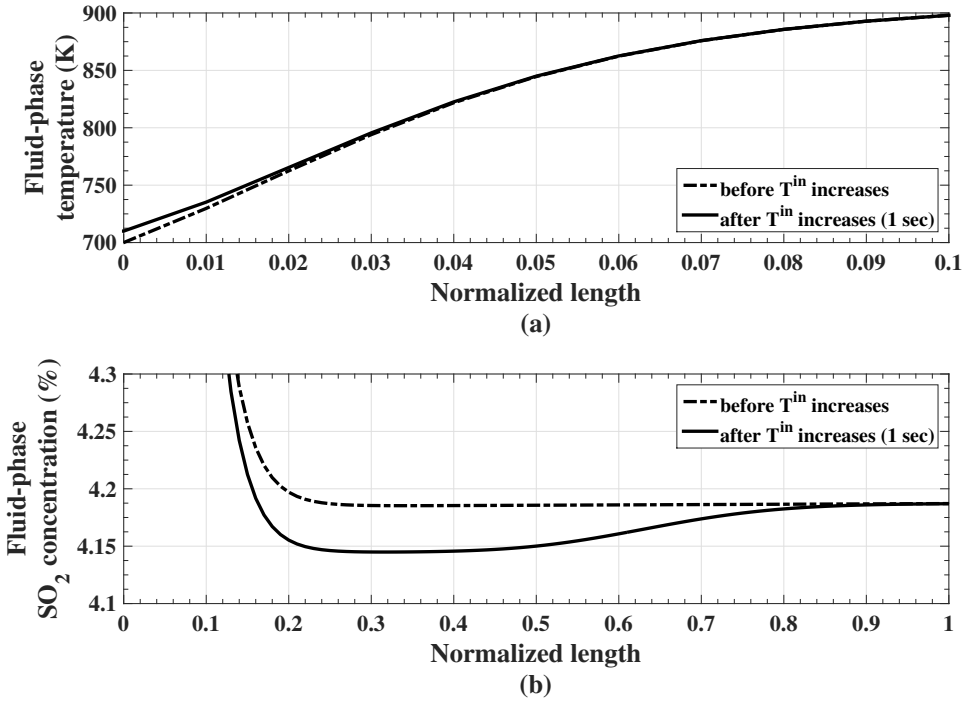


Figure 5.20: Simulated spatial profiles of fluid temperature and $SO_2$ concentration before and after inlet temperature increase

In Figure 5.18, The outlet temperature displays 5 minute time delay response. For $SO_2$ concentration, however, it responds to the inlet temperature changes almost simultaneously. As the inlet temperature increases, the $SO_2$ concentration decreases. We attempt to explore the mechanism behind the above observations from the dependence of reaction rate on the $SO_2$ concentration and gas temperature. Figure 5.19 presents the reaction rate contour regarding the $SO_2$ concentration and temperature. For a given $SO_2$ concentration, higher temperature is found to favor the reaction and lead to a higher reaction rate. Therefore, when a step increase occurs at the inlet temperature, reaction rate speeds up and more $SO_2$ is consumed at the top layer of catalyst leading to $SO_2$ concentration decrease.

Figure 5.20 show the spatial profiles of fluid temperature and $SO_2$ concentration in the converter stage when inlet temperature has a step increase. From Figure 5.20(b), after 1 second, the effect of $SO_2$ concentration decrease has been carried down by the gas flow and covered the top 80% of the catalyst. On the other hand, temperature increase is limited in the 10% of catalyst, as shown in Figure 5.20(a). Consequently, when feed temperature has a step increase of 10K, outlet $SO_2$ concentration experiences a fast drop almost simultaneously but outlet temperature remains constant for the first 5 minutes as shown in Figure 5.18. When the outlet temperature gradually escalates afterwards, outlet $SO_2$ concentration follows the change and a new steady state is reached. By observing the differential Equations (5.53 - 5.60), it is noticed that the heat capacity coefficient ($\rho c_p$) of the catalyst is larger than that of the fluid gas, leading to the slower variation of temperature comparing to those of the concentrations.

## 5.5 Industrial Data Comparison

At last, the two-phase dynamic model for the $SO_2$ catalytic converter is used to simulate some more realistic situations. With the estimated parameters in Section 5.3, one period of the industrial feed data are used as the feed conditions, and the process performance is simulated. The simulated outlet gas temperature of four converter stages is compared with the measured

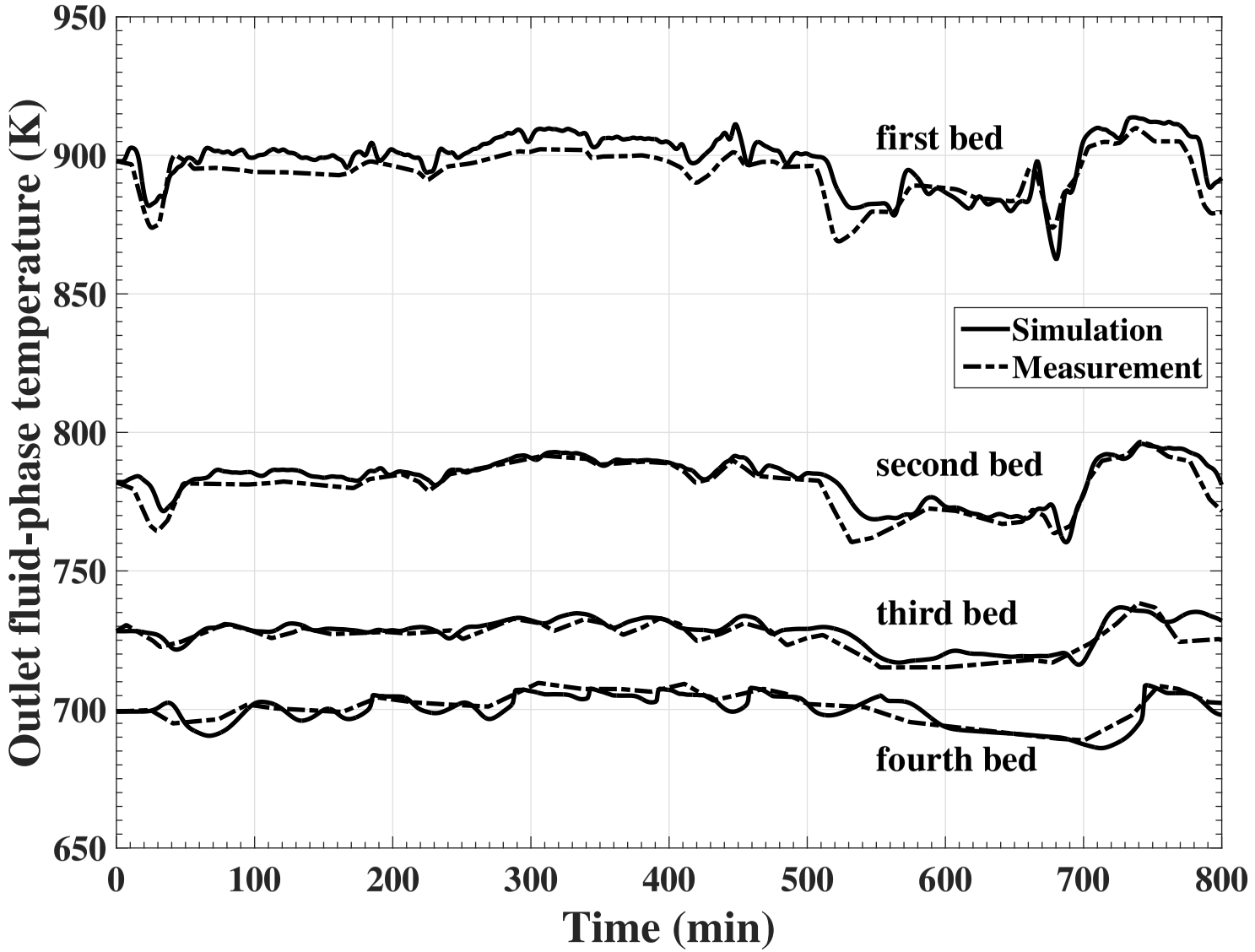


Figure 5.21: Comparison of one period of measured and predicted outlet gas temperature for four catalyst beds

temperature in Figure 5.21. It is observed that the simulated outlet gas temperature tracks the measurements reasonably well when the measurement varies slowly. This indicates that the model has a good validity in describing the industrial system. Existence of mismatch between the simulated temperature and the measurements is reasonable as the mechanistic model contains many parameters that can only approximately be estimated, while the industrial system may have unknown noises. In addition, other factors can also contribute to the mismatch, such as the neglected heat loss of the converter to the environment, the channelling effect in the catalyst bed, missing information about the oxygen concentrations from the collected data, and/or inaccurate estimated parameters.

## 5.6 Summary

In order to have a better understanding of the $SO_2$ conversion process, detailed modelling on the $SO_2$ converter is necessary. This chapter develops the dynamic model by applying the mass and energy conservations on both fluid- and solid-phase gas mixtures. This developed two-phase dynamic model takes the form of partial differential equations (PDE) and provides a mathematical tool to explore the interaction between gas flow and catalyst during normal industrial operation.

Based on the proposed model, simulations are run to examine the spatial variations of the temperatures and $SO_2$ concentrations within three $SO_2$ converter stages under given feed conditions. It shows that chemical reaction mainly occurs in the top layer of the catalyst beds. Comparisons are also given between the simulated and equilibrium outlet $SO_2$ concentrations and conversion ratios.

The $SO_2$ cut-off and restoring cases are simulated by the developed two-phase model. Simulation results provide the detailed two-phase temperature and $SO_2$ concentration spatial profiles varying with time. Studies indicate that $SO_2$ concentration diminishes quickly after $SO_2$ is cut-off and then the catalyst temperature decreases only through gradual heat loss to the

gas stream. The cold inlet gas continuously carries the released energy away and eventually cools down the catalyst bed. As for $SO_2$ supply restoring case, intensive reaction occurs at the top layer of catalyst and energy is continuously discharged from catalyst to gas flow by heat transfer. The heated gas flow delivers the energy into downstream and heats up the subsequent catalyst through energy exchange. Comparison between the heat loss flux rate after $SO_2$ stops and the heat gain flux rate from reaction after $SO_2$ restores indicates that the catalyst bed receives the reaction heat faster and speeds up the restoring process. Industrial data are examined and similar variation exists in variable dynamics.

Effects of the inlet flowrate and temperature are investigated using the developed PDE model. The simulation results show that changes in inlet flowrate barely affect the outlet steady states of temperature and $SO_2$ concentration, but affect the responding time delay and the variation speed of the system. With an inlet temperature increase, new higher steady state is observed in the outlet temperature and $SO_2$ concentration. The steady-state gain ratio of outlet to inlet temperatures is found around 0.5. The outlet $SO_2$ concentration is noticed to have a faster response to the feed temperature changes than the outlet temperature because the heat capacity difference between the gas and catalyst defers the energy variations.

With the estimated parameters, outlet gas temperature is predicted through dynamic simulations using the two-phase model with collected feed data. The prediction results show a good match with the industrial measurements.

# Chapter 6

# Conclusions and Future Work

Sulfuric acid plants that capture $SO_2$ from industrial off-gas emissions are essential for the modern process industry. The core unit is the catalytic $SO_2$ converter as this determines $SO_2$ conversion and, therefore, sulfuric acid production.

The focus of this thesis is to develop mathematical models for $SO_2$ converters for various applications. The developed models will be used to describe the performance of $SO_2$ converters and provide a fundamental tool for future process analysis, optimization and control.

## 6.1 Conclusions

In Chapter 2, steady-state modelling of the catalytic $SO_2$ converter is carried out based on steady-state mass and energy conservation. The obtained steady-state model provides an explicit relation between the $SO_2$ conversion ratio and gas temperature. This steady-state relationship is used to generate a heat-up path. By combining the heat-up path with the equilibrium curve of reaction (1.2), the equilibrium $SO_2$ conversion ratio and temperature can be calculated. The equilibrium conversion ratio reflects the theoretical maximum conversion which a $SO_2$ converter can achieve under given feed conditions. A heat-up path simulation is performed on a three-stage converter and the results indicate that the majority of conversion

is in the first catalyst bed. Heat-up paths under different inlet gas temperatures and $SO_2$ concentrations are explored and the proposed steady-state models should serve as a tool for the dynamic modelling and simplification.

$SO_2$ concentration and conversion ratio are important variables for the $SO_2$ converter operation, but they are little measured in many smelters due to hardware constraints. Chapter 3 established mathematical soft sensors for these essential variables so that they can be estimated from available measured variables. The soft sensors are built based on the steady-state models and industrial dynamic data analysis. From the industrial data, correlation examination discovers that outlet gas temperature is highly related to the inlet $SO_2$ concentration and the maximum correlation coefficient is derived when delay time equals to 9 minutes. A first-order exponential data filter is introduced and applied to the inlet $SO_2$ data to achieve the synchronization with outlet temperature. Using the filter's $SO_2$ concentration signals, the mathematical soft sensors generate a reasonable and useful estimation of outlet $SO_2$ concentration and conversion ratio. This provides helpful information to examine the performance of the converter.

A dynamic model of the $SO_2$ converter is obtained in Chapter 4 using dynamic mass and energy conservation. This developed dynamic model takes the form of ordinary differential equations (ODE) and uses the $SO_2$ conversion ratio as a key variable in the model development. In comparison with existing models, introducing the $SO_2$ conversion ratio into modelling avoids the necessity of reaction kinetics knowledge or expressions which sometimes are difficult to confirm due to too many parameters. Outlet gas temperature is predicted by the ODE model based on the available feed data. Comparison between the collected industrial measurements and prediction verifies the validity of the proposed model in describing the converter. With the proposed dynamic model, simulations are carried out to explore the effects of input variables. Inlet flowrate is found to effect the system dynamic speed, while outlet gas temperature exhibits slow dynamics in relation to inlet $SO_2$ changes. In addition, through steady-state observations,

a higher inlet $SO_2$ concentration results in more $SO_2$ conversion, but a lower $SO_2$ conversion ratio. This dynamic model incorporating the $SO_2$ conversion ratio can be conveniently applied to many $SO_2$ converters with easy parameter estimation using available operating data. It could be also used as the base equations for design when process control enhancement is required for the converters.

Detailed dynamic modelling is performed on the $SO_2$ converters by implementing mass and energy continuities on both fluid- and solid-phase gas mixtures. The two-phase dynamic model, established in the form of partial differential equations (PDE), is able to describe the $SO_2$ converter with time and space. In contrast with the existing dynamic models of the converters, difference between gas and catalyst temperature changes is considered so that the energy interaction between gas and catalyst can be studied. With the evaluated parameters, industrial feed data are applied to the two-phase dynamic model to produce a prediction of outlet gas temperature. The prediction fits well with industrial measurement and thus validates the detailed dynamic model.

Spatial variations of the fluid- and solid-phase temperatures and $SO_2$ concentrations in three-stage $SO_2$ converter are generated by dynamic simulations with the two-phase model. Chemical reaction is found to happen within the top layer of catalyst beds. Comparison between the simulated and equilibrium outlet $SO_2$ concentrations, and conversion ratios, are provided and the results show that the simulated conversion cannot exceed the equilibrium.

Simulations are carried out to explore the feed $SO_2$ cut-off and restoring cases and their effects. When inlet $SO_2$ cut-off occurs, $SO_2$ concentration inside the converter rapidly falls by flow and chemical reaction. The decline of both gas and catalyst temperatures in the converter are observed and their variations are determined by the energy transfer between gas and catalyst along with the continuous inlet gas flow. Effect of energy transfer gradually dies out with time, leading to the slow dynamics of the gas temperature. For inlet $SO_2$ supply restoration, fast reaction happens within the top layer of the catalyst bed, and this strengthens energy transfer

from the catalyst to the gas. The gas flow carries the received energy down to subsequent catalyst and releases it back to the catalyst. With the constantly fast reaction at the top catalyst layer, the strengthened energy transfer and gas movements lead to fast dynamics in outlet temperature in comparison with the case when the $SO_2$ cut-off occurs. By comparing the heat loss flux rate of the catalyst bed for $SO_2$ cut-off and the heat gain flux rate of the catalyst bed for $SO_2$ restoration, it is noted that the catalyst bed absorbs the reaction heat from the restored reaction faster than it losing heat when $SO_2$ is cut off. This heat flux rate difference directly leads to the fast response dynamics on the outlet temperature when the $SO_2$ restoration occurs. Simulations show that the developed two-phase model provides clear and detailed profiles of the $SO_2$ converter behaviour. Observation from the industrial data shows a similar response and dynamic pattern for the outlet temperature to $SO_2$ concentration changes.

The proposed detailed dynamic model is also used to investigate the effects of inlet flowrate and temperature on the $SO_2$ converter outlet. From the simulation results, inlet flowrate variations, as typically happens in industrial operations, hardly impact outlet steady states. System response time delay and dynamics, on the other hand, are significantly impacted by flowrate changes. Inlet temperature changes causes variations on the outlet temperature and $SO_2$ concentration. Higher steady-state outlet temperature and $SO_2$ concentration are obtained as a result of a feed temperature increase. The outlet $SO_2$ concentration is found to almost simultaneously respond to the sudden changes in inlet temperature.

## 6.2 Future Work

Modelling of the catalytic $SO_2$ converter is important for sulfuric acid plant control. A good model on the $SO_2$ converter is presented to provide valuable information while describing the behaviour of the converting process and can eventually help with improvement of the sulfuric acid plant. In this thesis, detailed dynamic modelling has been performed on the $SO_2$ converters, including steady-state model, dynamic model in the form of ODE incorporating with $SO_2$

conversion ratio, and detailed PDE dynamic model dividing the gas mixture into two phases. Based on the current work, there are still some open problems and investigations that may be addressed for by future research.

In this thesis, a dynamic model is established by using the $SO_2$ conversion ratio as the key variable. In order to connect the $SO_2$ conversion ratio only with the inlet variables, a linear relation is proposed between the actual and equilibrium conversion ratios. Even though the proposed dynamic model gives a good match with the data, challenges still remain to establish a more accurate relation between the actual and equilibrium conversion ratios. Achieving this will eventually improve the performance of the dynamic model, as well as the $SO_2$ conversion ratio estimation.

The detailed two-phase dynamic models in this thesis contain many process parameters. Most of them are estimated based on empirical expressions from existing work. Estimation of a large number of unknown parameters from a set of partial differential equations is always challenging. Especially for the kinetics parameters in the reaction rate expression, they should be varied if different catalyst is applied. A good estimation of the parameters will improve the accuracy of the dynamic model and extend its applications.

For a $SO_2$ converter located in a sulfuric acid plant within an industrial smelter, process control development is always important and necessary to deal with varying process disturbances. A stable and constantly high conversion of $SO_2$ is beneficial to acid product production. Control strategy investigation will, therefore, be necessary in future research.

# References

M. Amazouz and R. Platon. Soft-sensors for real-time monitoring and control of a black liquor concentration process. In *Proceedings of the 2011 International Conference on Data Mining*, pages 22 – 27, 2011.

G. Amhalhel and P. Furmanski. Problems of modeling flow and heat transfer in porous media. *Journal of Power Technologies*, 85:55 –88, 1997.

A. Amiri and K. Vafai. Analysis of dispersion effects and non-thermal equilibrium, non-darcian, variable porosity incompressible flow through porous media. *International Journal of Heat and Mass Transfer*, 37:939 – 954, 1994.

N.G. Ashar and K.R. Golwalkar. *A practical guild to the manufacture of sulfuric acid, oleums, and sulfonating agents*. Springer INternational Publishing, 2013.

A. Bousri, K. Bouhadef, H. Beji, R. Bennacer, and R. Nebbali. Heat and mass transfer in reactive porous media with local nonequilibrium conditions. *Journal of Porous Media*, 15: 329 – 341, 2012.

H. Byrdziak, J. Dobrzanski, J. Garbaczewski, and J. Kotarski. Sulfur dioxide emission reduction by the polish copper industry. In *Proceeding of the 1996 125th TMS Annual Meeting*, pages 1005 – 1013, 1996.

W.H. Chan, R.J. Vet, Chul-Un Ro, A.J.S. Tang, and M.A. Lusis. Impact of INCO smelter emissions on wet and dry deposition on the sudbury area. *Atmospheric Environment*, 18(5), 1984a.

W.H. Chan, R.J. Vet, Chul-Un Ro, A.J.S. Tang, and M.A. Lusis. Long-term precipitation quality and wet deposition fields in the Sudbury Basin. *Atmospheric Environment*, 18(6):1175 – 1188, 1984b.

Jr. Chase, M.W. Nist-janaf themochemical tables, fourth edition. *Journal of Physical and Chemical Reference Data, Monograph 9*, pages 1–1951, 1998.

A. Ciccone and J. Storbeck. Fugitive $SO_2$ and particulate emissions from a smelter complex. In *Proceedings of the Air & Waste Management Association's Annual Meeting & Exhibition*, 1997.

A.K. Coker. Ludwig's applied process design for chemical and petrochemical plants, 2007.

H. Darcy. Les fontaines publiques de la ville de dijon, 1856.

W.G. Davenport and M.J. King. *Sulphuric Acid Manufacture*. Elsevier, 2006.

A. Di Bella, L. Fortuna, S. Graziani, G. Napoli, and M.G. Xibilia. Soft sensor design for a sulfur recovery unit using genetic algorithms. In *2007 IEEE International Symposium on Intelligent Signal Processing, WISP*, 2007.

D. Dong, T.J. McAvoy, and L.J. Chang. Emission monitoring using multivariate soft sensors. In *Proceedings of the 1995 American Control Conference*, volume 1, pages 761 – 765, 1995.

J.R. Donovan, J.S. Palermo, and R.M. Smith. Sulfuric acid converter optimization. *CEP (Chemical Engineering Progress)*, 74(9):51 – 54, 1978.

ECCC. Environment and Climate Change Canada, canadian environmental sustainability indicators: Air pollutant emissions, 2017. URL www.ec.gc.ca/indicateurs-indicators/default.asp?lang=en&n=E79F4C12-1. (consulted in January 2018).

A. Fick. Ueber diffusion. *Annalen der Physik*, 94, 1855.

L. Fortuna, S. Graziani, A. Rizzo, and M.G. Xibilia. Soft sensors for monitoring and control of industrial processes, 2007.

L.J. Friedman. Analysis of recent advances in sulfuric acid plant systems and designs (contact area). In *4th International Conference COPPER 99-COBRE 99*, volume 5, pages 95 – 117, 1999.

L.J. Friedman and S.J. Friedman. The metallurgical sulfuric acid plant design, operating materials considerations 2006 update. In *2006 TMS Fall Extraction and Processing Division: Sohn International Symposium*, volume 8, pages 437 – 455, 2006.

G.F. Froment and K.B. Bischoff. *Chemical reactor analysis and design*. Wiley, 1979.

K. Gosiewski. Dynamic modelling of industrial $SO_2$ oxidation reactors. part 1. model of 'hot' and 'cold' start-ups of the plant. *Chemical Engineering and Processing*, 32:111 – 129, 1993.

K. Gosiewski. Unsteady states in metallurgical sulphuric acid plants after $SO_2$ concentration drop in the feed gas. *Canadian Journal of Chemical Engineering*, 74(5):621 – 625, 1996.

K. Gosiewski and W. Klaudel. Dynamic flowsheeting as a tool for a sulphuric acid plant start-up analysis. In *Proceedings, 6th International Conference - Large Chemical Plants*, pages 297 – 310, 1985.

A.A. Guenkel and G.M. Cameron. Packed towers in sulfuric acid plants - review of current industry practice. *Sulphur 2000 preprints*, pages 399 – 417, 2000.

J. Gunn, W. Keller, J. Negusanti, R. Potvin, P. Beckett, and K. Winterhalder. Ecosystem recovery after emission reductions: Sudbury, Canada. *Water, Air, Soil Pollut.*, 85(3):1783 – 1788, 1995.

A.S. Gupta and G. Thodos. Direct analogy between mass and heat transfer to beds of spheres. *AIChE Journal*, 9, 1963.

I.N. Hamdhan and B.G. Clarke. Determination of thermal conductivity of coarse and fine sand soils. In *Proceedings of World Geothermal Congress*, 2010.

P.H. Holst and K. Aziz. Transient three-dimensional natural convection in confined porous media. *International Journal of Heat and Mass Transfer*, 15:73 – 90, 1972.

R. Hong, X. Li, H. Li, and W. Yuan. Modeling and simulation of $SO_2$ oxidation in a fixed-bed reactor with periodic flow reversal. *Catalysis Today*, 38(1):47 – 58, 1997.

J. Humphris, M. J.and Liu and F. Javor. Gas cleaning and acid plant operations at the Inco Copper Cliff Smelter. In *Proceedings of the Nickel-Cobalt 97 International Symposium*, volume 3, 1997.

W.D. Hunter Jr., J.C. Fedoruk, A.W. Michener, and J.E. Harris. The allied chemical sulfur dioxide reduction process for metallurgical emissions. *Advances in Chemistry*, 139:23 – 34, 1975.

W.S. Janna. Engineering heat transfer, second edition, 1999.

M. Kampa and E. Castanas. Human health effects of air pollution. *Environmental Pollution*, 151:362 – 367, 2008.

A.A. Kiss, C.S. Bildea, and J. Grievink. Dynamic modeling and process optimization of an industrial sulfuric acid plant. *Chemical Engineering Journal*, 158(2):241 – 249, 2010.

S.H. Lam. Multicomponet diffusion revisited. *Physics of Fluids*, 18:073101, 2006.

L. Liang and M. Liang. Preliminary study on model selection and installation of the instrumentation for newly built sulfuric acid plant. *Process Automation Instrumentation*, 34(4):91 – 94, 2013.

G. Liessmann, W. Schmidt, and S. Reiffarth. Recommended thermophysical data. *Data Compilation of the Saechsische Olefinwerke Boehlen, Germany*, page 31, 1995.

V. Lobanov, N. Ageev, and A. Pritchin. Reduction of sulfur dioxide emission. In *2008 Global Symposium on Recyling, Waste Treatment and Clean Technology*, pages 327 – 330, 2008.

S. Ma, Z. Wen, and Chen J. Scenario analysis of sulfur dioxide emissions reduction potential in China's iron and steel industry. *Journal of Industrial Ecology*, 16:506 – 517, 2012.

F. Manenti, D. Papasidero, G. Bozzano, and E. Ranzi. Model-based optimization of sulfur recovery units. *Computers and Chemical Engineering*, 66:244 – 251, 2014.

R. Mann. Controlling $SO_2$ emissions during start-up of multi-bed sulphuric acid converters. *Transactions of the Institute of Measurement and Control*, 8(3):144 – 150, 1986.

R. Mann, I.J. Gardner, and C. Morris. Reactor dynamics and strategies for minimizing $SO_2$ emissions during start-up of a contact sulphuric acid plant. *Chemical Engineering Science*, 35:185 – 192, 1980.

R. Mann, E. Stavridis, and K. Djamarani. Experimental fixed-bed reactor dynamics for $SO_2$ oxidation. *Chemical Engineering Research and Design*, 64:248 – 257, 1986.

MECC-$SO_2$. Monitored pollutants - sulphur dioxide, Ontario Ministry of the Environment and Climate Change. URL http://www.airqualityontario.com/science/pollutants/sulphur.php. (accessed in January 2018).

NIST-$N_2$. Gas phase thermochemistry data - nitrogen, National Institute of Standard and Technology. URL http://webbook.nist.gov/cgi/cbook.cgi?ID=C7727379&Mask=1. (accessed in January 2018).

NIST-$O_2$. Gas phase thermochemistry data - oxygen, National Institute of Standard and Technology. URL http://webbook.nist.gov/cgi/cbook.cgi?ID=C7782447&Mask=1. (accessed in January 2018).

NIST-$SO_2$. Gas phase thermochemistry data - sulfur dioxide, National Institute of Standard and Technology. URL http://webbook.nist.gov/cgi/cbook.cgi?ID=C7446095&Mask=1. (accessed in January 2018).

NIST-$SO_3$. Gas phase thermochemistry data - sulfur trioxide, National Institute of Standard and Technology. URL http://webbook.nist.gov/cgi/cbook.cgi?ID=C7446119&Mask=1. (accessed in January 2018).

H. Nouri and A. Ouederni. Experimental and modeling study of sulfur dioxide oxidation in packed-bed tubular reactor. *International Journal of Innovation and Applied Studies*, 3(4): 1045 – 1052, 2013.

O. Reg. 194/05. Ontario Regulation 194/05, environmental Protection Act, industry emission - nitrogen oxides and sulphur dioxides. URL https://www.ontario.ca/laws/regulation/050194/v1#BK36. (version for the period May 5, 2005 to July 27, 2017).

P.V. Ravindra, R.D. Prahlada, and M.S. Rao. A model for the oxidation of sulfur dioxide in a trickle-bed reactor. *Industrial and Engineering Chemistry Research*, 36(12):5125 – 5132, 1997.

J.F. Richardson, J.H. Harker, and J.R. Backhurst. Chemical engineering volume 2, fifth edition - particle technology and separation processes, 2013.

M.E. Schlesinger, M.J. King, K.C. Sole, and W.G. Davenport. *Extractive metallurgy of copper, fifth edition*. Elsevier Science, 2011.

S.A. Shahamiri and I. Wierzba. Modeling the reactive processes within a catalytic porous medium. *Applied Mathematical Modelling*, 35:1915 – 1925, 2011.

H. Shang, M. Dillabough, P. Nelson, and B. Salt. Dynamic modelling of an industrial smelter furnace and converter off-gas system. *American Journal of Environmental Sciences*, 4(1):22 – 30, 2008.

H. Shao, T. Nagel, C. Ro$\beta$kopf, M. Linder, A. Wörner, and O. Kolditz. Non-equilibrium thermo-chemical heat storage in porous media: Part 2 - a 1D computational model for a calcium hydroxide reaction system. *Energy*, 60:271 – 282, 2013.

J.D. Snyder and B. Subramaniam. Numerical simulation of a periodic flow reversal reactor for sulfur dioxide oxidation. *Chemical Engineering Science*, 48(24):4051 – 4064, 1993.

P.A. Sørensen, M. Møllerhøj, and K.A. Christensen. New dynamic models for simulation of industrial $SO_2$ oxidation reactors and wet gas sulfuric acid plants. *Chemical Engineering Journal*, 278:421 – 429, 2015.

M.P. Sudbury and G.A. Crawford. Sulphur abatement at ontario operations of Falconbridge Limited. In *Proceedings - A&WMA Annual Meeting*, volume 5, 1989.

M. Thirumaleshwar. Fundamentals of heat and mass transfer, 2009.

N.V. Vernikovskaya, A.N. Zagoruiko, and A.S. Noskov. $SO_2$ oxidation method. mathematical modeling taking into account dynamic properties of the catalyst. *Chemical Engineering Science*, 54(20):4475 – 4482, 1999.

J. Warna and T. Salmi. Dynamic modelling of catalytic three phase reactors. *Computers and Chemical Engineering*, 20(1):39 – 47, 1996.

J.R. Welty, C.E. Wicks, R.E. Wilson, and G.L. Rorrer. Fundamentals of momentum, heat, and mass transfer, 2008.

H. Wu, S. Zhang, and C. Li. Study of unsteady-state catalytic oxidation of sulfur dioxide by periodic flow reversal. *Canadian Journal of Chemical Engineering*, 74(5):766 – 771, 1996.

Y. Wu and X. Luo. A design of soft sensor based on data fusion. In *Proceedings - 2009 International Conference on Information Engineering and Computer Science*, 2009.

W.D. Xiao and W.K. Yuan. Modelling and experimental studies on unsteady-state $SO_2$ converters. *Canadian Journal of Chemical Engineering*, 74(5):772 – 782, 1996.

W.D. Xiao, H. Wang, and W.K. Yuan. An $SO_2$ converter with flow reversal and interstage heat removal: From laboratory to industry. *Chemical Engineering Science*, 54(10):1307 – 1311, 1999.

X. Yan, N. Tu, and H. Fu. Hybrid method for prediction of coal and gas outburst based on data fusion and soft sensor. In *ICEMI 2009 - Proceedings of 9th International Conference on Electronic Measurement and Instruments*, 2009.